This project was supported by the Centre for Global Eco-Innovation and is part financed by the European Regional Development Fund.

HVAC-based Hierarchical Energy Management System for Microgrids

By

Jie Ma

In collaboration with

Entrust Microgrid LLP

European Union
European Regional Development Fund

Abstract

With the high penetration of renewable energy into the grid, power fluctuations and supply-demand power mismatch are becoming more prominent, which pose a great challenge for the power system to eliminate negative effects through demand side management (DSM). The flexible load, such as heating, ventilation, air conditioning (HVAC) system, has a great potential to provide demand response services in the electricity grids.

In this thesis, a comprehensive framework based on a forecasting-management-optimization approach is proposed to coordinate multiple HVAC systems to deal with uncertainties from renewable energy resources and maximize the energy efficiency. In the forecasting stage, a hybrid model based on Multiple Aggregation Prediction Algorithm with exogenous variables (MAPAx)-Principal Components Analysis (PCA) is proposed to predict changes of local solar radiance, vy using the local observation dataset and real-time meteorological indexes acquired from the weather forecast spot. The forecast result is then compared with the statistical benchmark models and assessed by performance evaluation indexes. In the management stage, a novel distributed algorithm is developed to coordinate power consumption of HVAC sys-

tems by varying the compressors' frequency to maintain the supply-demand balance. It demonstrates that the cost and capacity of energy storage systems can be curtailed, since HVACs can absorb excessive power generation. More importantly, the method addresses a consensus problem under a switching communication topology by using Lyapunov argument, which relaxes the communication requirement. In the optimization stage, a price-comfort optimization model regarding HVAC's end users is formulated and a proportional-integral-derivative (PID)-based distributed algorithm is thus developed to minimize the customer's total cost, whilst alleviating the global power imbalance. The end users are motivated to participate in energy trade through DSM scheme. Furthermore, the coordination scheme can be extended to accommodate battery energy storage systems (BESSs) and a hybrid BESS-HVAC system with increasing storage capacity is proved as a promising solution to enhance its self-regulation ability in a microgrid. Extensive case studies have been undertaken with the respective control strategies to investigate effectiveness of the algorithms under various scenarios.

The techniques developed in this thesis has helped the partnership company of this project to develop their smart immersion heaters for the customers with minimum energy cost and maximum photovoltaic efficiency.

Acknowledgements

In the process of my efforts to pursue the doctoral degree and of completing this thesis, I sincerely thank the following people for their great help.

First of all, I would like to express my sincere gratitude and respect to my first supervisor, Dr Xiandong Ma, who gives me a lot of useful suggestions for my academic research. He is a professional, patient and helpful scholar, and always encourages me when I meet difficulties in my academic life. His cautious attitude towards the academic research not only improve my research abilities, but also improve my problem-solving abilities in my whole life.

Then, I would like to thank my second Superior, Dr Suzana Ilics, who also gives me many useful guidance for my PhD. Her encourages and motivates me a lot when I feel depression on my research.

In addition, I would like to express my sincere gratitude to my industrial supervisor, Mr Xiongwei Liu, who is the director of Entrust Microgrid LLP and launched this industry-led PhD project. My practical skills is improved by participating in the construction of a "Smart Home" microgrid experiment platform. He helps me solving technical problems, such as a main direction of the research and platform testing. His

support is highly appreciated.

Also, I would like to thank my families, my father Qiucheng Ma, my mother Xianghui Xie, my colleagues in the Engineering Department at Lancaster University, my friends in Manchester and China. Without my family and friends' supports, loves, and encouragements, I will not be able to successfully complete my doctoral studies.

Declaration

I declare that the work in this thesis has been done by myself and has not been submitted elsewhere for the award of any other degree.

Jie Ma

Contents

List of Figures

List of Tables

List of Abbreviations

AC Alternating Curren t

AIC Akaike Information Criterion

ANN Artificial Neural Network

ANN-SFP ANN into Statistical Feature Parameters

ANFIS Adaptive Neural Fuzzy Inference System

ARIMA Autoregressive Integrated Moving Average

ARIMA Autoregressive Integrated Moving Average with exogenous variables

AR Autoregressive

BESS Battery Energy Storage System

CERTS Consortium for Electric Reliability Technology Solutions

CHP Combined Heat and Power

COP Coefficient of Performance

DC Direct Current

DER Distributed Energy Resources

DG Distributed Generators

DSM Demand Side Management

CNN Convolutional Neural Network

EMA Energy Market Agent

EMU Energy Management Unit

ELD Economic Load Dispatch

ESA Energy Storage Agent

ESS Energy Storage System

ETS Exponential Smoothing

EV Electric Vehicle

GA Genetic Algorithm

GHI Global Horizontal Irradiance

HANs Home Area Networks

HVAC Heating Ventilation Air Conditioning

IPM Intelligent Power Module

KKT Karush-Kuhn-Tucker

MA Moving Average

MAPA Multiple Aggregation Prediction Algorithm

MAPAx Multiple Aggregation Prediction Algorithm with exogenous variables

MAPE Mean Absolute Percentage Error

MAS Multi-agent System

MIEM Multi-objective Intelligent Energy Management

MLP Multiple Linear Regression

MO Multi-Objective

MPC Model Predictive Control

MPPT Maximum Power Point Tracking

NWP Numerical Weather Prediction

PCA Principle Components Analysis

PCC Point of Common Coupling

PEI Power Electronic Interfaces

PFC Power Factor Control

PID Proportional-Integral-Derivative

PSO Particle Swarm Optimization

PV Photovoltaic

PWM Pulse Width Modulation

RGA Renewable Generation Agents

RLA Responsive Load Agents

SARIMA seasonal-ARIMA

SoC State-of-Charging

SSL Shiftable Static Loads

SVM Support Vector Machine

TCL Thermostatically Controlled Load

ToU Time-of-Use

UCL Upper Control Level

UV Ultraviolet

V2G Vehicle-to-grid

WAN Wide Area Network

WFS Weather Forecast Service

List of Symbols

α_0	Level estimation
β_i	Coefficients of i^{th} dummy variable
γ_j	Coefficients of j^{th} explanatory variable
δ_k	Coefficients of k^{th} lag variable
$\mathcal{D}$	Dummy variable
$x_{j,t}$	j^{th} explanatory variable observation unit at time t
X_j	j^{th} explanatory variable time series
y_t	Solar radiance observation data at time t
Y	Solar radiance time series
y_{t-k}	Lag variable of y_t lagged by k hours
$\hat{y}_t$	The forecast value of solar radiance at time t
L	Lag operator
p	Order of autoregressive model
q	Order of moving average model
σ	Order of integration model
ϕ_i	The parameter of AR model

ψ_j	The parameter of MA model
e	Error term of ARIMA model
$Y^{[k]}$	The aggregated time series element with k aggregation level
l	The level of a time series
tr	The trend of a time series
s	The seasonal of a time series
h	Forecasting step
K	Maximum aggregation level
K'	The number of aggregation levels where seasonality is identified
ξ_j	The effect of exogenous variable
w_j	Weighting coefficient of exogenous variable
$\mathbb{Z}$	Intset
R^2	Coefficient of determination
SS_{res}	The sum of squared predicted output residuals
SS_{total}	The total sum of squares
I_{sc}	Short-circuit current of a solar PV module under standard condition
U_{oc}	Open circuit voltage of a solar PV module under standard condition
I_m	Maximum current of a solar PV module under standard condition
U_m	Maximum voltage of a solar PV module under standard condition
P_m	Maximum power output of a solar PV module under standard condition
S	Solar radiance
T	Temperature

S_{ref}	Solar radiance reference value under standard condition
T_{ref}	Temperature reference value under standard condition
θ_1	Constant parameter in empirical formula
θ_2	Constant parameter in empirical formula
θ_3	Constant parameter in empirical formula
N_{ss}	The number of modules connected in a string of PV array
N_{pp}	The number of strings in a PV array
I'_{sc}	Short-circuit current of a solar PV module under real scenario
U'_{oc}	Open circuit voltage of a solar PV module under real scenario
I'_m	Maximum current of a solar PV module under real scenario
U'_m	Maximum voltage of a solar PV module under real scenario
P'_m	The maximum power output of a PV array under real scenario
$\mathcal{G}$	Undirected graph
$\mathcal{V}$	Node set
$\mathcal{E}$	Edge set
(i, j)	Information exchange between vertex j and i
N_i	Union of neighbour vertexes for vertex i
a_{ij}	Weighting coefficient for (i, j)
ℓ_{ij}	Elements of Laplacian matrix
$\mathcal{L}$	Laplacian matrix
d_{ij}	(i, j) entry of stochastic matrix D
D	Doubly stochastic matrix

x_i	State of agent i
1_n	A column vector of all ones
λ	eigenvalues
f	Compressor frequency
u	Load ramp rates of HVAC
v	Initial power of HVAC
Q_{AC}	Cooling capacity of HVAC
$P_{AC,i}$	Power output of HVAC i
$P_{D,i}$	Power mismatch at bus i
$\overline{P}_{AC}$	Maximum power consumption of HVAC
$\underline{P}_{AC}$	Minimum power consumption of HVAC
f^{ref}	Compressor frequency reference
P_{AC}^{ref}	HVAC power output reference
P_G	Distributed power generation
P_L	Uncontrollable load demand
P_d	Total Power mismatch
f^*	Desired compressor frequency
P_{AC}^*	Desired power output of HVAC
Γ_{AC}	Subset of saturated HVAC units
ϵ_i	State feedback gain of unit i
F	Column vectors of f_i
P_D	Column vectors of $P_{D,i}$

P_{AC}	Column vectors of $P_{AC,i}$
V	Column vectors of v_i
E	Diagonal matrix of ϵ_i
U	Diagonal matrix of u_i
W	System matrix
$\overline{f}$	Maximum compressor frequency
$\underline{f}$	Minimum compressor frequency
c_i	Switching parameter
D'	Doubly stochastic matrix under switching topology
$\overline{m}(f)$	Maximum frequency signal among all HVACs
$\underline{m}(f)$	Minimum frequency signal among all HVACs
f_a	Frequency convergence value
$\Omega(f_a)$	Trajectory of state variables converges to consensus point
κ	Switching times
Δ_k	Auxiliary function
inf	Infimum
V	Lyapunov function
T_s	Simulation time
T_c	Control cycle
C_a	Discomfort cost function
ω_a	Constant coefficient of Discomfort cost function
$\hat{P}_{AC}$	Normal power consumption at the comfortable level

Δ	Maximum power deviation for HVAC
A	Cost of action
ρ	ToU price
C_p	Electricity cost
ν_1	Weighting coefficient
ν_2	Weighting coefficient
L	Lagrangian function
μ	Lagrangian multiplier
$\mathbb{R}$	Real number field
μ^*	Optimal KKT point
u_{pid}	Control signal given by PID controller
K_P	Proportional coefficient
K_I	Integral coefficient
K_D	Derivative coefficient
Θ_1	Positive constant coefficient
Θ_2	Positive constant coefficient
z	Auxiliary variable
Z	Column vector of auxiliary variable
$\otimes$	Kronecker product
U_{pid}	Column vector of PID control signal
$\mathcal{Y}^*$	The solution set of Lagrange optimization problem
P_B^{cha}	Power stored in the BESS

P_B	input/output power of BESS
η_C	Charging efficiency of BESS
P_B^{dis}	Power extracted from the BESS
η_D	Discharging efficiency of BESS
S_B	The set of BESS
S_{AC}	The set of HVAC system
$\overline{P}_B$	Maximum power consumption of BESS
$\underline{P}_B$	Minimum power consumption of BESS
a_B	Coefficient of BESS cost function
b_B	Coefficient of BESS cost function
a_{AC}	Coefficient of HVAC cost function
b_{AC}	Coefficient of HVAC cost function
a_i	The set of a_B and a_{AC}
b_i	The set of b_B and b_{AC}
C	Cost functions
ε	State feedback gain
r	Incremental cost
B	Diagonal matrix of $1/a_i$
$\hat{B}$	Diagonal matrix of b_i'
R	Column vectors of r_i
G	Column vectors of$-b_i/a_i$
r^*	Optimal incremental cost

$\overline{P}_i$	Maximum power consumption of participant i
$\underline{P}_i$	Minimum power consumption of participant i
$\mathcal{X}$	Communication topology
T_d	information update cycle

Chapter 1

Introduction

1.1 Motivation and scope

Conventional power station mainly depends on the tradition resources, such as coal, petrol and gas, which is the major cause of greenhouse effect. On the other hand, most of the power plants are located in the rural area, which are far away from the end user. The power loss and construction cost are inevitable in the transmission. The large scale power outages have commonly caused chaos and a serious consequence on sensitive loads when happened with such as an over centralized grid structure. Therefore, an innovative concept called microgrid was proposed to develop a distributed energy structure in the utility. The microgrid system, as an autonomous subsystem integrating with the utility, consists of distributed energy resource (DER), storage devices and adjustable loads. It can maximize exploitation of the available onsite renewable energy sources, such as wind and solar, to provide a reliable, consistent power supply for local users.

The integration of wind turbines, solar photovoltaic (PV) and other intermittent DERs into the grid poses a great challenge to the safety and stability of the system, due to uncontrollable and unexpected weather conditions. It has become a common goal for the power industry to boom the low-carbon technology and improve the energy efficiency, thus reducing carbon emission. The electricity network, thus, is forced to upgrade self-regulation ability. Demand side management (DSM) is a portfolio of measures to improve the energy system at the side of consumption. It helps effectively restrain fluctuation of power flow and alleviate the supply-demand power mismatch. Flexible loads such as heating, ventilation, air conditioning (HVAC) system, as a promising demand response resource, can be directly controlled to participate in demand-side regulation and provide power balance services in electricity grids.

This thesis is completed based on industrial-led PhD project launched by Entrust Microgrid LLP. The company has been engaged in the design of a hybrid DC/AC microgrid for properties, buildings and communities [7]. In 2017, the company developed Smart immersion heater to provide hot water for the residents with minimum energy cost and maximum photovoltaic efficiency. The schematic diagram of the system is illustrated in Figure 1.1.1. However, the key issues of generic importance to the microgrids, for example how to convert fluctuated renewable energy sources to controllable power output, how to reduce the occurrence of 'solar curtailment' and how to utilize existing controllable loads to alleviate energy storage pressure, remain to be addressed. In response to these problems, this study is dedicated to investigating the control strategy for distributed controllable loads to strengthen the balance

between renewable generations and variable load demands in microgrid system.

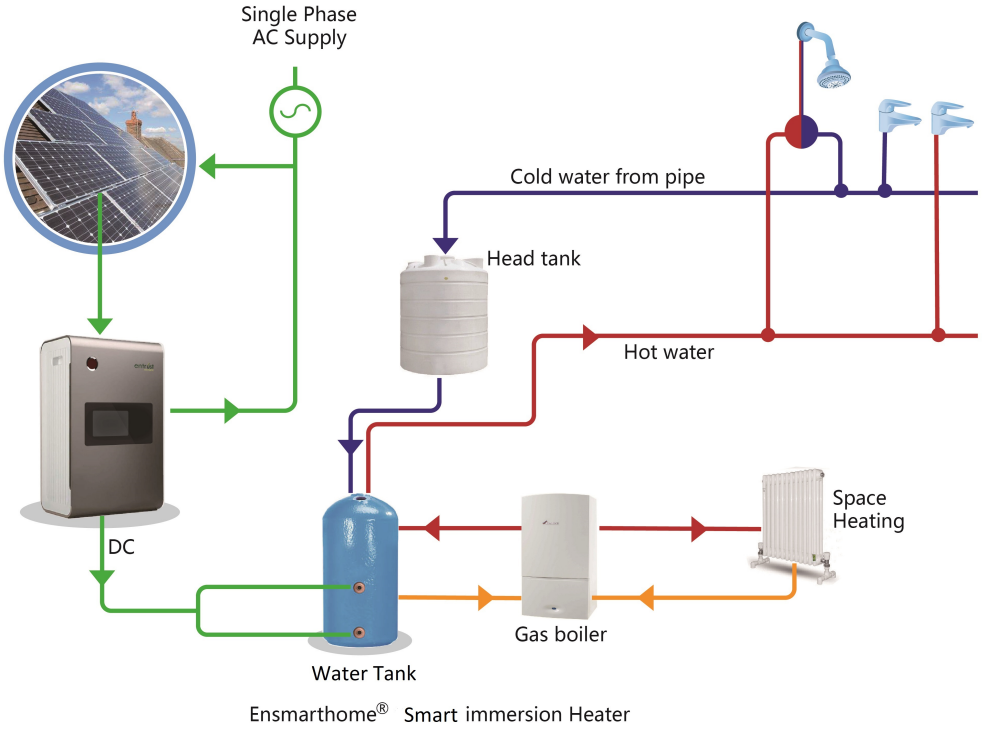

Figure 1.1.1: Schematic diagram of Smart immersion heater [1]

The thesis proposes a comprehensive framework based on a forecasting-management-optimization approach for a microgrid with the HVACs as the controllable loads. A short-term local solar radiance is forecast with a hybrid model and national weather forecast information. Based on the HVAC electrical model, a distributed control strategy is proposed to control its power consumption. A 24-hour ahead energy scheduling plan for HVAC unit is presented considering solar power forecasts. In order to evaluate the financial cost and discomfort level for the users, a price-comfort optimization model is formulated and a PID-based distributed algorithm is proposed to address

the problem. Meanwhile, the distributed algorithm can be extended to accommodate the battery energy storage system (BESS), where a hybrid system namely as HVAC-BESS is presented to improve storage capacity and enhance the flexibility of the system. The research developed in the thesis consists of following structural parts:

- A hybrid forecast model is developed to predict short-term solar radiance in a small-scale area. In order to increase the forecast accuracy of local solar irradiation, a multiple aggregation prediction algorithm with exogenous variables-principle components analysis (MAPAx-PCA) model is proposed by incorporating the information derived from weather forecast service (WFS) and the local weather historical data, where the multicollinearity problem can be avoided simultaneously [8]. The strongly-correlated weather indexes and time-series variables, such as dummy variable and lag variable, are selected to build the model. Furthermore, the hybrid model is compared with classic statistical models to show its outperformance. The obtained solar power curve is further utilized as the input signal for dynamic test of the control strategy.

- A well-designed cooperative control strategy is proposed to integrate multiple HVAC systems to minimize the global supply-demand mismatch through the demand response. The microgrid system with HVAC units is considered as a multi-agent system (MAS) with communication network and the local bus connected with HVAC is assigned as an agent. The approach provides a desirable operating frequency signal for each HVAC based on power mismatch value occurring on each local bus. The method addresses a consensus problem under a

switching communication topology by using Lyapunov argument, in comparison with the existing distributed algorithm under a fixed communication topology. It is verified that a jointly strongly connected topology is a sufficient condition in order to achieve average consensus under switching topology. Furthermore, a trend of convergence speed against feedback gain is obtained through the simulation model. The effectiveness and robustness of the algorithms against power constraints, dynamic behaviours, anti-damage characteristics, scalability and time-varying communication topology are investigated by simulation cases.

- To study the effects of comfortability and electricity cost on end users, the discomfort cost model and electricity cost model regarding the HVAC system are established. A price-comfort optimization model is formulated and a proportional-integral-derivative (PID)-based distributed algorithm is proposed to solve the convex optimization problem. The method aims to deal with the power imbalance and time-of-use (ToU) price, while minimizing the user's total cost. Case studies are conducted to investigate the algorithm under various scenarios.

- To enhance the flexibility of the microgrid, the BESS-HVAC hybrid energy storage system is investigated in DSM program and the BESS and HVAC system are modelled respectively, where the coordination scheme for HVAC system is extended to accommodate BESSs. The local bus connected to MAS participates in discovering the optimal incremental cost and local active power. The simulation studies are carried out under various conditions to validate the feasibility of the proposed solution.

1.2 Contributions of the resesarch

There are four main contributions of the thesis that can be summarized as follows:

1. A hierarchical demand side management architecture gives a forecasting-management-optimization solution based on the distributed HVACs. In response to the company's goal, it provides a system solution for next generation energy and power system for buildings and communities, for meeting the global challenge in energy security, affordability and sustainability, and battling climate change and environment pollution. The proposed system solution provides a theoretical and technical support for company's home micorgrid program. The exploitation of potential commercial value of the energy management controller can be further developed to provide local residence with financial incentive.

2. In order to achieve an intelligent energy management system, a key priority is to improve the forecasting capabilities of the power production. Time series forecasting algorithms investigated in this research give an explicit mathematical model, which is simple and feasible for hardware implementation. The proposed hybrid model can fully extract features of time-series data, which outperforms the conventional statistical methods in simulation results. Although statistical-based approach is not as good as machine learning algorithms in terms of self-learning capability, it would be a practical and low-cost solution for implementation.

3. Due to the unexpected change in the power generation, high-frequent control

update and high-speed processor is required. Thus, the proposed distributed approach takes advantage of its flexibility and scalability, which has a promising prospect in the future. On the other hand, participants in microgrid system may not be willing to release their cost function to other neighbouring agents, indicating the proposed solution could be implemented without broadcasting private information. Additionally, the distributed algorithm can be extended to accommodate BESS-HVAC hybrid energy storage system (ESS) thus increasing flexibility to provide ancillary service to users from the microgrid. It is worth highlighting that the distributed consensus algorithms presented in this thesis are, for the first time, designed to accommodate the HVAC system under switching interaction topologies to address the power mismatch in microgrid.

4. The utilization of HVAC units reduces the capacity and investment cost of ESS in the microgrid system, because the load consumption pattern can be modulated by HVACs according to total available power generation. Thus, the HVAC can be a low-cost option to construct or complement ESS. On the other hand, since the benefits of the end user may be enhanced by participating in DSM, an optimization problem is formulated where the discomfort cost and electricity cost are taken into account. Thus, a PID-based consensus algorithm is designed to achieve an optimal operation for customers.

5. A number of case studies are simulated and presented through the IEEE 14-, 30- and 57- bus systems, respectively, to investigate the feasibility and scalability of the proposed distributed algorithms.

1.3 Roadmap through this dissertation

Chapter 2 gives an overview of the microgrid system, DSM technology and current challenges. The solar power forecasting techniques and energy management algorithms are summarized and categorized in this chapter. The MAS-based distributed algorithms are discussed in the literature review. The applications of thermal controlled load (TCL) and HVAC system in the DSM are also reviewed, respectively.

Chapter 3 introduces three statistical techniques to obtain solar radiance forecasting results, by selecting highly-related time series components and weather indexes. The MAPAx-PCA model is focused with training dataset introduced. The forecasting accuracy of hybrid model is compared with benchmark models by means of performance evaluation indexes.

Chapter 4 proposes a cooperative algorithm for the distributed HVAC systems. The electrical model and physical hardware control circuit of the HVAC system are introduced. The algorithms under fixed and switching communication network based on the graph theory are presented, respectively. Furthermore, the stability proof of the algorithm under switching topology is emphatically demonstrated. The flowchart of the algorithm implementation is given accordingly. The feedback gain that has significant influence on the performance of control strategy is also investigated. Comprehensive case studies are conducted on the effectiveness of algorithm under the influence of power constraints, time-varying renewable energy, HVAC system failure, scalability test from 5-bus to IEEE 30-bus system and intermittent communication topology, respectively. Furthermore, an energy dispatch scheme is developed for

HVAC systems, based on the solar power forecasting results in Chapter 3.

Chapter 5 takes account of the comfortable cost and electricity payment of the end user, by formulating a HVAC system optimization model. A novel PID-based distributed algorithm is proposed and PID parameter tuning results are studied. A comparison study is conducted to present the advantage of the algorithm in eliminating steady-state error. The simulation models are developed to examine the feasibility of proposed algorithm to respond the dynamic ToU price, time-varying power mismatch, 24-hour solar power forecasts and the scalability on the IEEE 57-bus system.

Chapter 6 explores the cooperative control of HVAC-BESS hybrid system integrated into IEEE 14-bus system, by establishing cost function models for HVAC and BESS, respectively. Case studies are carried out to evaluate the performance of hybrid system, when the microgrid is facing power constraints, dynamic power mismatch, short-term solar power forecasts or hybrid system failures.

Chapter 7 summarizes the contributions and outcomes of the thesis. Future work that can be carried out following the findings of this work is also discussed.

1.4 Publications

Journal article:

Jie Ma, Xiandong Ma and Suzana Ilic, "HVAC-based Cooperative Algorithms for Demand Side Management in a Microgrid," *Energies*, 2019, 12(22), pp. 4276

Jie Ma and Xiandong Ma, "A review of forecasting algorithms and energy management strategies for microgrids" *System Science & Control Engineering*, 2018, 6(1), pp 237-

248

doi: 10.1080/21642583.2018.1480979

Conference paper:

Jie Ma and Xiandong Ma, "Distributed control of battery energy storage system in a microgrid", Proceedings of the 8th International Conference on Renewable Energy Research and Applications, Brasov, Romania. 2019. 11

doi: 10.1109/ICRERA47325.2019.8996504

Jie Ma and Xiandong Ma, "Consensus-based Hierarchical Demand Side Management in Microgrid", Proceeding of the 25th IEEE International Conference on Automation & Computing, Lancaster, United Kingdom, 2019. 09.

doi: 10.23919/IConAC.2019.8895118

Jie Ma and Xiandong Ma, "State-of-the-art forecasting algorithms for microgrids", Proceeding of the 23rd IEEE International Conference on Automation & Computing, Huddersfield, United Kingdom, 2017. 09.

doi: 10.23919/IConAC.2017.8082049

Chapter 2

Literature Review

Distributed energy resources (DERs), which are more scalable than the central power stations and can be locally or flexibly integrated into the power system, are gradually replacing the conventional generation and playing a vital role in future smart grid. In order to coordinate the contradiction between the large power system and DERs and fully exploit the benefit of DERs, the concept of microgrid has emerged. In this chapter, the concept of microgrid system is firstly introduced in Section 2.1, with its components, architecture and operation model introduced. Furthermore, the distribution systems of the microgrid with its applications in the test-bed are highlighted in Section 2.1.3. One of the key issues in the energy management is to obtain an accurate forecasting curve to describe the change of local weather condition. Therefore, a range of forecasting techniques applied to solar power prediction are classified and discussed in Section 2.2. More importantly, the microgrid controller is a key technique to achieve power flow management and maintain a dynamic balance between the supply side and demand side. The widely-used microgrid control system can be categorized

into centralized, decentralised and distributed controllers, which are summarized in Section 2.3, respectively. On the other hand, the energy consumption curve can be reshaped by DSM schemes and activities. The fundamentals and methods of DSM are given in the Section 2.4.1 and the utilization of TCL appliances in DSM is emphasized in Section 2.4.2. Moreover, the HVAC system with its application examples is highlighted in Section 2.4.3.

2.1 Overview of microgird system

Conventional power station mainly depends on the nonrenewable fossil fuels such as coal, oil and gas, which emits a large amount of greenhouse gases. The large-scale power outages pose huge risks for sensitive loads, when the mechanical or electrical faults occur at the over-centralized power station [9]. Moreover, the traditional, centralized electricity grid also causes losses in the transmission system.

With the integration of DERs and various loads in a electricity network, building a modern, localized, small-scale grid in a limited geographical area can maximize the usage of on-site resources and reduce the economy and energy losses during the power transmission. As an autonomous subsystem connected with the utility, the development of microgrids is beneficial for enhancing stability of the main grid, shifting the peak load demand, providing voltage support, thus creating an innovative environmentally-friendly technology [10].

2.1.1 Microgrids structure & operation mode

A microgrid system typically comprises five components: DER, distribution systems, alternating current (AC) and direct current (DC) loads, storage units and control and communication modules [11, 12]. The power supply in the microgrid mostly relies on DER devices or/and conventional power generators, such as diesel generators. The DER consists of solar PV arrays, wind turbines, small hydro, biogas and fuel cells, where the micro-turbines and fuel cell can provide combined heat and power (CHP) generation. These on-site DERs aim to maximize benefits of the local resources and minimize the electricity and financial costs caused by long-distance high-voltage transmission. The energy storage system (ESS) in the microgrid not only stores the excess power generated by DERs, but also acts as a power regulator to provide consistent power for the sensitive loads and eliminate supply-demand mismatch. The commonly-used storage devices involve flywheels, batteries and super-capacitors. Due to some DERs are operated in maximum power point tracking (MPPT) mode to maximize the power output, the employment of ESS can generate controllable power output to facilitate the matching of power generation and load demand. The control and communication modules can be realized by a centralized controller or multiple distributed controllers in cooperation with power electronic interfaces (PEIs), thus, plug-and-play functionality and power conversion can be achieved. The microgrid controller plays a vital role in automated operation and control of microgrid by generating and sending control signals to PEIs [13]. It is used for automatic state switching, reference signal assignment and state monitoring of physical devices [14].

A microgrid system normally operates in two modes: grid-connected mode and the island mode. Under the grid-connected mode, the microgrid system makes benefits from selling the excessive electricity to the utility, when the on-site power generation is over the local demand. Otherwise, it is required to purchase supplementary electricity from the main grid. If the power quality from the utility exceeds a threshold level, the microgrids should be seamlessly switched to island mode, for the sake of maintaining stability and avoiding the disturbance of the utility failure [9].

2.1.2 Distribution systems

The distribution system represents a common bus to interconnect all physical devices. The microgrid system is generally classified into AC microgrid and DC microgrid, depending on the type of distribution system. The configuration in the AC and DC distribution network with the application of microgrid system is extensively reviewed in [15]. Figure 2.1.1 gives a typical microgrid architecture with AC-line configuration, where all of the non-AC micro-generators and loads are converted to 50 Hz AC grid with the power converter. The microgrid is connected the main grid via the point of common coupling (PCC), which is located on the primary side of the step-up main transformer. It is worth noting that the impact of considerable power loss and harmonic voltage in the power conversion are non-negligible. In reference [16], three separate regulators: voltage, active power and reactive power regulator are developed in AC microgrid. The global voltage regulation and proportional reactive load sharing can be handled. Furthermore, the existing microgrid testbeds are mainly implemented on the AC grid, such as consortium for electric reliability technology so-

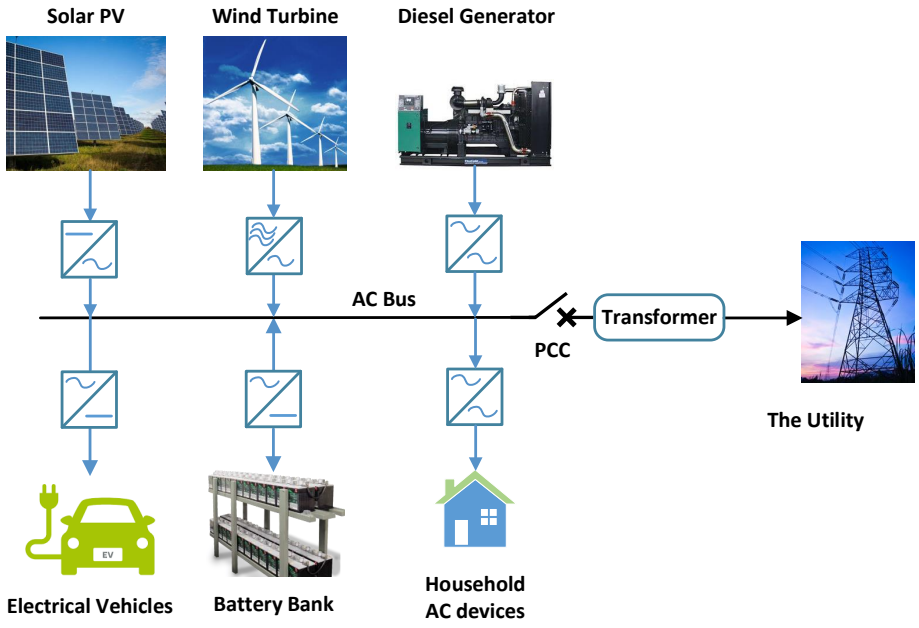

Figure 2.1.1: Vision of microgrid in AC-link configuation.

lutions(CERTS) testbed in America and microgrid project in Europe. CERTS testbed is a leading practical project launched by American Electrical Power, aiming at implementing the seamless transition between grid-connected and island operation in terms of reconnected and resynchronized process and maintaining the stability of voltage and frequency in microgrids when working on island condition. The testbed consists of three feeders for sensitive loads and a feeder for non-sensitive loads. In each sensitive feeder, sub-controller, breaker and more than one DER device are set to ensure a consistent power supply for sensitive loads, where the sub-controller is introduced to realize 'plug-and-play' and 'peer-to-peer' functionality [13, 17, 18]. Standing on the history perspectives, AC power network has become the main choice for commercial power system, as it is easy to transform AC voltage into multiple levels to accommodate various applications with the capability to transmit power over a long distance.

AC power network has existed more than a century along with AC loads dominated the entire market.

Meanwhile, the development of the DC-microgrid system has attracted researchers' attentions in recent years, with the booming of DC loads, batteries and DC distributed generators [19, 20]. It is expected that DC distribution network will become an alternative way to partly replace the AC bus to supply all electricity equipments in the future[15]. Presently, most of household appliance (computer, variable speed drives, lights), business and industrial appliance are fundamentally powered by DC voltage. In the existing AC grid system, DC-based generator is required to complete DC-AC-DC power conversion, in order to supply power to DC loads in customer side. It causes substantial energy loss and financial cost. The DC distribution network is a new technique to tackle the problems in AC distribution system and point the way for future power network. It ensures a higher power quality for the customer and facilitate the installation of more distributed generator units [21].

2.2 Renewable power forecasting

The wind turbine and solar PV are typical DERs in microgrid system. The wind and solar energy are weather-related resources, where their variability ranges from minutely/hourly to yearly. In order to alleviate the power fluctuation with energy management approach, it is vital to provide forecasting results of renewable power generation for the grid operator. Thus, a number of methodologies have been developed and combined to predict wind speed or/and wind power on varied forecast scale,

such as [22–27]. Since this research pays a attention the home/community microgrid system, the prediction of solar energy and solar power is the research focus. An effective control system should be capable of handling the uncertainty and fluctuation of the power generated by solar PV. In this case, solar power forecasting is a crucial precondition to ensure optimal energy scheduling. The forecasting time horizon is classified into the very short-term (from second to half an hour), short-term (half an hour to 6 hours), medium-term (6 hours–1 day), long-term (1 day–1 week), based on different energy management requirements. For instance, very short-term forecasting aims at achieving dynamic control for renewable power generators and load tracking. Short-term forecasting is used for scheduling energy flow among power sources, loads and storage devices. Medium-term and long-term forecasting are responsible for price settlement, load dispatch and maintenance scheduling, respectively.

The development of solar radiance prediction and solar power prediction has been reviewed in many literatures [28–31]. The developed forecasting tools can be classified into three approaches: physical model, statistical model and artificial intelligence model, which is shown in Figure 2.2.1. The numerical weather prediction (NWP) model is the basis of physical approach, where the variability of meteorological processes is described by atmospheric mesoscale model or global databases of meteorological measurements [28]. Since meteorological modelling is not the focus of the thesis, its literature review will not be further introduced. Statistical models mainly discuss the influence of historical data on forecast value. The frequently used statistical methods include Auto-Regression(AR), Moving Average(MA), Auto-Regression Moving Average(ARMA), Auto-Regression Integrated Moving Average(ARIMA). It is

remarkable that Box-Jenkins approach is an effective tool to identify the components and parameters in time series model. Kalman filter technique is another typical parametric model based on the historical data [32]. The artificial intelligent algorithm investigates the relationship between input variables and output variables without taking the physical process into account. It can be a single model or hybrid model. The popular single model include fuzzy logic, artificial neural network(ANN) [33], support vector machine(SVM) [34], fuzzy logic [35], multilayer perception(MLP) [36], genetic algorithm (GA), particle swarm optimization (PSO), expert systems. The hybrid system is combining one or more algorithms to pursue a higher forecasting accuracy [35, 37, 38]. The most widely accepted hybrid model is adaptive neural fuzzy inference system(ANFIS) [39].

Currently, the state-of-art in machine learning is deep learning. The improved technique can predict the outcome by perceiving the pattern from the voluminous inputs in the context related to forecasting. Various conditions such as time stamp, forecast horizon, input correlation analysis, data pre and post-processing, weather classification, network optimization, uncertainty quantification and performance evaluations have been considered [40]. The most popular deep learning models involve conventional neural network [41, 42], recurrent neural network [43].

2.2.1 Statistical techniques

The statistical approaches aim to build the relation between the past meteorological parameters and future solar radiance. [44] proposes three different ARIMA models to forecast next hour global horizontal irradiance(GHI) based on feasible meteorological

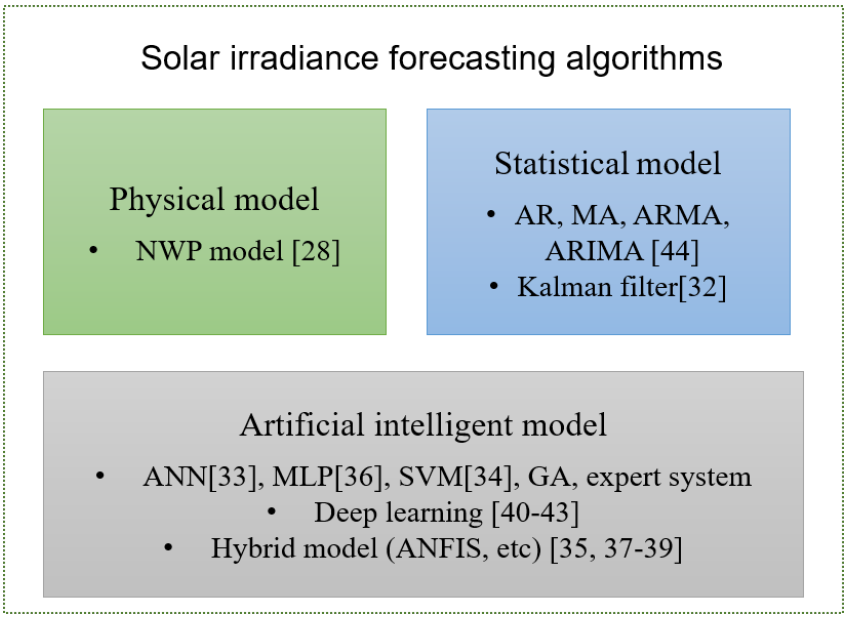

Figure 2.2.1: Overview of solar irradiation forecasting techniques

variables, such as GHI, diffuse horizontal irradiance, direct normal irradiance and cloud cover, as input parameters. It is demonstrated that the cloud cover formation improves forecast accuracy. In [45], the authors propose a novel multitime-scale data-driven model to improve the accuracy of solar PV generation forecast. The model takes advantage of both spatial and temporal correlations among neighbouring solar sites. It is pointed out the trade-off between the computation cost and forecast accuracy. However, the above model are based on historical daily average data instead of intra-day dynamic pattern. The authors in [46] develop a partial functional linear regression model with the consideration of intra-day dynamic pattern of solar power output. The forecasting results outperform that of ANN and traditional regression model. In order to capture the stochastic nature of PV power output, a nonparameteric model named as multivariate adaptive regression splines is introduced in [47], which is more effective than machines learning algorithms. On the other hand, some

literatures utilize available NWP information to forecast on-site PV power generation. Taken [48] as an example, the multilinear adaptive regression spines model is established based on the information from US Global Forecasting Services. The model is tested by power generation data of a PV plant in Borkum, Germany.

2.2.2 Intelligent algorithms

In recent 20 years, most researchers focused on developing computational algorithms in exploring a non-linear map without studying the inner physical model. Many case studies demonstrated that machine learning algorithms can simplify the forecasting process compared with other forecasting models. However, one of the challenges in nonlinear forecast model is the selection of appropriate input variables. For example, [49] selects daily sunshine duration, air temperature and global solar radiance as input variables, on the bases of one-year historical data. It is indicated that the proposed model can successfully be used for prediction, with correlation coefficient being 98.9%. Whereas, the mean daily solar radiance and air temperature are used for building a multilayer perception model in [33] to forecast the solar irradiance in 24 hours. The proposed model is identified to perform well, where the correlation coefficient is in the range 98–99% for sunny days and 94–96% for cloudy days. Following this idea, researchers do further research on developing different solar power forecasting models for different weather types. Therefore, three distinct ANN models are developed for sunny, partly cloudy and overcast weather condition [50]. A comparison study of day-ahead solar power forecasting model based on seasonal-ARIMA (SARIMA) model and ANN model is proposed in [51], where the SARIMA model incorporates solar

radiance information derived form NWP. These models are validated by PV plants dataset. It is obvious that developing the model for a specific PV plant is relatively easy than establishing a unified forecast model for PV roof of thousands of home in the entire grid. In order to overcome this challenge, the authors in [29] explore a site-specific forecast model to accommodate the diversity of sites. The model utilizes SVM-based techniques combined with the national weather service forecast results.

With the development of AI, the deep learning algorithms are applied to improve photovoltaic power forecast accuracy. In [52], the convolutional neural network (CNN), long short-term memory network and a hybrid model based on these two models are proposed. The results demonstrate that the size and characteristics of input sequence is closely related to the model accuracy and the prediction performance resulting from the hybrid model is the best. Similarly, a hybridized deep learning framework is designed in [41], which integrates the CNN for input feature extraction with the long short-term memory network for half-hourly global solar radiation forecasting. Another CNN framework is introduced in [42] based on meteorological data from surrounding sites with different sampling times. A chaotic GA/PSO hybrid algorithm is applied to optimize the hyper parameters of the novel framework. The superiority of the novel framework is fully demonstrated by comparing with CNN model. In [43], a recurrent neural network model is developed to investigate the performances of the deep learning algorithms for the solar radiation prediction, where the meteorological data from a local weather station is used for the training process and variable scenarios about different sampling frequencies and moving window algorithms are considered.

2.2.3 Hybrid models

Generally, the hybrid model developed for forecasting can be divided into two types. The first type combines statistical method and intelligent approach [53–55], while the second type combines multiple intelligent methods [56–59]. In terms of first type of model, [60] focuses on integrating ANN into statistical feature parameters (ANN-SFP) to predict solar irradiance. The ANN-SFP model performs well in a cloudy day compared with conventional models. In [61], an improved forecasting model is developed to enhance the prediction accuracy under the extremely weather condition, where the aerosol index is regarded as a key component to indicate solar radiation attenuation. The authors in [62] present a hybrid technique consisting of SARIMA and SVM. The forecast accuracy shows its outperformance than either of them. In second type of models, a hybrid model incorporating fuzzy logic and neural network is proposed in [63], where the temperature, sky information and solar irradiance level are grouped under the fuzzification process. The accuracy of hybrid model is compared with single intelligent algorithms. Apparently, the hybrid model with more complex model gives a better forecasting performance than single technique. However, our aim is to implement the forecasting algorithm within an embedded system, which is easy to install in the customer side. A highly integrated energy management controller would be relatively easily accepted by the market. Apparently, AI methods and hybrid models are not feasible for hardware implementation due to the limitation of computation speed and storage capacity. Standing on the practical point of view, the statistical method is an appropriate solution in this research.

2.3 Energy management algorithm in microgrid

The operation and control of microgrid is different from the conventional electricity network, since the components in PEIs are with the properties of small inertia and fast response. The operation of the system is required to achieve the optimal unit commitment (UC), the stability of voltage and frequency, the power balance among DERs, storage devices and variable loads. Therefore, the energy distribution in the microgrid is a comprehensive multi-objectives problem, including load sharing, voltage and frequency regulation and power quality monitoring [64]. There are three mainstream solutions proposed to effectively address these issues, namely centralized controllers, decentralized schemes and distributed control strategies, which are reviewed in this section.

2.3.1 Centralized/Decentralized algorithms

The centralized energy management system is calculating and assigning direct commands to each DER and monitoring the operation state of microgrid system to achieve optimal resources management. The technique is based on power generation and load consumption, without exploring physical models of DER and various loads. In [65], authors employ an online approach called rolling horizon strategy to schedule energy storage and solve UC issues by using mixed integer programming optimization. The result shows that the operation cost is minimized by proposed UC rolling horizon method compared with offline UC approach. The authors in [64] design a central controller, which is composed of multi-stage economic load dispatch(ELD) block,

generation/load forecasting block and UC block. UC block is responsible for deciding the ON-OFF state of dispatchable DERs and condition monitoring of microgrid units. Multi-stage ELD block designs and implements energy dispatch plan for DER by considering the power forecasting results obtained by generation/load forecasting block. On the other hand, the energy management problem can be formulated as a multi-objective problem, where the multi-objective intelligent energy management (MIEM) algorithm is presented in [66]. The MIEM combines multi-objective (MO) linear programming and fuzzy logic-based expert system. The MO optimization is used for generating power reference signal and expert system is responsible for battery scheduling. The financial cost, the environmental impact and network operation conditions are considered in MO optimization model. Another congeneric model described in [67] aims at minimizing financial cost and maintaining the temperature at a lower cost, with the consideration of the real-time pricing and properties of appliance. Meanwhile, these researches have not considered the presence of energy uncertainties, In [68], the authors discuss the impact of wind power uncertainties, operating cost and voltage stability by formulating a multi-objective stochastic optimal power flow problem, in order to reduce the risk of voltage instability and forecast the voltage collapse point.

However, the biggest problem for centralized control scheme is over-dependent on a single control system, which may cause huge risks when the controller breaks down. On the other hand, a wider communication bandwidth is required to achieve bidirectional communication between the controller and each microgrid component. The uncertainty due to time delays in the communication process might be inevitable,

thus, the measurement and control signal may be not accurate enough or get lost in the communication channel [69]. Moreover, the sampling rates of measurement or control signal should be as fast as possible, while the memory and computation of the central controller are limited. In the case of a central controller in a bulk power system, the research and development costs is increased, while the stability of system will be unavoidably defective.

The decentralized scheme is designed to address problems in centralized controller [70]. This technique is capable of tolerating the communication failure and has a better plug-and-play ability, which facilitate the system scalability [71]. Nevertheless, there are still some inevitable drawbacks that have not been solved in the published research. For example, in practical applications [72], the synchronization signals must be provided to all DER units, which deteriorates the robustness of the system. On the other hand, the voltage frequency is a global signal in the microgrid system [71]. If local controllers regulate the grid frequency simultaneously, the system stability would be destroyed. Therefore, the coordination of local controllers is big challenging problem for decentralized controller.

2.3.2 MAS-based distributed algorithms

Recently, multiagent system (MAS) is widely used in microgrid control technique. The main idea of the MAS is dividing a complex large-scale system into multiple subsystems. Each subsystem possess the features of autonomy, coordination and communication with each other. Each agent has characteristic of intelligence and perception, which means they are able to respond to changes in the environment. The

communication protocol is feasible for each agents and it has ability to coordinate agents in compliant mode. Therefore, instead of utilizing bi-direction communication channel, the command information can cover the entire network under a certain communication topology, which outperforms the conventional centralized control scheme. Integration of graph theory and consensus control is a promising approach to solve cooperative control problem in the various fields. Specifically, the topology model is built on the communication network in the MAS. Consensus protocol is a unified state updating rule for all agents in the complex system, based on the information communication between the agent and their neighbours. All agents in MAS achieving consensus is the objective of cooperative control. A variety of MAS-based consensus control schemes are systematically reviewed in [73]. One of the key problems in MAS is how to realize the communication link in an efficient and effective way. Ethernet, worldwide interoperability for microwave access(WiMAX) and wireless fidelity (WiFi) are good options for communication. The MAS concept has wide applications in the area of unmanned aerial vehicles, unmanned ground vehicles and unmanned underwater vehicles.

Recently, the massive applications of the MAS in microgrid system have been presented in [74–76]. Figure 2.3.1 gives a typical MAS-based energy management system in a microgrid, where various agents are included, such as renewable generation agents (RGA), responsive load agents (RLA), energy market agent (EMA) and energy storage agent (ESA). Among these agents, RGA, RLA and ESA collect the data from DER and customers and ESS, respectively. EMA is responsible for electricity price regulation [2]. It is remarkable that the grid frequency is an significant signal

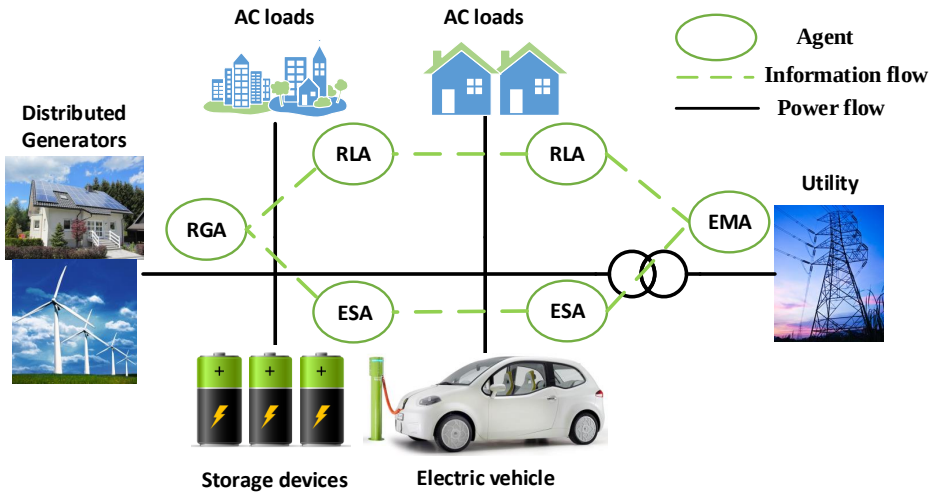

Figure 2.3.1: Multi-agent based distributed energy management system for microgrid [2]

to be managed in energy dispatch problem. The integration of decentralised MAS methods and frequency control strategy would be an effective way to achieve frequency recovery through primary and frequency control and multi-stage load shedding [77]. To overcome the power imbalance in the microgrid, reference [78] develops a fully distributed control scheme to discover the references for DERs, energy storages and loads.

Neither AC microgrid nor DC microgrid is easy to stabilize the bus voltage, frequency and power under dynamic weather condition and load demand [19]. Thus, the BESS plays a vital role in supporting bus voltage and frequency and maintaining power balance. Under a BESS-based MAS framework, each storage device is considered as an agent having access to its neighbouring agent under a communication topology to share the power mismatch in a cooperative way. In terms of heteroge-

neous BESSs, a consensus-based strategy is presented in [79] to achieve energy level balancing, active/reactive power sharing and voltage/frequency synchronization in microgrid system. As for homogeneous battery agents, a cooperative distributed control scheme demonstrated in [78] is applied to reduce the global power mismatch and maximize the energy efficiency of the batteries, whilst the robustness and plug-and-play capability of the algorithm are considered. However, the above literatures fail to include the impact of energy uncertainties. Thus, the consensus model in [6] focuses on the wind power uncertainties and protection of agent's privacy. Similarly, in [80], a dynamically updated energy management schedule is presented by using the demand response of batteries and controllable loads to overcome the forecast errors and system uncertainties. On the other hand, it is inevitably to concern the transient responses of BESSs. In [81], an adaptive droop control is proposed for balancing the SoC (state of charge) of distributed BESSs. Regarding the DC microgrid system, a MAS-based cooperative control strategy is presented in [82] to configure a hybrid ESS, consisting of ultracapacitors and batteries, to achieve power-sharing under different conditions.

2.4 Demand side management

2.4.1 The fundamental of DSM

DSM aims to plan, implement and monitor the utility activities that are developed to influence the consumer use of electricity. The load profile is modified in time horizon and magnitude scale by the DSM programs. The objective of DSM is to motivate

the customer to use less electricity during the peak time or shift energy demand to off-peak hours to flatten the load curve, or even to follow the generation pattern to purse a desired outcome. There are various DSM techniques and six generic load management programs, including peak clipping, valley filling, load shifting, strategic conservation, strategic load growth and flexible load shaping [83].

Architecture and components of DSM

The architecture of DSM is composed of customer domain and smart grid domain. Customer domain is a home-based subsystem including local generator, smart devices, sensors, energy storage systems and energy management unit(EMU). Specifically, EMU can be a centralized controller to connect other components via home area networks (HANs). By constructing an interaction network among these components, the residential user can manage the electric resources, monitor and control appliances through an intelligent DSM mechanism. The functionality of smart grid domain involves distribution system, grid operator, energy market and service provider. In addition to home network, the smart grid domain has interaction with the customer domain by connecting EMU via wide area network (WAN) [3, 84]. A typical DSM framework is shown in Figure 2.4.1.

Classification of DSM

A number of DSM techniques can be found in the existing literatures, which can be categorized depending on the time horizon, impact of applied measures on the customer process and optimization methods.

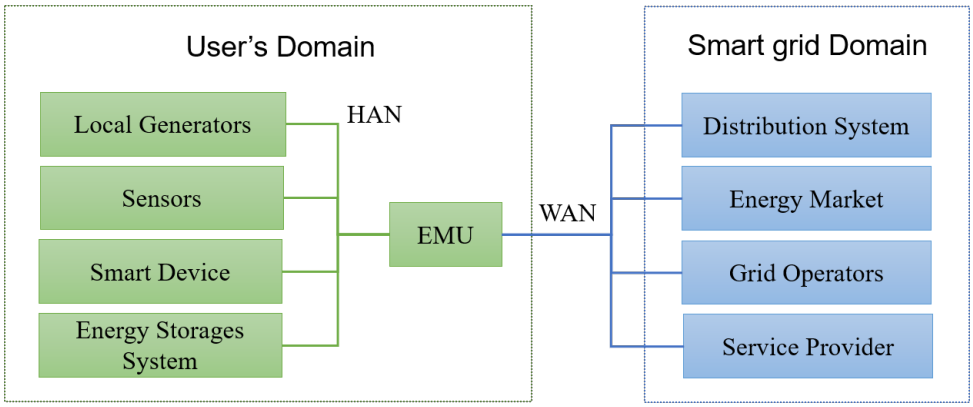

Figure 2.4.1: Architecture of DSM framework [3]

Based on the timing and impact of applied measures on the customer process, DSM methods can be categorized into three sub-categories. The first method is energy efficiency, which includes all permanent changes on equipments or improvement on the physical properties of the system. Such measures aim at eternal energy and emission savings and can be the most popular methods. ToU price can be another effective measure for DSM. It goes up on certain period when the demand is high, so that the customer are forced to rearrange their behaviour to minimize the electricity bill. Demand response aims to motivate end-users respond to changes in price or available electricity by changing their normal behaviour of electricity use. It can only influence the demand pattern, instead of curtailing load consumption. There are two types of demand response, namely market demand response and physical demand response. Market demand response includes real-time pricing, price signals and incentives, which mainly depends on the transaction in the energy market. Real-time pricing reflects the real time figures of an energy spot market without delay. In fact, the limited customer elasticity and physical situation that cannot be mapped onto prices result in the load

shedding in the grid that fails to be done by price alone. Physical demand response is responsible for sending out emergency signal when the grid and its infrastructure fail to operate in a normal performance due to the failure or maintenance. Therefore, a good mixture of the both is necessary to make an operational scheme [85, 86].

The optimization approaches in DSM can be classified based on two characteristics, which are summarized in Figure 2.4.2. Firstly, the DSM system can be designed to obtain the optimal resource allocation through either individual customers or a cluster of cooperative customers. Maximum benefits of individual user can be achieved by the means of independent management. In this case, the global cost and objectives for the utility will be neglected. If the end users can collaborate together to rearrange their operation plan, the performance of the grid can be facilitated. Mathematically, it ensures the participants in the grid are operating in a global optimum through an effective DSM methods. Also, the DSM system can be classified by different time scales to manage the resources of customers, such as day-ahead and real time. In the day-ahead stage, the energy dispatch scheme for electrical resource of end user is determined in the next 24-hours time period. DSM mechanism requires predictions/estimation of electricity information obtained from the network, such as the energy supply of local source, electricity price and appliances usage preference for the next day. The data from sensors, smart meters or other resources will be used for training the forecast model which is executed in EMU. In the real-time stage, the device usage preference can be altered according to real-time event and data. Typically, the real-time DSM are based on stochastic techniques, since the model is designed to cope with uncertainties in dataset [3].

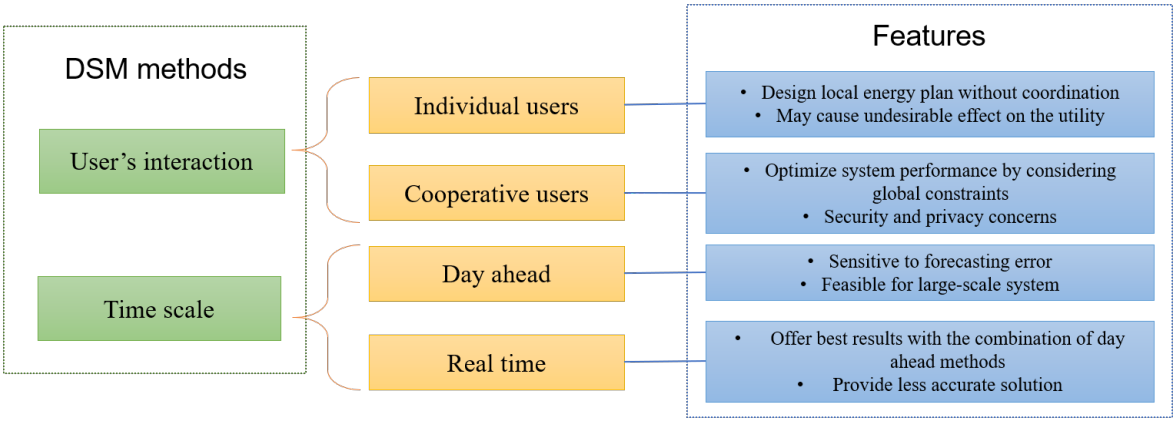

Figure 2.4.2: Various DSM methods and features [3]

2.4.2 Demand response of thermal controlled load

To accomplish load shaping, deferrable load is a necessary source for demand response program. The deferrable appliances can be divided into thermal loads and shiftable static loads (SSL) [87]. The SSL implies that the device runs at a set period of time and consumes a certain amount of energy, while thermal loads are more dependent on the usage and environment temperature. It is expected that by strengthening DSM technologies, the electricity usage for heating in UK can be reduced significantly with the energy efficiency being maximized. One of the way of maximizing efficiency is by introducing thermal controlled load (TCL), as a potential supplier to enhance system elasticity. TCL includes electrical heaters, HVACs and refrigerators, which is capable of modulating short-term power consumption profile to alleviate the pressure on the utility at peak time. For example, a second-order thermal parameter model is utilized to define a typical cooling/heating system, while a distinctive control strategy is employed to provide an ancillary service to ensure power balance [88, 89]. Furthermore, a stochastic control strategy under decentralized framework is proposed in [90],

with the aim of modulating the profile of heterogeneous appliances. Clearly, a large number of heterogeneous TCLs can be unified as an aggregated model for centralized control. There are two significant variables in aggregated TCL model, such as binary state variable (ON/OFF) and time-varying environment variable (temperature). A population model for aggregated heterogeneous TCLs is developed by [91], where a distributed model predictive control (MPC) scheme is proposed to manage a population of TCLs for grid regulation service. As for homogeneous loads, a hierarchical DSM framework is proposed in [92] to regulate the primary frequency with aggregated HVAC units. However, the published study fails to address power imbalance problem in the microgrid system with the use of TCLs.

2.4.3 The application of HVAC in DSM

The HVAC system in homes and buildings shows a particular advantage in demand response, which reshapes the load consumptions in response to grid emergencies or high-price signal [93]. Presently, the HVAC system in the market can be divided into fixed frequency air conditioner and inverter air conditioner, based on the compressor driving mode. The fixed frequency HVACs only operates in ON/OFF model with constant power output, which are mostly denoted by aggregated TCL model. However, the authors in [94] propose a novel bilinear partial differential equation (PDE) model to build distributed air conditioners. Clearly, the HVAC system has become a popular research topic in published papers. For example, a ON/OFF scheduling scheme is developed for air conditioners and other household electrical appliances by applying learning-based MPC approach to maintain desired room temperature [95].

Other research [92] focuses on solving primary frequency regulation problem. A complex control system is designed to manage a population of HVAC loads, where the trigger frequency and ON/OFF command are calculated and sent to each HVAC unit. An aggregated model investigated in [96] is to describe the dynamic behaviour of a large population of responsive loads, in order to achieve frequency regulation and peak load reduction without sacrificing user's comfort level.

The fixed frequency air conditioner has limitation on improving the flexibility of the utility. Instead, the inverter air conditioner has been developed to operate in a wide power range, which is appropriate to participate in demand response program. It has won remarkable market share, due to the high energy efficiency. In [97], the authors design a comprehensive model involving the room thermal model and inverter air conditioner model. A MPC strategy integrated into the model is utilized to adjust the operating frequency of inverter air conditioner, whilst various external conditions, such as weather conditions, occupancy and time-varying electricity prices, are taken into account. A generalised piecewise model is proposed in [98] to evaluate comfort level regarding HVAC systems, plug-in electric vehicles and electric water heaters. Additionally, the operating cost model of the HVAC system can be normalized to fit the scale of comfort level, which implies a trade-off between the comfort level and operating cost. In [99], a novel model-based DSM strategy is presented for inverter air conditioners, in response to day-ahead ToU prices. The GA approach is employed to schedule the indoor air temperature set-point, in order to balance the relationship among the electricity bills, thermal comfortability and peak load reduction. Furthermore, how to maintain comfort level while meeting the needs of the grid become a

new challenge. Authors in [100] propose a control system based on consensus theory and inverter air conditioner group to compensate the total net power mismatch with a fair scheme, while the distinct comfort level of different users can be satisfied.

2.5 Summary and discussion

In this chapter, the introduction of microgid system with its challenges and key issues is given. The energy forecasting is a prerequisite for an energy dispatch scheme. Therefore, a variety of solar power forecasting algorithms are reviewed and summarized. The key issue in the microgrid is to maintain the system stability under the high penetration of DERs, while strengthening the utilization of distributed resources. A survey of intelligent energy management methods is presented, where pros and cons are introduced. Due to the diversity of load demand, a number of DSM strategies are introduced to help grid operator reshape the load profile, through which the ancillary service can be provided and total cost of end users can be minimized. The DSM methods on TCL appliance are briefed and the applications of HVAC are emphasized.

Based on the comprehensive understanding about challenges and gaps in a microgrid system, a hierarchical energy management architecture is proposed in Figure 2.5.1, taken the 5-bus system as an example [101]. The architecture is composed of the data acquisition, renewable energy forecasting and energy management technique, where these functions are realized through external layer, prediction layer and operational layer, respectively. The external layer is designed for data acquisition and data storage in data centre, including to extract the information from a nearby

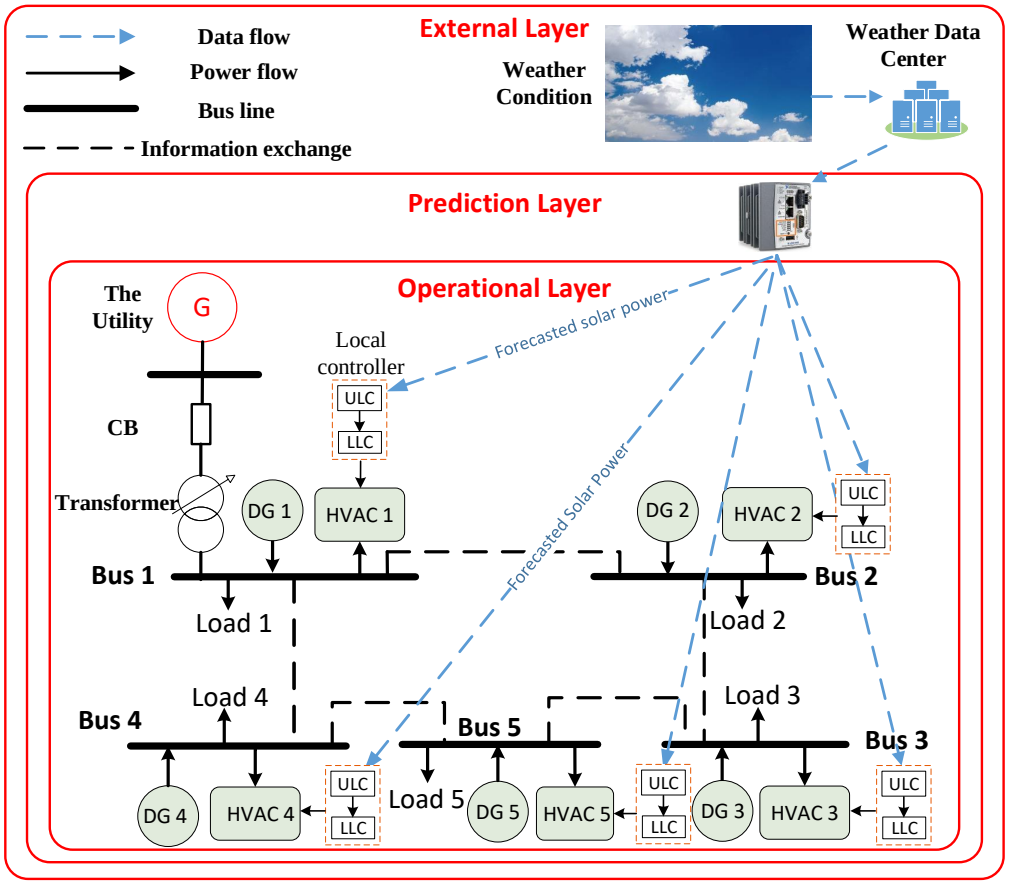

Figure 2.5.1: A hierarchical energy management architecture

weather forecast spot and acquire local weather observation historical dataset. As for the prediction layer, a proper forecast algorithm is utilized for analysing the data given by the external layer to predict local weather condition. The algorithm is implemented by an embedded controller to receive weather information, calculate solar power generation in a day ahead and send results to local controller of each HVAC. In the operational layer, each bus line can be considered as an individual agent and the bus system is regarded as a MAS framework. In Figure 2.5.1, the thin black solid lines signify the information exchange between neighbouring agents, where the

communication topology is formed. It is different from the power connection, which is described by black lines with arrow. The blue dash line with arrow represent solar power forecast issued by prediction layer. A well-designed energy management algorithm or/and an optimization method can be implemented in the local controller of HVAC systems based on the estimated solar power generation. A detailed discussions on each layer in proposed framework are given in Chapter 3, 4, 5 and 6 respectively.

Chapter 3

Solar power forecasting model

This chapter investigates energy forecasting technologies based on the weather forecast service (WFS) information and historical weather data to predict weather conditions in a small scale area. The most significant weather factors (such as: temperature) and time series factors (such as: level and trend) are selected to build solar radiance forecasting model. Multiple linear regression (MLR) models [47, 48] and autoregressive integrated moving average with exogenous variable (ARIMAX) models [102], as widely-used statistic techniques, are utilized as benchmarks to solve time-series forecasting problem. Meanwhile, a hybrid multiple aggregation prediction algorithm with exogenous variables -principal components analysis (MAPAx-PCA) models is presented to capture more information in different temporal aggregation levels [8]. The results show that the hybrid model outperforms the benchmark models, which are assessed by performance evaluation indexes in terms of model accuracy. Furthermore, a day-ahead solar power generation for a PV array is estimated correspondingly by taking advantage of its output characteristics.

3.1 Data acquisition

Met Office is a national WFS in the UK, which makes meteorological predictions across all time scales from weather forecasts to climate change. Met Office Data Point provides a free service to access available Met Office data for scientific research. It includes forecasts for approximately 5000 sites and observations for approximately 140 sites across the UK. The website provides weather forecast for the next five days updated every 3 hours, whilst the data is updated in real time, as shown in Figure A.0.1 in Appendix. The closest weather forecast site to Lancaster is called Walney Island, which is an island off the west coast of England, at the western end of Morecambe Bay in the Irish Sea. Quite a few weather forecast indexes are given in the Data Point, such as UV index, temperature, wind speed, weather types. The Table 3.1.1 summarizes weather forecast information in a day from the Figure A.0.1. It is worthwhile to note that the ultraviolet (UV) index specifies the strength of the sun's ultraviolet radiation, which combines effects of the position of the sun in the sky, forecast cloud cover and ozone amounts in the stratosphere. Although the solar radiance is not given directly, it can be predicted indirectly by using highly related meteorological components, such as: UV index, temperature and weather type, that are provided in Data point [103, 104]. Furthermore, information in the forecast site cannot directly represent the local weather condition, due to geographical differences. The Hazelrigg site of Lancaster University is selected as the forecasting site, where its historical observation data can be provided. The dummy variable and lag variable are used to specify the time series characteristics in dataset, where dummy variables

imply the seasonality and lag variables emphasize the impact of historical data on forecast value. A forecasting model is established by taking advantage of WFS and local observation data, in order to accurately reveal the local weather condition.

3.2 Solar irradiation forecasting model

A time series is a sequence of data points, measured typically at successive times, spaced at uniform time intervals. Time series prediction is the use of a model to predict future states based on the past states. In this section, MLR and ARIMAX, as two mainstream statistical methods, are employed to solve the time-series predication problem, which are regarded as benchmark models to compare with the advanced algorithms.

3.2.1 MLR model

In time series domain, the most obvious form is a time plot in which the data are plotted over time. A time plot reveals various features of the data, such as: level, trend, seasonality and cyclical behaviour. Therefore, by obtaining time map of historical solar radiance, features can be discomposed from time series data.

MLR attempts to model the relationship between time-series components with the forecasting variable by fitting a linear equation to observed data. The local solar radiance observation data y_t and $t = 1, 2, ..n$ sampled at a certain frequency. UV index, temperature and weather type in the WFS are used as input variables $x_{j,t}, j = 1, 2, 3$, in the forecasting model. Considering the data update frequency in the WFS,

Table 3.1.1: A summary of weather index in Metoffice Data point

Date	**2017-04-01**							
Time	**00**	**03**	**06**	**09**	**12**	**15**	**18**	**21**
Max UV index [1]	0	0	1	1	3	2	1	0
Weather Type [1]	12	12	12	15	12	7	3	0
Temperature (°C)	10	9	9	9	10	10	9	8
Wind Speed (mph)	4	4	2	7	9	11	11	13
Wind Direction	SE	SSW	E	ENE	WNW	WNW	WNW	NW
Relative Humidity (%)	91	97	97	92	92	86	87	89
Precipitation Probability (%)	78	57	85	81	53	8	6	0
Feel Like Temperature (°C)	7	9	9	8	8	8	6	5

[1] The code definition refers to website: https://www.metoffice.gov.uk/services/data/datapoint/code-definitions

the local solar radiance can be predicted every 3 hours accordingly. The mathematical model regarding solar radiance prediction $\hat{y}_t$ is shown as below:

$$\hat{y}_t = \alpha_0 + \sum_{i=1}^{8} \beta_i \mathcal{D}_i + \sum_{j=1}^{3} \gamma_j x_{j,t} + \sum_{k=1,2,8} \delta_k y_{t-k} \tag{3.2.1}$$

where β_i, γ_j, δ_k are coefficients of different regressors, α_0 is an estimation of true level. Dummy variable $\mathcal{D}_i$ is introduced to describe 3-hourly seasonality. y_{t-1}, y_{t-2}, y_{t-8} represent the lag variables (lagged approximately by 3, 6 and 24 hours, respectively) to analyse the effects of historical data on forecast value $\hat{y}_t$.

3.2.2 ARIMAX model

The autoregressive moving average (ARMA) model is one of the most popular time series forecasting methods. It is composed of autoregressive (AR) part and moving average (MA) parts. AR explains that the forecast variable is regressed on its own lag values. MA term indicates the regression error is a linear combination of error terms whose value occurs at various times in the past. ARMA models are very flexible due to their benefits in representing different types of times series with different orders. Note that ARMA model is only available for stationary series. ARIMA technique is proposed to address this problem by using I (integration) part to differentiate the data at appropriate time, so that it is suitable for non-stationary series. The model is indicated as ARIMA(p, σ, q), where the non-negative parameters p,σ and q are the order of AR, I and MA models, respectively. Because the input variables are combined in the ARIMA model, ARIMA with exogenous variable (ARIMAX) model transforms ARIMA into a multiple regression model. It is suitable to analyse additional variables

that have direct effects on the predicted values. The mathematical model can be written as [102]:

$$(1 - \sum_{i=1}^{p} \varphi_i \mathrm{L}^i)(1 - \mathrm{L})^{\sigma} y_t = \sum_{j=1}^{n} \gamma_j' x_{j,t} + (1 + \sum_{i=1}^{q} \psi_i \mathrm{L}^i) e_t \tag{3.2.2}$$

where L is the lag operator, for example, $\mathrm{L}^i y_t = y_{t-i}$ and $\mathrm{L}^i e_t = e_{t-i}$. φ_i and ψ_i are parameters of AR and MA of model, respectively and e_t is error terms. γ_i' is the coefficients of exogenous variables. Generally, ARIMAX model can be estimated with Box-Jenkins approach, where a range of candidate models can be evaluated by akaike information criterion (AIC), in order to investigate the optimal order and parameters in the model.

3.2.3 MAPA model

The model selection and parameter identification are the keys of forecasting, as they are tried to achieve accurate and reliable prediction. Multiple aggregation prediction algorithm (MAPA) is proposed to mitigate the importance of model selection, while improving forecasting accuracy. It plays a vital role in strengthening different characteristics in a time series by transforming the original data to different time frequencies. A time series can be aggregated into multiple low frequency series, i.e., a daily time series become weekly, monthly, quarterly and so on. Different features of time series at each aggregation level are highlighted or attenuated. As for high frequency time series(low aggregation level), periodic components (i.e. seasonality) will be strengthened. With the increase of aggregation level, the high frequency feature such as seasonality and outlier components can be filtered out, while the low frequency

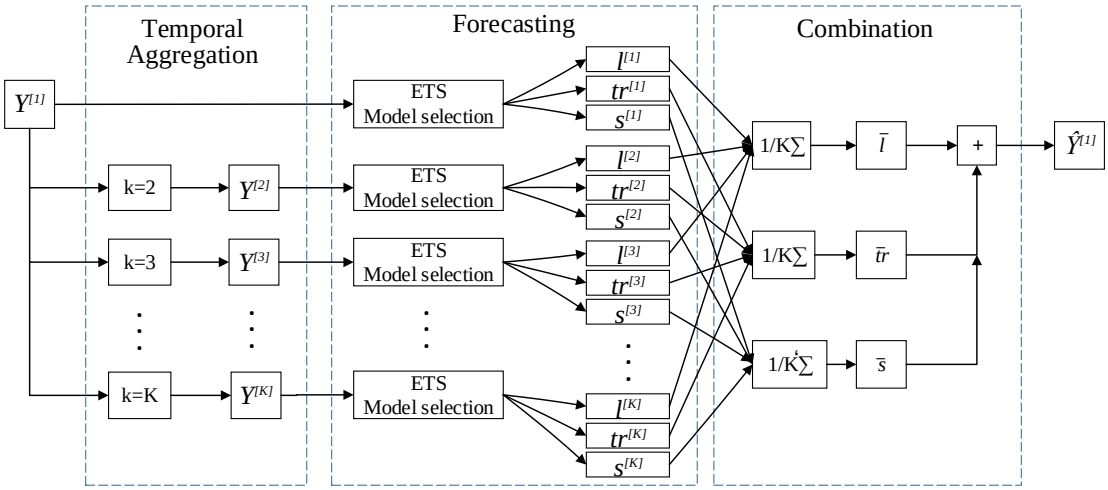

Figure 3.2.1: Flowchart of the multiple aggregation prediction algorithm (MAPA) [4]

component such as level and trend of time series will be prominent. Intuitively, it is expected to capture the seasonal elements of a time series better at low aggregation levels. Conversely, the level and trend are highlighted at high aggregation levels.

Intuitively, the framework of MAPA algorithm consists of three steps: temporal aggregation, forecasting and combination, as shown in Figure 3.2.1 [8]. In the temporal aggregation stage, Let Y be time series with the observation units y_t and $t = 1, 2, ..., n$ sampled at a certain frequency. This time series is aggregated into multiple reconstructed series by means of length k and the temporal aggregated time series is defined as $Y^{[k]}$ with the observation units y_i^k and $i = 1, 2, ..., n/k$, $k = 1, 2, ..., K$, such that:

$$y_i^{[k]} = k^{-1} \sum_{t=1+(i-1)k}^{ik} y_t \tag{3.2.3}$$

Clearly, for $k = 1$, $y_i^{[1]} = y_t$. The aggregated time series $y^{[k]}$ has n/k observations. If the reminder of n/k is not zero for a specific aggregation level k, $n-[n/k]$ observations

from the beginning or end of original time series can be removed, in order to form a complete temporal aggregation group. Practically, the number of observation units should satisfy $n >> k$ in order to leave adequate samples for temporal aggregation.

Although, theoretically, MAPA can use any forecasting methods at each aggregation level, exponential smoothing (ETS) model is appropriate, as it splits a time series into level (l_i), trend (tr_i) and seasonal (s_i) components during modelling [4]. These components are smoothed and the level of smoothing is controlled by the smoothing parameters of ETS. The smoothed components are combined to give a forecast. With the consideration of the nature for each time series, these may interact in an additive or multiplicative way. Note that the trend can be linear or damped by parameter ϕ. Furthermore, the error correction form of ETS model cannot be neglected, where the additive/multiplicative error correction form for ETS model can be referred to [5]. To identify a proper form of ETS for each time series and temporal aggregation level, AIC is used for ETS modelling. It is worthwhile to mention that MAPA is interested in the last state of ETS, in order to produce forecasts for desired horizon. However, the additive and multiplicative components are not comparable in the same scale. For example, an additive ETS can fit one of the aggregation levels and multiplicative fit another one. To overcome these difficulties, Table 3.2.1 is given to transform multiplicative components into additive components and give components prediction for h step ahead forecasting. The following notations are used: **N** for none, **Md** for multiplicative damped, **M** for multiplicative, **Ad** for additive damped and **A** for additive. In the last step, a combination methods is proposed to combine time series components across all aggregation levels. Two combination scheme, namely

Table 3.2.1: Component prediction in the additive formulation [5]

Trend	**Seasonal**		
	N	**A**	**M**
N	$l_{i+h} = l_i$	$l_{i+h} = l_i$	$l_{i+h} = l_i$
		$s_{i-m+h} = s_{i-m+h}$	$s_{i-m+h} = (s_{i-m+h} - 1)l_{i+h}$
A	$l_{i+h} = l_i$	$l_{i+h} = l_i$	$l_{i+h} = l_i$
	$tr_{i+h} = htr_i$	$tr_{i+h} = htr_i$	$tr_{i+h} = htr_i$
		$s_{i-m+h} = s_{i-m+h}$	$s_{i-m+h} = (s_{i-m+h} - 1)(l_{i+h} + tr_{i+h})$
Ad	$l_{i+h} = l_i$	$l_{i+h} = l_i$	$l_{i+h} = l_i$
	$tr_{i+h} = \sum_{j=1}^{h} \phi^j tr_i$	$tr_{i+h} = \sum_{j=1}^{h} \phi^j tr_i$	$tr_{i+h} = \sum_{j=1}^{h} \phi^j tr_i$
		$s_{i-m+h} = s_{i-m+h}$	$s_{i-m+h} = (s_{i-m+h} - 1)(l_{i+h} + tr_{i+h})$
M	$l_{i+h} = l_i$	$l_{i+h} = l_i$	$l_{i+h} = l_i$
	$tr_{i+h} = (tr_i^h - 1)l_{i+h}$	$tr_{i+h} = (tr_i^h - 1)l_{i+h}$	$tr_{i+h} = (tr_i^h - 1)l_{i+h}$
		$s_{i-m+h} = s_{i-m+h}$	$s_{i-m+h} = s_{i-m+h}$
Md	$l_{i+h} = l_i$	$l_{i+h} = l_i$	$l_{i+h} = l_i$
	$tr_{i+h} = (b_i^{\sum_{j=1}^{h}} - 1)l_{i+h}$	$tr_{i+h} = (b_i^{\sum_{j=1}^{h}} - 1)l_{i+h}$	$tr_{i+h} = (b_i^{\sum_{j=1}^{h}} - 1)l_{i+h}$
		$s_{i-m+h} = s_{i-m+h}$	$s_{i-m+h} = (s_{i-m+h} - 1)(l_{i+h} + tr_{i+h})$

unweighted mean and median, are identified to perform similarly. Each component is calculated as [4, 5]:

$$\bar{l}_{t+h} = K^{-1} \sum_{k=1}^{K} l_{t+h}^{[k]} \tag{3.2.4}$$

$$\overline{tr}_{t+h} = K^{-1} \sum_{k=1}^{K} tr_{t+h}^{[k]} \tag{3.2.5}$$

$$\overline{s}_{t+h} = K'^{-1} \sum_{k=1}^{K'} s_{t+h}^{[k]}, \text{ if } \frac{m}{k} \in \mathbb{Z} \text{ and } k < m \tag{3.2.6}$$

where K is the maximum aggregation level. Normally, the maximum aggregation level is equal to the period of original time series. K' specifies the number of aggregation levels where seasonality is identified. A example is given to illustrate this: suppose that a monthly sampled time series, then $K' = 1, 3, 6, 12$, which indicate the seasonality estimated and combined at monthly, quarterly, semi-annual and annual data.

In order to produce the final forecast for h steps ahead, the time series components can be added together, as they have been already predicted respectively [4].

$$\hat{y}_{t+h}^{[1]} = \bar{l}_{t+h} + \overline{tr}_{t+h} + \overline{s}_{t-m+h} \tag{3.2.7}$$

3.2.4 MAPAx-PCA model

MAPA algorithm also can be extended to include exogenous variables. The revised algorithm is named as MAPAx. Let define X_j as jth explanatory variable with the observations $x_{j,t}$ and $j = 1, ..., J$. $\xi_{j,t}$ is introduced to indicate the effect of each X_j variable at time t and w_j is weighting coefficients, where $\xi_{j,t}$ can be defined as [4]:

$$\xi_{j,t} = w_j x_{j,t} \tag{3.2.8}$$

The effect of each variable is measured separately in $\xi_{j,t}$, allowing to be incorporated into the MAPA framework. The estimation of w_j can be done by least square, maximum likelihood estimation. At each aggregation level k, $\xi_j^{[k]}$ is calculated by multiplying the estimated $w_j^{[k]}$ and $x_j^{[k]}$. At each temporal aggregation level k, a separate $\xi_{j,t}^{[k]}$ is calculated based on the estimated $w_j^{[k]}$ and temporally aggregated $X_j^{[k]}$. The resulting vector with coefficients are combined into a single effect across all aggregation levels for each variable X_j

$$\overline{\xi}_{j,t+k} = K^{-1} \sum_{k=1}^{K} \xi_{j,t+h}^{[k]} \tag{3.2.9}$$

Finally, the equation 3.2.7 used for univariate forecast can be revised to adapt to the multi exogenous variables and investigate their effect on forecasting accuracy [4].

$$\hat{y}_{t+h}^{[1]} = \overline{l}_{t+h} + \overline{tr}_{t+h} + \overline{s}_{t-m+h} + \sum_{j=1}^{J} \overline{\xi}_{j,t+h} \tag{3.2.10}$$

The structure of MAPAx algorithm is demonstrated in Figure 3.2.2.

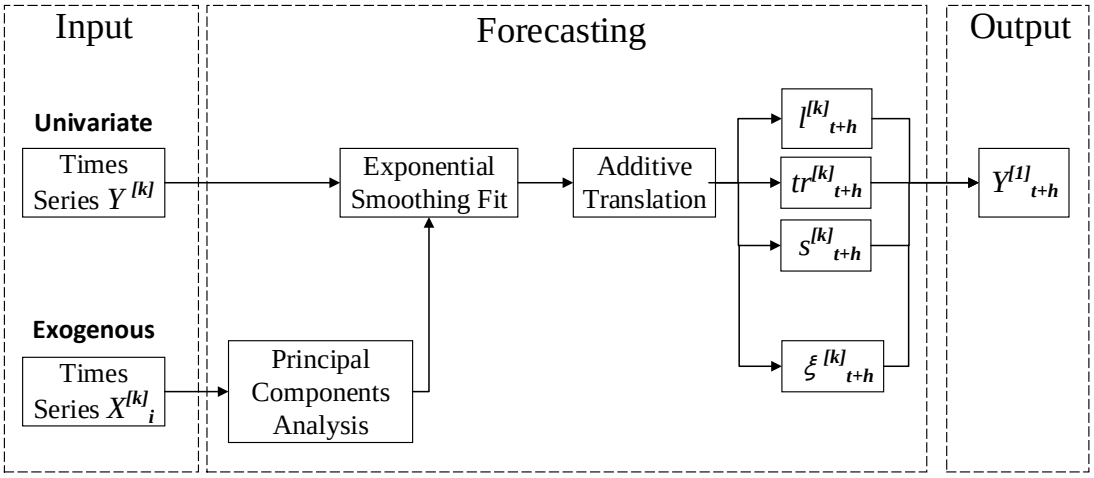

Figure 3.2.2: MAPAx algorithm diagram [5]

As the same way treated in the univariate case, the parameters of multivariate

ETS across each aggregation level can be optimized and the appropriate model will be selected with AIC. However, temporal aggregation causes additional complexity for the multivariate models. As X_j are aggregated, they become smoother. This changes the correlation between exogenous variables and potentially introduce multicollinearity at the higher aggregation levels, if more than one variable is included. As lag variables are employed as explanatory variables to predict solar radiance, collinearity phenomenon will appear at some aggregation levels. These variables can be merged to one vector, whilst the estimating coefficients w_j would not always exist. To avoid this, it is worthwhile to transform the variables into orthogonal variables by means of PCA method.

Mathematically, PCA is a statistical technique which employs an orthogonal transformation to convert a set of possibly correlated variables into a set of the linearly uncorrelated variables called principal components [105, 106]. The algorithm has characteristics that the first principle component has the greatest variance by some projection of the data and comes to lie on the first coordinate. The succeeding component on the second coordinate has second greatest variance under the constraint that it is orthogonal to the preceding component [107, 108]. In this study, a transformed set of variables X'_j is generated by PCA called as principal components, in response to the original correlated variables X_j, where $j = 1, ..., J$. The obtained principal components are orthogonal to each other. Thus, by replacing the original variables with the orthogonal principal components, the multicollinearity problem caused by temporal aggregating exogenous variables can be overcome. To produce the final forecast for h steps ahead, the algorithm implementation is shown in algorithm 1.

Algorithm 1 MAPAx algorithm for solar radiance forecasting.

Input: Time series of forecast variable y_t, forecast step h and exogenous variables $x_{j,t+h}$

Output: Forecast result $\hat{y}_{t+h}$

1: Given a time series forecast variable $Y = y_t$ and exogenous variables $X = x_{j,t+h}$ with $t = 1, 2, ..., N$, $j = 1, 2, ..., J$

2: Pre-process multicollinearity variables in exogenous variable with PCA to set a new exogenous variable set $X' = x'_{j,t+h}$

3: Temporally aggregating original time series (Y, X') to obtain aggregated series at each level $Y^{[k]}$ and $X'^{[k]}$ with equation 3.2.3 and the effect of $X'^{[k]}$ is reflected by $\xi_{t+h}^{[k]}$ with equation 3.2.8.

4: Fit ETS model components (level, trend and seasonality) at each aggregation level. Make the components prediction for h step by following the Table 3.2.1 to obtain $\{l_{t+h}^{[k]}, tr_{t+h}^{[k]}, s_{t+h}^{[k]}\}$

5: Combine time series components and effects of exogenous variables at each aggregation level with weights combination scheme (equation 3.2.4-3.2.6 and 3.2.9) to obtain forecast result $\hat{y}_{t+h}$, referred to equation 3.2.10

3.3 Weather forecasting results and comparison

In this section, solar radiance forecasting results and the data acquired from Lancaster University weather station will be compared and discussed by means of MLR model, ARIMAX model and MAPAx-PCA model. It is necessary to test the proposed forecasting methods with historical dataset and nearby weather forecast data. These two datasets range from 2017 April to 2017 July obtained from Lancaster Environment Center and Metoffice website. Due to the different time scales in two datasets, the sampling time is 10 minutes for Lancaster University weather station data, while the weather condition data from Metoffice are predicted every 3 hours. The historical data should be preprocessed with mean value method to adapt to the same time scale with Metoffice data. More specifically, first two months data (2017.04.01-2017.06.13) are employed for training the model, while the data from 2017.06.14 to 2017.07.03 are utilized for evaluating the performance of trained model.

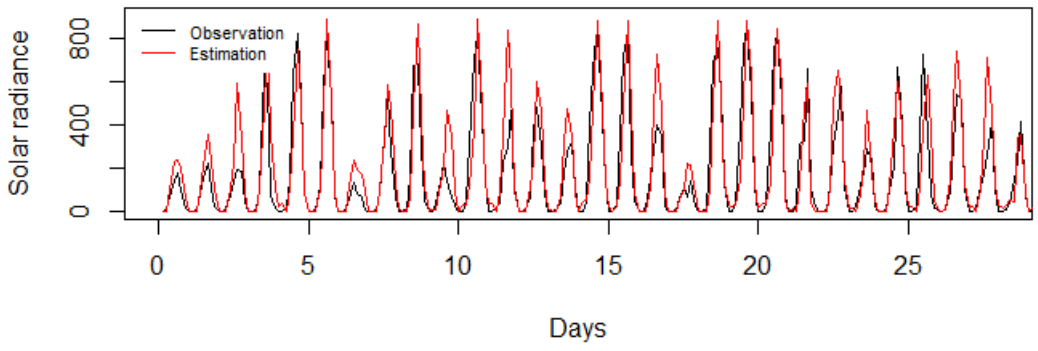

Figure 3.3.1: Forecasting results from the MLR model

Regarding the model evaluation, mean absolute percentage error (MAPE) can be

a good indicator to describe the prediction accuracy, which is defined as follows:

$$MAPE = \frac{1}{n}\sum_{t=1}^{n}\left|\frac{y_t - \hat{y}_t}{y_t}\right| \tag{3.3.1}$$

where y_t is the actual value and $\hat{y}_t$ is the forecast value. Additionally, another index called Coefficient of determination (R^2) is introduced to assess how well a model explain the actual output data and it is defined as:

$$R^2 = 1 - \frac{SS_{res}}{SS_{total}} \tag{3.3.2}$$

where SS_{res} is the sum of squared predicted output residuals, SS_{total} is the total sum of squares. If R^2 converges to unity, it indicates the model provide a good fit to real case. If R^2 approaches to zero, it means the theoretical model fails to fit real model, .

Figure 3.3.1 shows short-term solar radiance forecasting results with the MLR model. Clearly, the estimated value generally follow the observation data, with MAPE and R^2 being 69.27 and 0.745, respectively. In contrary, Figure 3.3.2 gives the forecasting result from the ARIMAX model, with MAPE and coefficient of determination being 86.67 and 0.78, respectively.

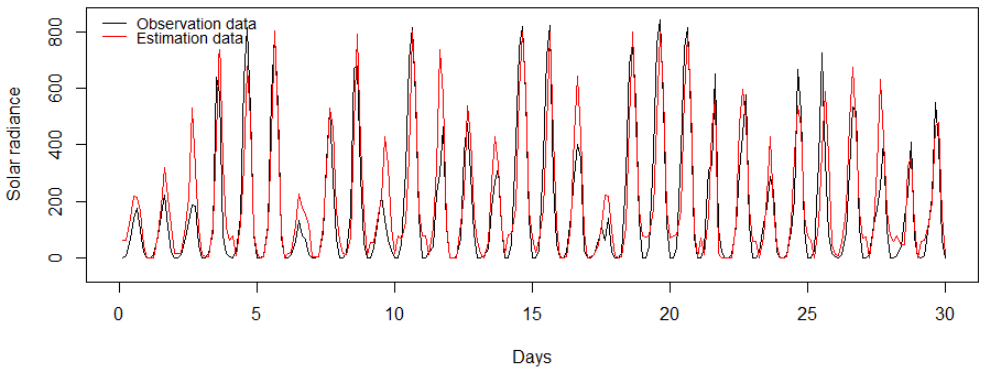

Figure 3.3.2: Forecasting results from ARIMAX model

The implementation of MAPAx is based on 'mapa' package in Rstudio. Rstudio is integrated development environment for R and is most commonly-used tool in statistic field. Figure 3.3.3 shows the identified ETS models at each temporal aggregation level. The components (error, trend, seasonality and exogenous variables) at different aggregation levels are identified and combined to fit the ETS model. Greyed cells indicate levels that no seasonality is estimated. **N**, **A**, **Ad**, **M** and **Md** indicate distinguishing combination schemes, as mentioned above. Figure 3.3.4 gives the final prediction results with the MAPAx-PCA model. Apparently, this hybrid MAPAx-PCA model best fits the test dataset, with MAPE equalling to 65.0355 and R^2 being 0.803, which outperforms the regression model in terms of goodness-of-fit of the predicted values. In summary, Table 3.3.1 is given to show the forecasting performance with three methods.

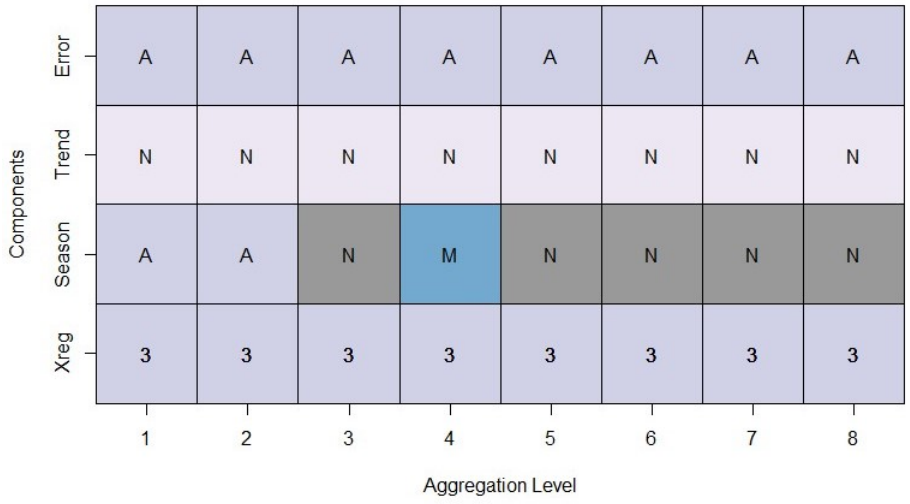

Figure 3.3.3: Identified ETS components for all temporal aggregation level

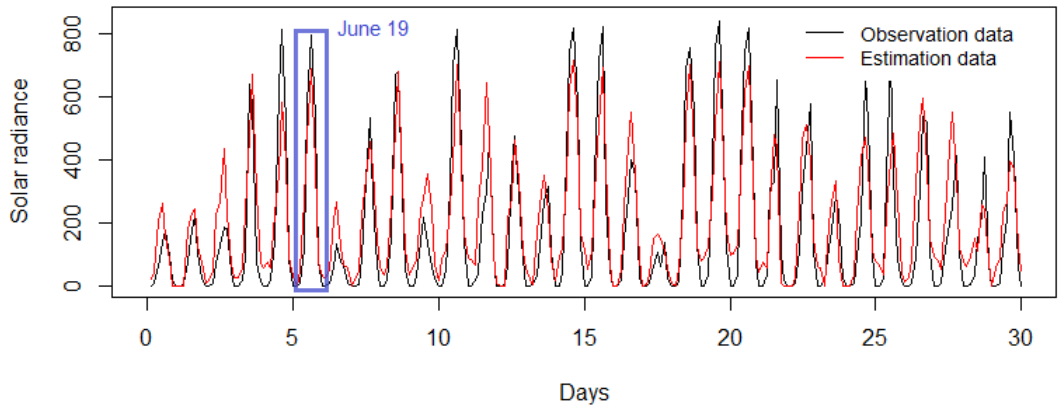

Figure 3.3.4: Forecasting results from MAPAx-PCA model

Table 3.3.1: The comparison of forecasting performance

	MLR	ARIMAX	MAPAx-PCA
MAPE (%)	69.27	86.67	65.035
R^2	0.745	0.78	0.803

3.4 Solar power system model

Based on the forecasting results generated by MAPAx-PCA model, a 24-hour solar power can be estimated by taking account of the specification of a solar PV panel and the size of the PV array. Table 3.4.1 gives a set of parameters for a single PV module from ISoltech with model No.ISTH-215-P, where I_{sc}, U_{oc}, I_m, U_m denote short-circuit current, open circuit voltage, maximum current and maximum voltage under standard condition. The standard condition indicates solar radiance reference value $S_{ref} = 1000W/m^2$ and temperature reference value $T_{ref} = 25^oC$. Figure 3.4.1 gives output power-voltage (P-V) and current-voltage (I-V) curve for single PV module under different solar radiance and temperature conditions. Clearly, the P-V curve of

Table 3.4.1: Specification of PV module

	Value
I_m(A)	7.35
U_m(V)	29
I_{sc}(A)	7.84
U_{oc}(V)	36.3
P_m(W)	213.15

a PV module shows a single peak under even irradiation environment. Many MPPT techniques have been proposed to adjust the peak power output and improve the generating efficiency of PV system. The perturb and observe method and the incremental conductance algorithm are most commonly applied MPPT algorithms[109].

Instead of utilizing conventional methods, it is straightforward to calculate key parameters in output curve with a set of mathematical model in reference [111], based on the change of solar radiance and temperature, which is given as follows:

$$I'_{sc} = I_{sc}\frac{S}{S_{ref}}(1 + \theta_1\Delta T) \tag{3.4.1}$$

$$U'_{oc} = U_{oc}(1 - \theta_3\Delta T)\ln(1 + \theta_2\Delta S) \tag{3.4.2}$$

$$I'_m = I_m\frac{S}{S_{ref}}(1 + \theta_1\Delta T) \tag{3.4.3}$$

$$U'_m = U_m(1 + \theta_3\Delta T)\ln(1 + \theta_2\Delta S) \tag{3.4.4}$$

where $\Delta T = T - T_{ref}$ and $\Delta S = S/S_{ref} - 1$. Assume that the shape of output characteristic remains unchanged, the parameters θ_1, θ_2 and θ_3 are set as $0.0025/^oC$, 0.5 and $0.00288/^oC$ respectively [111]. The maximum output current and voltage (I'_m, U'_m) are calculated by equation 3.4.3 and 3.4.4 and the total maximum power output

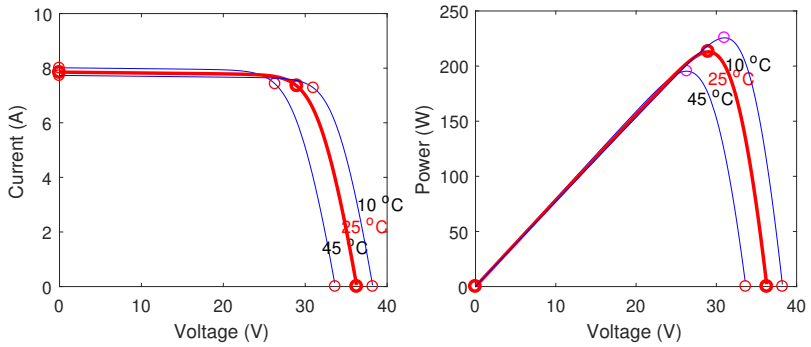

(a) PV output characteristics in different temperatures [110]

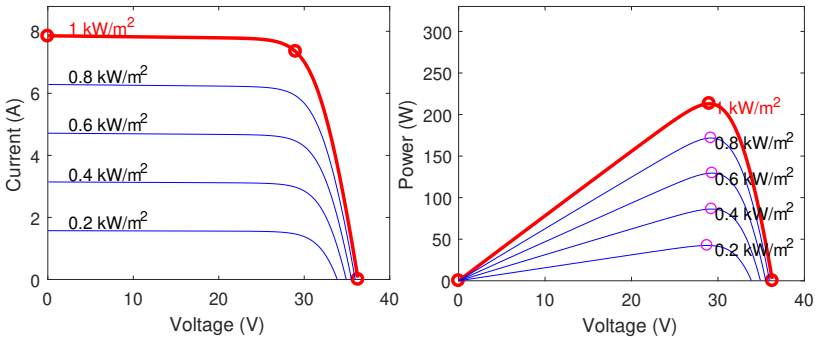

(b) PV utput characteristics in different solar radiances [110]

Figure 3.4.1: Output characteristics of PV module against different conditions

P'_m of a PV array can be expressed as:

$$P'_m = I_m U_m N_{ss} N_{pp} \tag{3.4.5}$$

where N_{ss} represents the number of modules connected in a string and N_{pp} is the number of strings in a PV array. Suppose there is a PV array with 4 parallel strings and 6 series-connected modules per string installed in a house roof. In fact, the shadow of obstructions and angle of installation are significant influencing factors that cannot be neglected. In this study, we assume these external factors are under ideal condition. Assume that the PV inverter always operates in MPPT mode to

maximize the utilization of energy efficiency, the forecast result on June 19 can be extracted as marked in Figure 3.3.4 and the daily solar energy curve is obtained in Figure 3.4.2(a). Since the forecast from Metoffice is updated every 3 hours, the solar power curve is expected to change every 3 hours correspondingly, as shown in Figure 3.4.2(b). The obtained solar power curve will be integrated into control strategy to evaluate the dynamics of distributed algorithm. More details will be elaborated in chapter 4 and chapter 5.

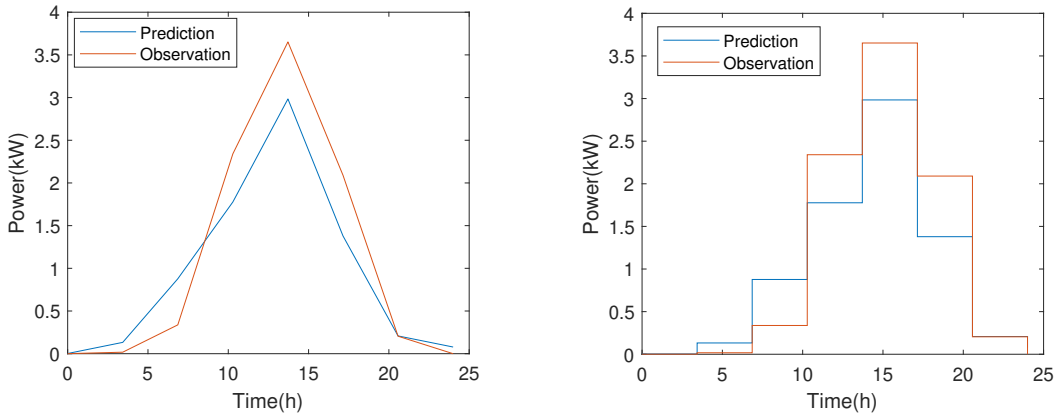

(a) (b)

Figure 3.4.2: A predicted solar power curve in a day

3.5 Summary and discussion

In this charter, the solar radiance can be predicted by multiple regression model, ARIMAX model and MAPAx-PCA hybrid model, respectively. These statistical-based models are trained and tested with historical weather observation dataset and weather forecast service data provided by Metoffice. The strongly correlated factors including

time series variable (lag variables, dummy variables) and meteorological indexes (UV index, temperature and weather type) are considered as exogenous variables.

A novel forecasting algorithm based on the MAPA-PCA model is developed to explore features in times series by aggregating original data into different temporal levels. A ETS model is established for each aggregation level and final prediction results are obtained by combining all ETS models with weighting coefficients. In comparison with classic models, the proposed hybrid method mitigates model uncertainty by introducing multiple ETS models and therefore improves the forecasting accuracy. Moreover, the power output of a PV array is modelled and then predicted with the forecasting solar radiances. The daily solar power forecasting curve will be provided for follow-up work in the subsequent chapters.

Chapter 4

HVAC-based Cooperative Algorithm

HVAC system, as a household appliance with high popularity, can be considered as an effective technology to deal with energy dispatch issue. This chapter presents novel distributed algorithms to solve supply-demand mismatch problem through the demand response, where the microgrid system with HVAC units is considered as a MAS framework. The approach helps reduce the quantity and capacity of energy storage devices potentially to be required. Compared with existing approaches focusing on the distributed algorithms under a fixed communication network, the proposed algorithm addresses a consensus problem under a switching topology by using Lyapunov argument and its consensus condition is given, correspondingly.

Section 4.1 describes preliminary knowledge involving graph theory and consensus algorithm. A mathematical model and physical model of HVAC system are presented in Section 4.2. Section 4.3 formulates a HVAC-based DSM problem, where distributed

energy management algorithms under the fixed and time-varying interaction topology are propossed respectively, with algorithm proofs given. Case studies and simulation results are presented and discussed in Section 4.4. Section 4.5 develops an energy dispatch scheme for HVAC systems, based on the solar power forecasting results obtained by MAPAx-PCA model. A summary is outlined in Section 4.6.

4.1 Preliminary

The preliminary knowledge including graph theory and consensus algorithm is given in this section, which lays a theoretical foundation for the introduction and proof of cooperative algorithm.

4.1.1 Graph theory

The communication topology among agents in MAS can be represented by an undirected graph $\mathcal{G} = (\mathcal{V}, \mathcal{E})$, where $\mathcal{V} = \{1, 2, ..., n\}$ is a node set and $\mathcal{E} = \{(i, j)|i, j \in \mathcal{V}\} \subseteq \mathcal{V} \times \mathcal{V}$ is a finite edge set. As for an undirected graph, the edge (i, j) represents the information exchange between vertex j and i. Nodes j and i are neighbouring nodes. Here, the self-loop edges are not considered in the topology. We only focus on the undirected graph. Let define $N_i = \{j|(i, j) \in \mathcal{E}\}$ as the union of neighbour vertexes for vertex i. If each node in an undirected graph has connection with any other nodes, the graph is called a strongly connected graph. In the microgrid diagram shown in the operational layer in Figure 2.5.1, each bus line is modelled as a node. The thin black solid lines signify the information exchange between neighbouring nodes and

hence, they form the communication topology. Clearly, the topology under Figure 2.5.1 is a strongly connected undirected graph. Mathematically, the communication topology can be described as a $n \times n$ matrix to indicate the interaction among agents, which will be demonstrated in the next section.

4.1.2 Consensus algorithm

When the interaction network among the agents allows continuous communication, the information state update of each agent is modelled by a differential equation. If the communication data arrives in discrete packets, then the information state is updated with a difference equation. Therefore, a scalar information state is updated by each agent using a first-order differential equation or a first-order difference equation.

According to the communication topology introduced above, the most common continuous consensus algorithm is given by [112]:

$$\dot{x}_i(t) = -\sum_{j=1}^{n} a_{ij} \left[x_i(t) - x_j(t) \right], i = 1, 2, ..., n \tag{4.1.1}$$

where a_{ij} indicates the weight for $(i, j) \in \mathcal{E}$ associated with $\mathcal{G}$ at time t and x_i is the information state of agent i. Note that $a_{ij} = 0$ denotes the fact that agent i cannot receive information from agent j ($(i, j) \notin \mathcal{E}$). Equation (4.1.1) represents that the state of agent is driven by the information transfer with its neighbouring agents. The consensus algorithm (4.1.1) is rewritten as in matrix form:

$$\dot{x}(t) = -\mathcal{L}(t)x(t) \tag{4.1.2}$$

where $x = [x_1, x_2, ..., x_n]^T$ is the information state column vector and $\mathcal{L} = \{\ell_{ij}\} \in \mathbb{R}^{n \times n}$ is a non-symmetrical Laplacian matrix associated with communication topology.

The Laplacian matrix is defined as [112]:

$$\ell_{ij} = \begin{cases} -a_{ij}, & (j,i) \in \mathcal{E} \\ \sum_{j=1, j\neq i}^{n} a_{ij}, & i = j \\ 0, & (j,i) \notin \mathcal{E} \end{cases} \tag{4.1.3}$$

For a undirected graph, Laplacian matrix is symmetrical with diagonal entries positive. It owns the following properties [113].

1. $\mathcal{L}$ is symmetric matrix with each row sum is zero. Thus, $\mathcal{L}$ exists at least a zero eigenvalue, with associated eigenvector $1_n = [1, 1, .., 1]^T$, satisfying $\mathcal{L}1_n = 0$

2. $\mathcal{L}$ is positive semi-definite matrix, with non-zero eigenvalue having non-negative real part.

If the communication between agents occurs at discrete instants, the information update of each agent relies on difference equation. Similar to continuous model, the commonly-used discrete-time consensus algorithm has the form:

$$x_i(k+1) = \sum_{j \in N_i} d_{ij} x_i(k) \tag{4.1.4}$$

where $x_i(k)$ is the state of agent i at the iteration k. d_{ij} is the (i, j) entry of a row stochastic matrix $D = \{d_{ij}\} \in \mathbb{R}^{n \times n}$ corresponding to an undirected graph. Equation (4.1.4) can be rewritten in terms of matrices as below

$$X(k+1) = DX(k) \tag{4.1.5}$$

Different methods have been used to define matrix D such as those used in refer-

ences [76, 101, 112]. Here, Vicsek model is adopted to define d_{ij} as follows [112]

$$d_{ij} = \begin{cases} \frac{1}{1+|N_i|}, & j \in N_i \\ 1 - \sum_{i \in N_i} \frac{1}{1+|N_i|}, & i = j \\ 0, & j \notin N_i \end{cases} \tag{4.1.6}$$

where $|N_i|$ represents the number of elements in set N_i. It can be seen that matrix D associated with a strongly connected graph is a positive doubly stochastic matrix, where the sum of entries in rows and columns are both equal to one. Matrix D satisfies following conditions[112, 113].

1. It satisfies $D1_n = 1_n$ and $1_n^T D = 1_n$. The stochastic matrix D has 1 as an eigenvalue with an associated eigenvector 1_n.

2. The spectral radius of matrix D is 1 and all of rest of eigenvalues are all positive.

3. The average consensus is achievable based on initial conditions of all agents, if the graph is strongly connected. The consensus state is calculated by $\lim_{k \to \infty} x_i(k) = \frac{1}{n} \sum_{i=1}^{n} x_i(0)$ and $x_i(0)$ denotes initial condition for agent i $(i = 1, 2, .., n)$

The above properties will be utilized for the proof of the distributed algorithm in Section 4.3. Examples of matrix D are given in Section 4.4.6 when dealing with switching topology test.

4.2 HVAC model

A HVAC system is physically composed of a compressor, an evaporator, condenser and expansion valves, sensors, electrical control parts and a central controller. The

compressors of air conditioner have evolved from fixed speed to variable speed units. The constant speed air conditioner only works in ON/OFF mode with a constant power consumption, based on the triggering temperature, which is not an adjustable load to participate in system operation. Moreover, there is a transient spike in the power consumption when it is turned on. After it is turned off, the air conditioner continues to cool for a few minutes, because of the inertial effect, which results in over cooling and inefficiency. Conversely, the inverter air conditioner has a variable-frequency drive to control the motor speed and cooling/heating output. With its flexibility and popularity, the inverter air conditioner has a promising application prospect in relieving the tension of supply-demand mismatch, strengthening the grid's ability of dealing with power fluctuation, improving energy efficiency and maintaining the occupant comfortable level. Specifically, the inverter air conditioner can be divided into AC inverter-based air conditioner and DC inverter-based air conditioner, which employs AC motor or DC motor to drive the compressor, respectively. In this thesis, we only discuss AC inverter-based air conditioner.

4.2.1 Electrical model of the HVAC system

The electrical model of inverter air conditioner system describes the relationship among compressor frequency, cooling capacity and power consumption. The power of inverter air conditioner system is mostly consumed by the compressor, whose Coefficient of Performance (CoP) is varied with different frequencies. Figure 4.2.1 shows the performance curves of a typical HVAC, demonstrating the relationship of compressor frequency against the cooling load, CoP and power consumption, respectively [114].

The relationship between operating frequency f_i and power consumption $P_{AC,i}$ with respect to i^{th} HVAC system is expressed approximately as [115].

$$P_{AC,i} = u_i f_i + v_i \qquad (\underline{P}_{AC,i} \leqslant P_{AC,i} \leqslant \overline{P}_{AC,i}) \tag{4.2.1}$$

where u_i and v_i are a pair of model coefficients. Physically, u_i and v_i denote load ramp rates and initial power of the HVAC unit, respectively. $\overline{P}_{AC,i}$ and $\underline{P}_{AC,i}$ denote the maximum and minimum power consumption of HVAC i, respectively. The power consumption of each HVAC system subjects to its power constraints. Similarly, the relationship between the cooling capacity $Q_{AC,i}$ and the frequency f_i also can be modelled as a first-order function. It can be seen that the operating frequency

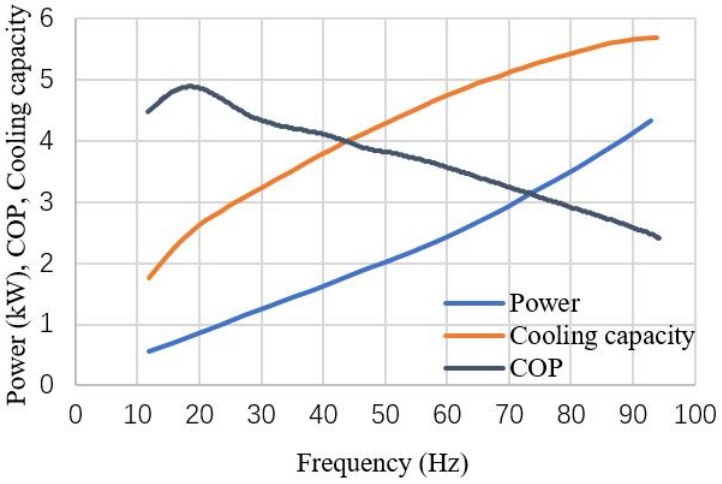

Figure 4.2.1: CoP, power consumption and cooling capacity of the HVAC against compressor frequency

increases with the increment of the cooling load. Then, the expansion valve will open more to ensure the system can operate at an optimal CoP value. Consequently, the power consumption increases with the growth of the operating frequency. A number

of performance tests carried out in [116] indicate that the power consumption of air conditioner depends on the compressor frequency instead of the temperature.

4.2.2 HVAC physical control

The motor in inverter air conditioner offers a wide operating range, which allows the unit to work even in extreme weather conditions. It is achieved by inverter technology and electro motors of the compressors. Figure 4.2.2 shows the schematic of a typical AC inverter-based air conditioner, demonstrating how the controller algorithms are integrated into power conversion of the HVAC system. In Figure 4.2.2, the power conversion circuit aims to achieve AC-DC-AC power conversion, which is composed of an AC filtering module, a rectifier, a power factor control (PFC) circuitry, a DC filtering module, and an intelligent power module (IPM). Firstly, a single-phase power supply is given to AC filtering module. Then, a stable DC voltage is obtained by connecting capacitors along with a PFC in the current path after the rectifier. The IPM module is utilized to convert DC to AC regulated by the pulse width modulation (PWM) signals as controlled to drive the compressor. There are two controllers in the HVAC unit. The upper controller implements the distributed algorithm and generates reference frequency and power signals (f_i^{ref}, $P_{AC,i}^{ref}$) in response to the local power mismatch ($P_{D,i}$) and collects local agent information, such as: power constraint ($\overline{P}_{AC,i}$, $\underline{P}_{AC,i}$) and frequency information (f_j) interaction with neighbouring HVAC units. Provided that the indoor and outdoor temperatures, frequency and power reference signals are given, the lower controller then generates PWM pulses to drive the insulated-gate bipolar transistor (IGBT) in the IPM module to secure the compressor

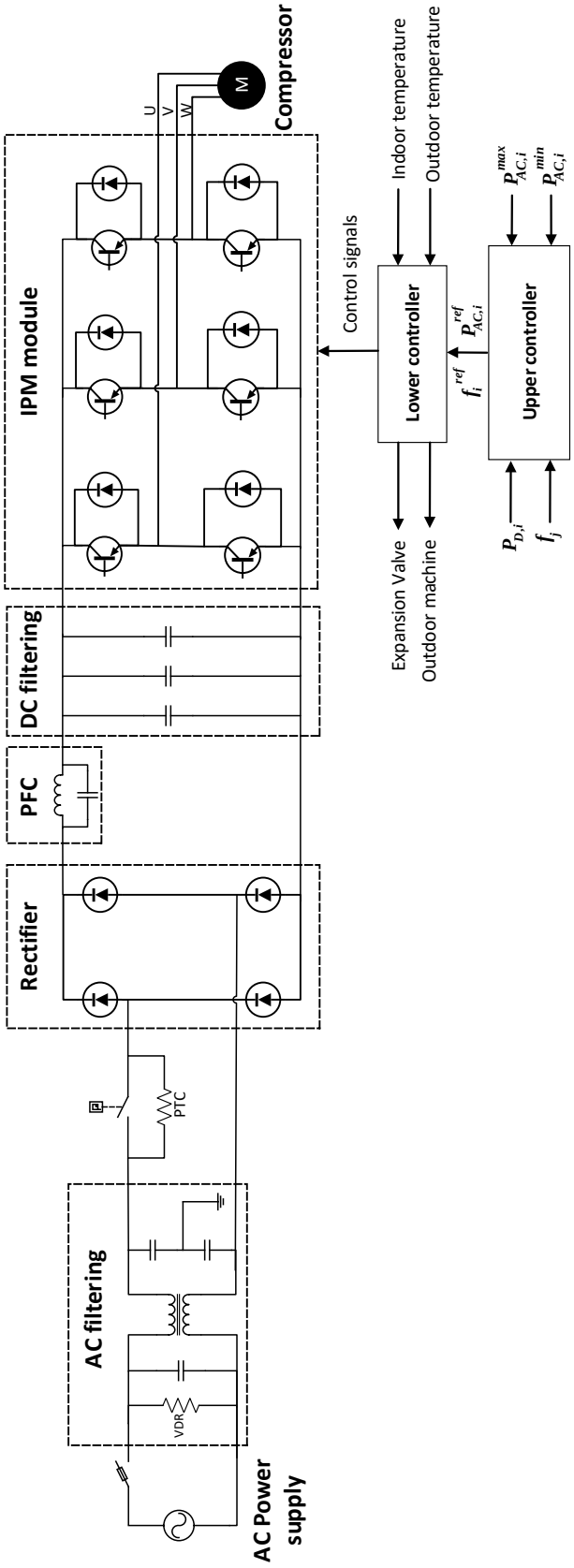

Figure 4.2.2: The schematic diagram of a typical inverter AC system

operates with referred frequency signal and consumes power as desired. Furthermore, the lower controller adjusts the operation state of the expansion valve and outdoor machine to assist its operation. Meanwhile, it is worthy highlighting that the control strategy in the lower controller is not the focus of this work.

4.3 Distributed HVAC systems energy management

In this session, a HVAC-based DSM problem is formulated. A distributed cooperative algorithm is presented by incorporating the HVAC model to address DSM problem in a stand-alone microgrid system. The main objective is to obtain a desired frequency f^* and power reference $P^*_{AC,i}$ for HVAC, while the consumption of aggregated HVAC systems can compensate the total power mismatch caused by unstable renewable energy. The convergence proof for the proposed algorithm under fixed communication topology and dynamic communication topology are provided.

4.3.1 Problem formulation

Considering an IEEE n-bus system to construct a microgrid system, the active power balance in an autonomous microgrid system without transmission loss can be represented as:

$$P_d = \sum_{i=1}^{n} P_{G,i} - \sum_{i=1}^{n} P_{L,i} \tag{4.3.1}$$

where P_d is total supply-demand mismatch for the entire microgrid system, $P_{G,i}$ is the distributed power generation at i^{th} local bus; $P_{L,i}$ denotes the non-adjustable load demand at bus i. An appropriate dispatching strategy therefore needs to be

implemented to share the total power mismatch P_d by regulating power consumption of the HVAC unit $P_{AC,i}$ $(i = 1, 2, ..., n)$ such that

$$P_d = \sum_{i=1}^{n} P_{AC,i} \tag{4.3.2}$$

When power consumption constraints for each HVAC are applied, the objective of coordinating multiple HVAC units is to minimize the cost function

$$\min \sum_{i=1}^{n} P_{G,i} - \sum_{i=1}^{n} P_{L,i} \tag{4.3.3}$$

$$s.t. \quad P_d = \sum_{i=1}^{n} P_{AC,i} \tag{4.3.4}$$

$$\sum_{i=1}^{n} \underline{P}_{AC,i} \leqslant P_d \leqslant \sum_{i=1}^{n} \overline{P}_{AC,i} \tag{4.3.5}$$

where $\underline{P}_{AC,i}$, $\overline{P}_{AC,i}$ are lower and upper power constraints for the i^{th} HVAC unit, respectively.

Assume there are n HVAC units in a microgrid system, according to equation (4.2.1) and (4.3.4), all frequency signals will eventually converge to an optimal common value, which is calculated as:

$$f^* = \left(P_d - \sum_{i=1}^{n} v_i \right) \sum_{i=1}^{n} \frac{1}{u_i} \tag{4.3.6}$$

The associated power consumption for each HVAC systems is therefore

$$P^*_{AC,i} = u_i f^* + v_i \tag{4.3.7}$$

Considering power constraints on HVACs, the frequency can be specified as:

$$\begin{cases} f^* = (P_{AC,i} - v_i)/u_i, & \underline{P}_{AC,i} < P_{AC,i} < \overline{P}_{AC,i} \\ f^* > (P_{AC,i} - v_i)/u_i, & P_{AC,i} = \overline{P}_{AC,i} \\ f^* < (P_{AC,i} - v_i)/u_i, & P_{AC,i} = \underline{P}_{AC,i} \end{cases} \tag{4.3.8}$$

Let define Γ_{AC} as a subset of the HVAC units where the power consumption is saturated, in order to achieve the optimal assignment, we have

$$f^* = \left(P_D - \sum_{i \in \Gamma_{AC}} P_{AC,i} - \sum_{i \notin \Gamma_{AC}} v_i \right) \sum_{i \notin \Gamma_{AC}} \frac{1}{u_i} \tag{4.3.9}$$

The power consumption for each HVAC can be described as:

$$P^*_{AC,i} = \begin{cases} u_i f^* + v_i, & i \notin \Gamma_{AC} \\ \overline{P}_{AC,i} \text{ or } \underline{P}_{AC,i}, & i \in \Gamma_{AC} \end{cases} \tag{4.3.10}$$

The results obtained in equation (4.3.10) are the solution to the DSM problem as formulated in equations (4.3.3)-(4.3.5) with HVAC power constraints being considered.

4.3.2 Algorithm design

Distinguished distributed algorithms are provided in response to the difference in fixed communication topology and time-varying topology.

Under fixed topology

Let $f_i(k)$ and $P_{AC,i}(k)$ be the operating frequency and power consumed for the i^{th} HVAC at the iteration k, respectively. $P_{D,i}$ denotes the power mismatch estimated between the local power generation and local load demand at bus i. ϵ_i is a positive coefficient affecting the convergence speed. The discrete time distributed algorithm is described as:

$$f_i(k+1) = \sum_{j \in N_i} d_{ij} f_j(k) + \epsilon_i P_{D,i}(k) \tag{4.3.11}$$

$$P_{D,i}(k+1) = \sum_{j \in N_i} d_{ij} P_{D,i}(k) - (P_{AC,i}(k+1) - P_{AC,i}(k)) \tag{4.3.12}$$

$$P_{AC,i}(k+1) = u_i f_i(k+1) + v_i \tag{4.3.13}$$

Remark 4.3.1: The update of f_i in the distributed algorithm (4.3.11) is obtained based on collaborative efforts of all neighbouring agents of i^{th} HVAC and its current state. The stability of the algorithm mainly relies on consensus term $\sum_{i\in N_i} d_{ij} f_j(k)$, which is determined by the associated communication topology. The surplus term $\epsilon_i P_{D,i}(k)$ provides a feedback mechanism to ensure the convergence and ϵ_i is called state feedback gain, which dominants the convergence speed of f_i when converging to optimal f^*.

Consider the initial conditions:

$$\begin{cases} f_i(0) = \frac{(P_{AC,i}(0)-v_i)}{u_i} \\ P_{AC,i}(0) \in \left[\overline{P}_{AC,i}, \underline{P}_{AC,i}\right] \\ P_{D,i}(0) = 0 \end{cases} \tag{4.3.14}$$

Let $P_{AC,i}(0)$ be any value within the power constraint boundary and total initial power consumed by HVAC devices is $P_{AC}(0) = \sum_{i=1}^{n} P_{AC,i}(0)$.

The equations (4.3.11), (4.3.12) and (4.3.13) can be rewritten in a matrix form as follows:

$$F(k+1) = DF(k) + EP_D(k) \tag{4.3.15}$$

$$P_D(k+1) = DP_D(k) - (P_{AC}(k+1) - P_{AC}(k)) \tag{4.3.16}$$

$$P_{AC}(k+1) = UF(k+1) + V \tag{4.3.17}$$

where F, P_D, P_{AC}, V are column vectors of f_i, $P_{D,i}$, $P_{AC,i}$, v_i, respectively with $i = 1, 2, ..., n$. Define $E = \text{diag}\{\epsilon_1, \epsilon_2, ..., \epsilon_n\}$, $U = \text{diag}\{u_1, u_2, ..., u_n\}$. It can be

reformatted as a matrix form

$$\begin{pmatrix} F(k+1) \\ P_D(k+1) \end{pmatrix} = W \begin{pmatrix} F(k) \\ P_D(k) \end{pmatrix}, \quad W = \begin{pmatrix} D & E \\ U(I-D) & D-UE \end{pmatrix} \tag{4.3.18}$$

W is called the system matrix. Denote

$$W_0 = \begin{pmatrix} D & 0 \\ U(I-D) & D \end{pmatrix}, \quad \Xi = \begin{pmatrix} 0 & E \\ 0 & -UE \end{pmatrix} \tag{4.3.19}$$

Here we introduce a metric for the distance between the spectrum of W and W_0; thus $W = W_0 + \Xi$. The matrix Ξ is dominated by a gain vector $[\epsilon_1(k), ..., \epsilon_n(k)]$. By analysing the optimal matching distance between the spectrum of W and W_0, the boundary of feedback gain can be obtained, which is demonstrated in next session.

Now consider power constraints on HVAC system; equation (4.3.13) is then revised to

$$P_{AC,i}(k+1) = \begin{cases} \underline{P}_{AC,i}, & f_i(k+1) < \underline{f}_i \\ u_i f_i(k+1) + v_i, & \underline{f}_i < f_i(k+1) < \overline{f}_i \\ \overline{P}_{AC,i}, & f_i(k+1) > \overline{f}_i \end{cases} \tag{4.3.20}$$

The $\underline{f}_i$ and $\overline{f}_i$ are minimum/maximum compressor frequency for HVAC i, where $\underline{f}_i = (\underline{P}_{AC,i} - v_i)/u_i$, $\overline{f}_i = (\overline{P}_{AC,i} - v_i)/u_i$. With the same initial values as given in (4.3.14), equation (4.3.18) is then revised to:

$$\begin{pmatrix} F(k+1) \\ P_D(k+1) \end{pmatrix} = \begin{pmatrix} D & E \\ U'(I-D) & D-U'E \end{pmatrix} \begin{pmatrix} F(k) \\ P_D(k) \end{pmatrix} \tag{4.3.21}$$

where $U' = \text{diag}\{u'_1, u'_2, ..., u'_n\}$ with

$$u'_i = \begin{cases} 0, & \text{if } P_{AC,i} \text{ is saturated} \\ u_i, & \text{otherwise} \end{cases} \tag{4.3.22}$$

Under time-varying topology

The consensus algorithms under a fixed communication topology is modified to address the case under time-varying interaction topology. Assume the communication network in the MAS is time varying, the equations (4.3.11) and (4.3.12) need to be improved to accommodate the average consensus in a dynamic topology.

$$f_i(k+1) = \sum_{j \in N_i} c_i(k) d_{ij} f_j(k) + \epsilon_i P_{D,i}(k) \tag{4.3.23}$$

$$P_{D,i}(k+1) = \sum_{j \in N_i} c_i(k) d_{ij} P_{D,i}(k) - (P_{AC,i}(k+1) - P_{AC,i}(k)) \tag{4.3.24}$$

where the switching parameter $c_i(k) = 1$, if the $\sum_{j \in N_i} d_{ij} \neq 0$, or otherwise $c_i(k) = 0$. Let us define $D'(k) = \{c_i(k) d_{ij}(k)\}$ is also a doubly stochastic matrix as D. This means that the agent updates its current state may only rely on its surplus term, if there is no direct information from in-neighbours during the time subinterval. Similarly, a matrix format is expressed as:

$$\begin{pmatrix} F(k+1) \\ \\ P_D(k+1) \end{pmatrix} = \begin{pmatrix} D'(k) & E \\ \\ U(I - D'(k)) & D'(k) - UE \end{pmatrix} \begin{pmatrix} F(k) \\ \\ P_D(k) \end{pmatrix} \tag{4.3.25}$$

The power information of each HVAC unit is updated with equation (4.3.13) and the initial conditions satisfy equation (4.3.14).

4.3.3 Convergence analysis for fixed communication topology

With the updating rule of HVAC systems expressed in equations (4.3.11)-(4.3.13), we have the following theorem to demonstrate the stability proof of distributed algorithm under fixed topology [101].

Theorem 4.3.1. *Suppose a communication topology $\mathcal{G}$ is strongly connected, if the feedback gain ϵ_i is properly small, distributed algorithm eqs (4.3.11)-(4.3.13) with the initial condition eq (4.3.14) solves DSM problem eq (4.3.3). That is, f_i and $P_{D,i}$ can asymptotically converge to the optimal value f^* and P_D^*, respectively.*

Proof. Firstly, if the feedback gain ϵ is sufficiently small to be neglected, we prove that the eigenvalue of $W_{2n\times 2n}$ satisfy

$$|\lambda I_{2n} - W| = \left| \begin{pmatrix} \lambda I_n - D & -\epsilon I_n \\ U(D - I_n) & \lambda I_n - D + \epsilon I_n U \end{pmatrix}_{2n\times 2n} \right| \approx |\lambda I_n - D|^2 \tag{4.3.26}$$

where W has the repeated eigenvalue sets as D. I_n is a identity matrix with size of $n \times n$. Since the matrix D is designed as equation (4.1.6), it is a doubly stochastic matrix with the property demonstrated in Section 4.1.2. Therefore, the eigenvector with respect to $\lambda = 1$ should be $[1_n, 0_n]^T$, which satisfies

$$W \begin{pmatrix} 1_n \\ 0_n \end{pmatrix} = \lambda \begin{pmatrix} 1_n \\ 0_n \end{pmatrix}$$

$$\Rightarrow \begin{pmatrix} D & \epsilon I_n \\ U(I_n - D) & D - \epsilon I_n U \end{pmatrix}_{2n\times 2n} \begin{pmatrix} 1_n \\ 0_n \end{pmatrix}_{2n\times 1} = \lambda \begin{pmatrix} 1_n \\ 0_n \end{pmatrix}_{2n\times 1}$$

$$\Rightarrow \begin{pmatrix} D1_n \\ U(I_n - D)1_n \end{pmatrix} = \begin{pmatrix} 1_n \\ 0_n \end{pmatrix}$$

According to the proof in [101, 117], the system converges to region $[1_n, 0_n]^T$, as time goes to infinity

$$\begin{pmatrix} F(\infty) \\ P_D(\infty) \end{pmatrix}_{2n\times 1} = f^* \begin{pmatrix} 1_n \\ 0_n \end{pmatrix} \tag{4.3.27}$$

Thus, the compressor frequency will converge to a common value f^* and the local power mismatch will converge to 0. On the other hand, the matrix perturbation theory can also be used to analyse the convergence of the algorithm by discussing the eigenvalue characteristic of system matrix W. □

Note that the selection of gain ϵ_i depends on the topology structure and number of agents. Denote $\lambda(W_0) = \lambda_1, ..., \lambda_{2n}$ and $\lambda(W) = \lambda_1(\epsilon), ..., \lambda_{2n}(\epsilon)$, where $|\lambda_1| \geq |\lambda_2| \geq ... \geq |\lambda_{2n}|$ and $|\lambda_1(\epsilon)| \geq |\lambda_2(\epsilon)| \geq ... \geq |\lambda_{2n}|(\epsilon)$. There is a result of the distance metric $d(\lambda(W_0), \lambda(W))$

Lemma 4.3.2. *[118] An upper bound on $d(\lambda(W_0), \lambda(W))$ is given by:*

$$d(\lambda(W_0), \lambda(W)) \leq 4(\|W_0\|_\infty + \|W\|_\infty)^{1-\frac{1}{2n}} \|\Xi(t)\|_\infty^{\frac{1}{2n}}$$

Proposition 4.3.3. *Suppose a communication topology $\mathcal{G}$ is strongly connected, then there exists a positive $\bar{\epsilon}$, which has the following form,*

$$\bar{\epsilon} = \frac{1}{(8+4n)^{2n}}(1-\lambda_3)^{2n} \tag{4.3.28}$$

where λ_3 is the third largest eigenvalues of W_0. When the feedback gain ϵ_i satisfies $\epsilon_i \in (0, \bar{\epsilon})$, algorithm (4.3.11)-(4.3.13) converge to the optimal solution of problem eq (4.3.3).

Proof. From the definition of D, we conclude that $\|D\|_\infty = 1$, and it is easy to obtain that $\|W_0\|_\infty = 1$. Lets define $\bar{\epsilon} = \max_{i \in n} \epsilon_i$. In general, $\bar{\epsilon} < n$. Given by [101], we obtain $\|\Xi(\epsilon)\|_\infty = \bar{\epsilon}$ thus

$$\|W\|_\infty \leq \|W_0\|_\infty + \|\Xi\|_\infty = 1 + \|\Xi(\epsilon)\|_\infty < 1 + n \tag{4.3.29}$$

From eq 4.3.28 and 4.3.29, we can obtain

$$\begin{aligned} d(\lambda(W_0), \lambda(W)) &\leq 4(\|W_0\|_\infty + \|W\|_\infty)^{1-\frac{1}{2n}} \|\Xi(\epsilon)\|_\infty^{\frac{1}{2n}} \\ &\leq 4(2\|W_0\|_\infty + \|\Xi\|_\infty)^{1-\frac{1}{2n}} \|\Xi(\epsilon)\|_\infty^{\frac{1}{2n}} \\ &\leq 4(2+n)\|\Xi(\epsilon)\|_\infty^{\frac{1}{2n}} \\ &\leq 1 - |\lambda_3|. \end{aligned} \tag{4.3.30}$$

From the proof of Lemma 11 in [117], the unperturbed eigenvalues $\lambda_3, ..., \lambda_{2n}$ of W_0 lie strictly inside the unit circle. Therefore, perturbing the eigenvalues $\lambda_3(\epsilon), ..., \lambda_{2n}(\epsilon)$ by a value less than $\bar{\epsilon}$ will remain in the unit circle. Furthermore, $\lambda_2(\epsilon)$ is also lie in the unit circle and $\lambda_1(\epsilon) = 1$ for $\epsilon_i \in (0, \bar{\epsilon})$. Therefore, an upper bound of ϵ_i can guarantee that algorithm (4.3.11)-(4.3.13) converge to the optimal solution of problem (4.3.3). □

Meanwhile, the summation of $P_{AC,i}$ and $P_{D,i}$ is preserved during the consensus iterations k, which can be verified by multiplying 1_n^T on both side of equation (4.3.16)

$$\begin{aligned} 1_n^T(P_D(k+1) + P_{AC}(k+1)) &= 1_n^T(DP_D(k) + P_{AC}(k)) \\ &= 1_n^T(P_D(k) + P_{AC}(k)) \\ \Rightarrow 1_n^T(P_D(k) + P_{AC}(k)) &= 1_n^T(P_D(0) + P_{AC}(0)) \end{aligned} \tag{4.3.31}$$

With the initial condition that $P_D(0) = 0$, we have $\sum_{i=1}^n P_{D,i}(k) = \sum_{i=1}^n (P_{AC,i}(0) - P_{AC,i}(k))$. If $P_{D,i}(k) \to 0$ when $k \to \infty$ for $i = 1, 2, ..., n$, power imbalance problem is solved for each bus.

4.3.4 Stability proof for switching communication topology

To verify the convergence condition for the distributed algorithm under switching topology, we derive the following theorem

Theorem 4.3.4. *The revised equation 4.3.23 and 4.3.24 can solve the average consensus under a dynamically changing interaction topology if the union of the directed graph across each interval is strongly connected.*

Because the state matrix in equation (4.3.25) fails to be divided into a deterministic matrix and parameter matrix due to the appearance of D', the matrix perturbation theory is thus not applicable to prove a dynamic topology. The convergence proof of equation (4.3.25) is now conducted based on the Lyapunov-type argument. In reference [118], the gain parameter is given within $(0, 1)$, which specifies the amount of power mismatch used for compressor frequency update. Due to the model diversity, the trend of ϵ against the convergence speed is obtained to fit our case, through a number of simulation experiments. As shown in Figure 4.3.1, the algorithm performance is optimized when $\epsilon \in (1, 3)$. The system convergence become weak if out of this range. When ϵ is over 8, the system become divergence.

In order to design a Lyapunov candidate function, we introduce the maximum and minimum frequency state $\overline{m}(f)$ and $\underline{m}(f)$ with regard to Equation 4.3.23 satisfying

$$\overline{m}(f) = \max_{i \in n}(f_i) \qquad \underline{m}(f) = \min_{i \in n}(f_i) \tag{4.3.32}$$

As demonstrated in reference [118], the minimum value $\underline{m}(f)$ is a non-decreasing variable for each iteration. It satisfies $\underline{m}(f) \leq f_a$, if f_a is the convergence value.

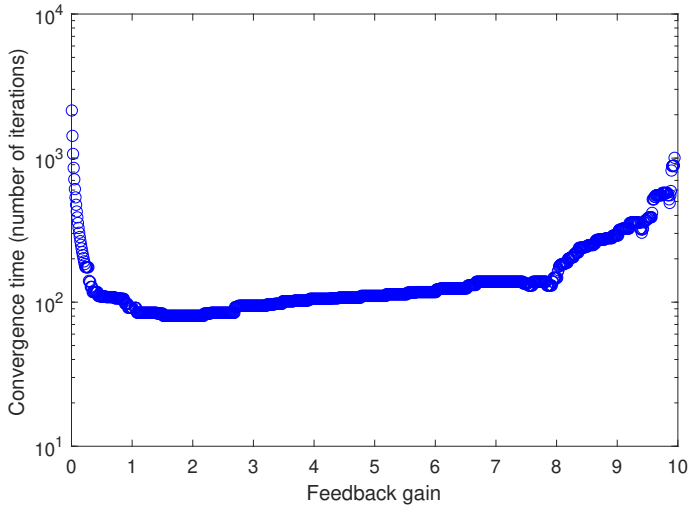

Figure 4.3.1: Convergence time with varying feedback gain under switching topology

When $\underline{m}(f) = f_a$, all agents satisfy average consensus condition at which $f_i(k) = f_a$ and $P_{D,i}(k) = 0$. The final equilibrium point will be $(f_a 1_n, 0_n)$, where 0_n is a column vector that all elements must be zero.

Similar to the derivation in fixed topology case as equation 4.3.31, we then obtain

$$1_n^T(P_D(k) + UF(k)) = ... = 1_n^T(P_D(0) + UF(0))$$

This implies that $P_D(k) + UF(k)$ is a constant quality for all k. Given the initial condition $(F(0), P_D(0))$, the steady state value for each agent converges to consensus point $(f_a, 0)$, where the scalar $f_a = \frac{\sum_{i=1}^n u_i f_i(0)}{\sum_{i=1}^n u_i}$. We define a set to describe the change of states (F, P_D) when they approach and converge to the consensus point.

$$\Omega(f_a) = \left\{ (F, P_D) \in \mathbb{R}^{2n} : \frac{1_n^T(P_D + UF)}{\sum_{i=1}^n u_i} = f_a, P_D > 0 \right\} \subset \mathbb{R}^{2n} \tag{4.3.33}$$

Lemma 4.3.1: [118, 119] Suppose that $\Delta_k(F, P_D)$ and $V(F, P_D)$ are positive bounded functions with respect to the equilibrium point. There exist finite times κ satisfies

that each state $F(k), P_D(k) \in \Omega(f_a)$ meets.

$$V(F(k+\kappa), P_D(k+\kappa)) - V(F(k), P_D(k)) \leq -\Delta_k(F(k), P_D(k))$$

Then, the network of agents achieves uniform average consensus.

We will construct two functions that satisfy the conditions in Lemma 4.3.1. We firstly introduce a Lyapunov candidate function $V(F, P_D)$ as below:

$$V(F, P_D) = \frac{1_n^T(P_D + UF)}{\sum_{i=1}^n u_i} - \underline{m}(f) \tag{4.3.34}$$

Clearly, V is a continuous and bounded function with respect to (F, P_D), because both $\frac{1_n^T(P_D+UF)}{\sum_{i=1}^n u_i}$ and $\underline{m}(f)$ are restricted. With the definition of both terms as mentioned above, $V(F, P_D)$ is positive definite when $(F, P_D) \in \Omega(f_a) - (f_a 1_n, 0_n)$, while $V(F, P_D) = 0$, if the state converges to the consensus point $(f_a 1_n, 0_n)$.

Assuming that κ denotes switching times occurring time interval $[k, k+1]$, we consider an auxiliary function $\Delta_k(F, P_D)$, where $(F, P_D) \in \Omega(f_a)$, which satisfies:

$$\Delta_k(F, P_D) = \inf(V(F_0, P_D 0) - V(F_\kappa, P_{D\kappa})) \tag{4.3.35}$$

where the function experiences all possible sequences $(F_0, P_{D0}), (F_1, P_{D1}), ..., (F_\kappa, P_{D\kappa}) \in \Omega(f_a)$, satisfying Equation (4.3.25). Thus, $(F_\kappa, P_{D\kappa})$ is a pair of reachable state from (F_0, P_{D0}). From Equation 4.3.35, if $V(F, P_D) = 0$, the only solution is $(F, P_D) = (f_a 1_n, \mathbf{0})$ and $\Delta_k(f_a 1_n, \mathbf{0}) = 0$, thus $\Delta_k(F, P_D) = 0$, which indicates the system reaches the average consensus point. Then, we introduce Lemma 4.3.2 as below, in order to demonstrate the positive definite property of the $\Delta_k(F, P_D)$ when $(F, P_D) \in \Omega(f_a) - (f_a 1_n, 0_n)$.

Lemma 4.3.2: If a dynamic digraph is jointly strongly connected during each time interval, there is a finite switching times κ happens in $[k, k+1]$, when $V(F, P_D)$ and $\Delta_k(F, P_D)$ both satisfy the strictly positive condition.

Since the preconditions of positive definite property of $\Delta_k(F, P_D)$ and $V(F, P_D)$ are based on the non-decreasing property of minimum state, it satisfies $\underline{m}(f(k)) < \underline{m}(f(k+\kappa))$. The proof of Lemma 4.3.2 relies on the graphical condition of jointly strongly connected topology, dynamic state information and surplus updating as described in equations (4.3.23) and (4.3.24), which is organized by two steps. Firstly, suppose that some nodes in a network have positive surplus, all nodes will then have positive surplus in a finite time, due to a jointly strongly connected graph. Secondly, by using the positive surplus, the node having a minimum state of the updated graph will not decrease with the non-negative property of the minimum state. More detailed proof can be found in [118].

Proof. Assume that $\mathcal{G}(k)$ denotes a dynamic communication network under a multi-agent system, which is jointly strongly connected. We then define a Lyapunov candidate function (Equation 4.3.34) and an auxiliary function (Equation 4.3.35) with both satisfying the condition in Lemma 4.3.2. According to second method of Lyapunov, the stability of presented algorithm (4.3.23) and (4.3.24) is verified and a uniform average consensus is achievable. □

On the other hand, the consensus problem under the fixed topology can be considered as special case of switching topology, when switching sequences κ is sufficient during each iteration and dynamic topology $\mathcal{G}$ is jointly strongly connected. There-

fore, it is potential to apply the proof used in the switching topology to the consensus problem under fixed topology. Intuitively, let us define another an auxiliary function Δ' as below:

$$\Delta'(F, P_D) = \inf V(F(k), P_D(k)) - V(F(k+1), P_D(k+1)) \tag{4.3.36}$$

The inequality in Lemma 4.3.1 can be revised as

$$V(F(k+1), P_D(k+1)) - V(F(k), P_D(k)) \leq -\Delta'(F(k), P_D(k))$$

Following from Lemmas 4.3.1 and 4.3.2 with the function defined in Equation (4.3.36) and the function V defined in 4.3.34, it can prove that the average consensus is achieved.

4.3.5 Algorithm implementation

It is worth emphasizing that the state feedback gain matrix $E = \{\epsilon_i\}$ is a crucial parameter that dominates the stability and convergence rate of the distributed algorithm. Suppose that all elements in matrix E are identical, Figure 4.3.2 illustrates the change of convergence time with feedback gain ϵ_i under a fixed topology. It can be clearly seen that the convergence time decreases exponentially when $0.1 < \epsilon_i < 3.6$. Then, the convergence rate is growing slightly when ϵ_i rises to 9 and the system becomes unstable when $\epsilon_i > 9$. Apparently, the optimal value of ϵ_i lies at the corner point of the curve, which is 3.6, resulting in a fastest consensus time and 35 iterations associated with settling time. Similar trends are also found for the revised algorithm under the time-varying topology. Essentially, reference [120] concludes that the second largest eigenvalue of the system matrix governs the convergence speed. With the

increase of feedback gain, the second largest eigenvalue decreases in the beginning and increases and eventually divergence occurs.

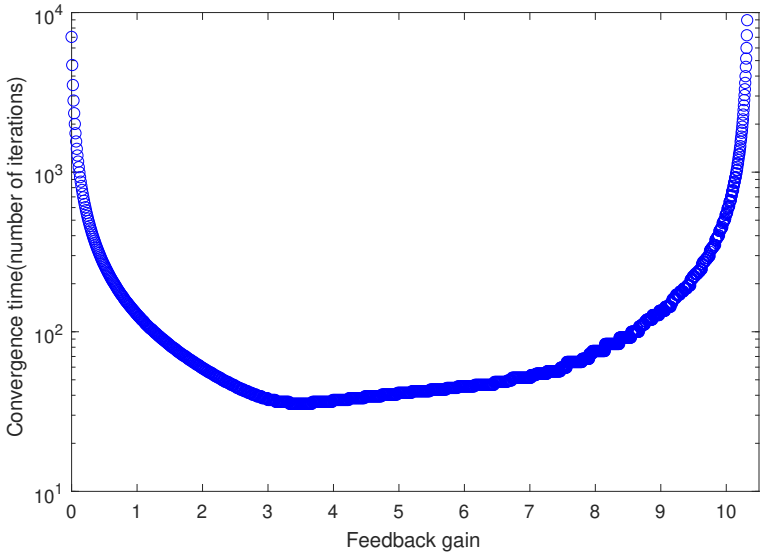

Figure 4.3.2: Convergence time with varying feedback gain

The implementation of distributed algorithm is explained in flow chart 4.3.3. Based on the communication network under MAS framework, the stochastic matrix is determined with the definition in equation 4.1.6. The initial conditions of state variables are specified in equation (4.3.14). Let set a certain simulation time T_s, the duration of each control cycle is T_c, where $T_c = 0.01s$. During each control cycle, each agent implements the distributed algorithm to calculate the desired frequency and the power reference for each HVAC, which is composed of three function blocks, namely communication block, optimal frequency discovery block and local information update block. Communication block exchanges information of frequency and the estimated power mismatch with neighbouring agents according to the topology. The optimal frequency discovery block updates its state according to equation (4.3.11).

Local information update block calculates the HVAC power consumption and local power mismatch reference signals, as calculated by equation (4.3.13) (4.3.12). Afterwards, the estimated power output of HVAC system should be constrained by the operating power range for different HVACs, referred to equation (4.3.20). The power reference signal will be provided to the lower controller of HVAC. The lower controller is responsible for controlling the associated component to track the frequency and power reference signals, which is specifically described in Section 4.2.2 and Figure 4.2.2. Until the simulation time T_s is over, the algorithm simulation is completed.

4.4 Simulation studies and discussion

The microgrid system under test is a 5-bus system, as shown in Figure 2.5.1. Each bus connects a distributed generator, HVAC unit and other uncontrollable loads. Circuit breaker is utilized to realize switching of the microgrid between the island mode and grid-connected mode. In the Figure 2.5.1, thick solid lines and lines with arrow represent the local buses and power flow, respectively, while the thin solid lines show the information exchange between agents. The blue dotted lines with arrow represent the reference information issued by the centralized controller to each HVAC device. Suppose that the system operates in island mode, which has no power exchange with the main grid. The interaction topology matrix regarding the communication topology can be determined with equation (4.1.6). Referring to specifications of typical HVAC systems with their frequency-power characteristics curves, table 4.4.1 gives the parameters of HVAC capacities and power generation of local buses. The feedback gain ϵ_i

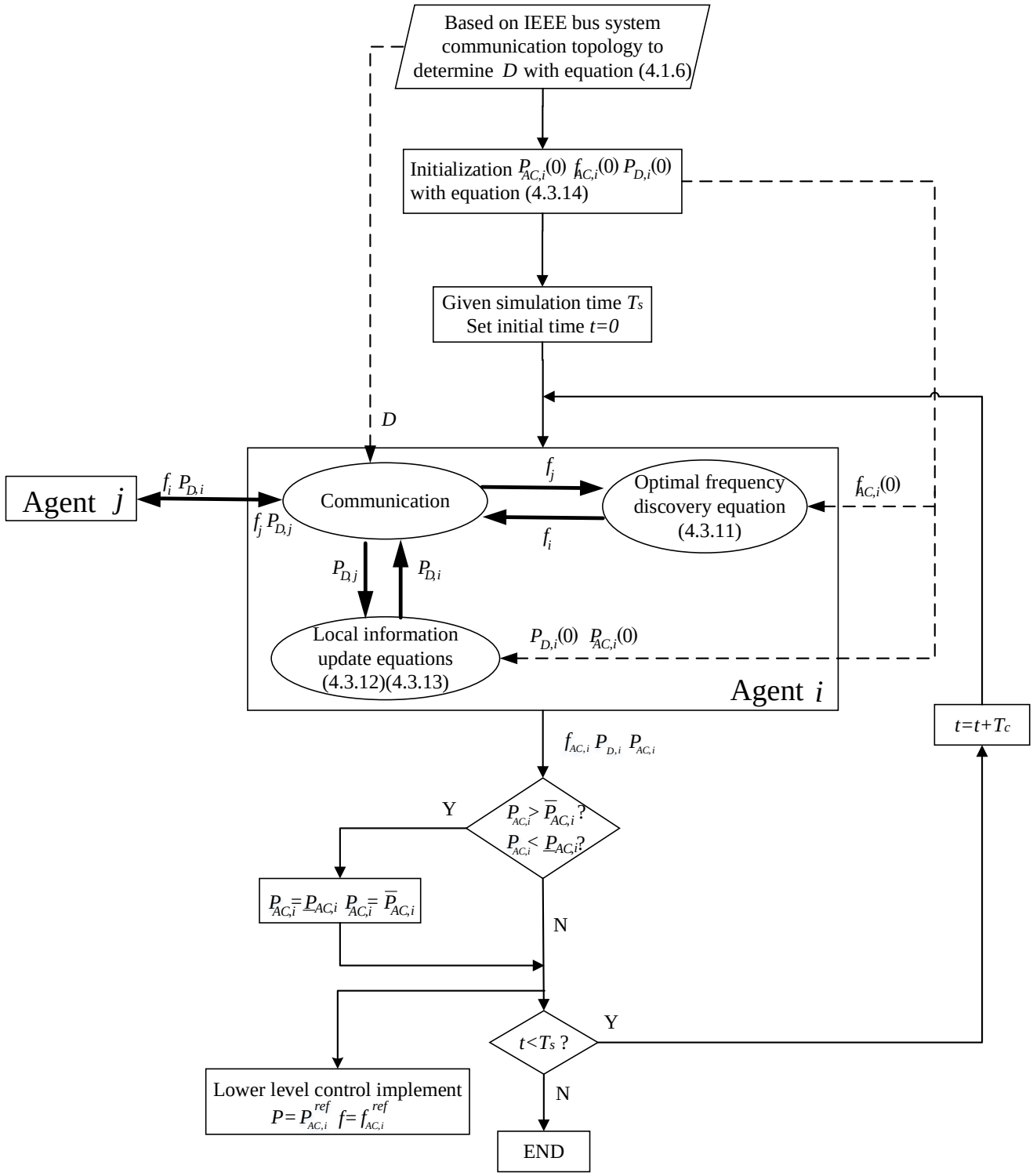

Figure 4.3.3: Flow chart of a distributed algorithm implementation

Table 4.4.1: Parameters of the HVAC in 5-bus system

	u_i	v_i	$\overline{P}_{AC,i}(kW)$	$\overline{P}_{AC,i}(kW)$	$P_{G,i}(0)(kW)$
Bus1	0.057	-0.995	2	0.5	0.943
Bus2	0.07	-1.12	4.8	2	2.64
Bus3	0.04	-0.75	3.5	0.2	3.25
Bus4	0.06	-1.06	4	1.6	1.64
Bus5	0.035	-0.558	4.5	1	3.08

for each bus is assumed identical to simplify the problem. Based on equation (4.3.14) and HVAC specifications, initial values are selected as $F(0) = [34, 57, 28, 45, 67]$ Hz, $P_D(0) = [0, 0, 0, 0, 0]$ kW, $P_G(0) = [0.943, 2.64, 3.25, 1.64, 3.08]$ kW. Referred to the trend of convergence rate against feedback gain as shown in Figure 4.3.2, E is supposed to be a scalar matrix with all its main diagonal entries $\epsilon = 3.6$ in the case studies unless otherwise specified. In this section, the feasibility of the proposed algorithms (4.3.18) and (4.3.21) for power constraint and unconstrained cases are firstly studied in Case 1 and Case 2, respectively. Then, the power unconstrained case is revised to test the time-varying power generation scenarios caused by renewable energy generators, which is simulated in Case 3. In Case 4, the robustness of the algorithms is discussed when the HVAC is considered to be broken down or removed from the microgrid system in order to evaluate the anti-damage capability of the microgrid. Additionally, a IEEE 30-bus systme is introduced to undertake the scalability test for cooperative algorithm as shown in Case 5. The performance of the network with time-varying topology to verify the algorithm (4.3.25) is lastly assessed and demonstrated in Case 6. All of simulations are performed with MATLAB/SIMULINK.

4.4.1 Case study 1: with no HVAC constraints

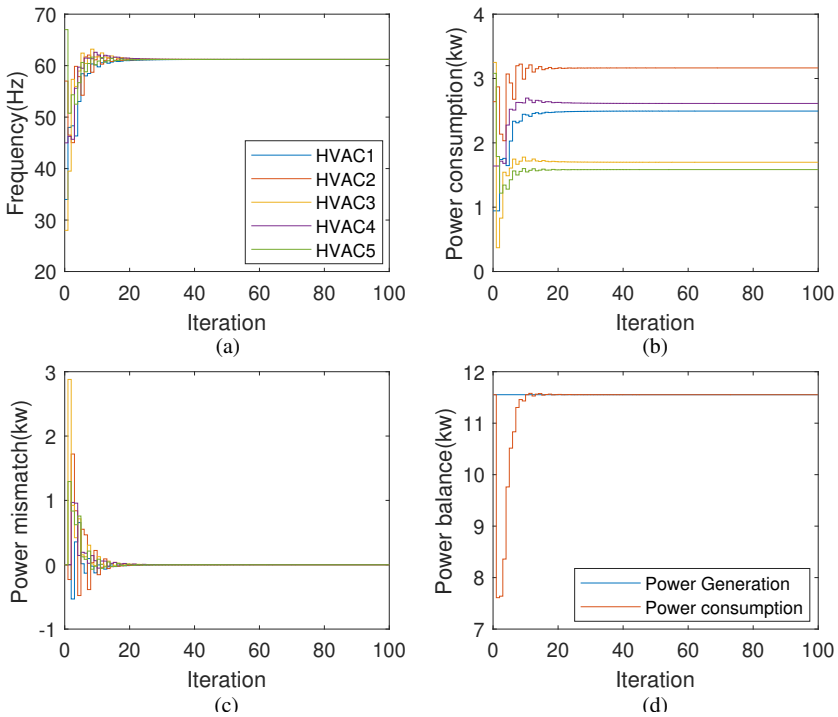

Figure 4.4.1: Results of HVAC-based consensus algorithm without power constraints: (a) Frequency; (b) HVAC power consumption; (c) Estimated power mismatch and (d) Power balance. (The legends in (a) adapts to (b) and (c) in the figure; this also applies to the subsequent cases)

In this case study, power constraints of HVAC units are not imposed. Figure 4.4.1 shows the update of frequency signal, power consumption, local bus supply-demand mismatch and total energy consumption (as demanded to be 11.55 kW in total). After 35 iterations, local power mismatch goes to zero, as shown in Figure 4.4.1(c), while power consumed matches the power supplied as shown in Figure 4.4.1(d). The operating frequency of all HVAC units converges to a common value $f^* = 60.206$ Hz, as seen from Figure 4.4.1(a). The power consumption for each HVAC is $P_{AC,1} = 2.494$

kW, $P_{AC,2} = 3.164$ kW, $P_{AC,3} = 1.698$ kW, $P_{AC,4} = 2.612$ kW, and $P_{AC,5} = 1.584$ kW, respectively, as seen from Figure 4.4.1(b). It is noted that the power output of the HVAC 1 should be saturated if power constraints are applied.

4.4.2 Case study 2: with HVAC constraints

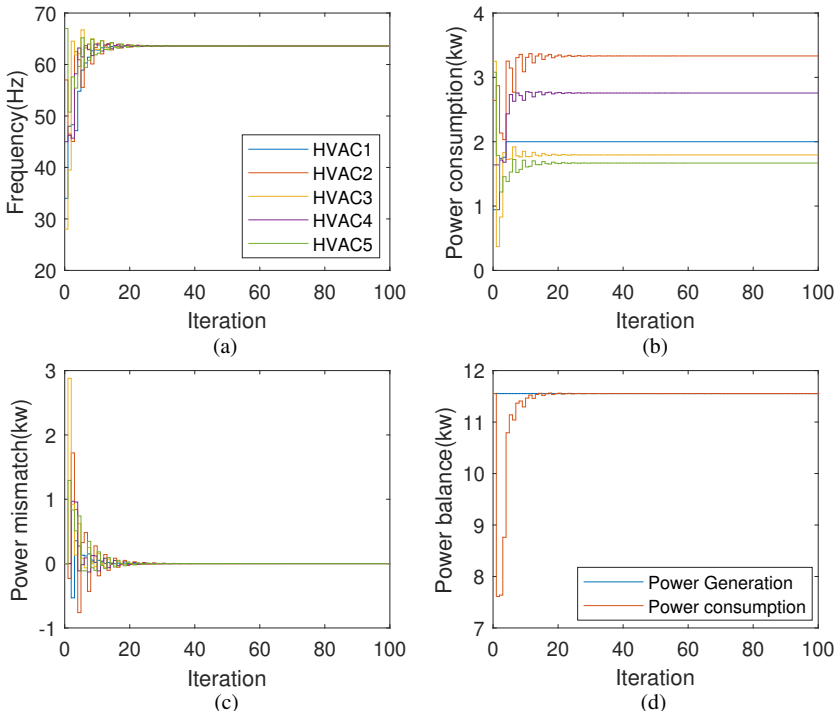

Figure 4.4.2: Results of HVAC-based consensus algorithm with power constraints: (a) Frequency; (b) HVAC power consumption; (c) Estimated power mismatch and (d) Power balance.

Following results in Case 1, Figure 4.4.2 illustrates results for the case considering HVAC power constraint. Also after 35^{th} iterations, the units converge to a new frequency, which in this case $f^* = 63.6146$ Hz. The power consumption for each HVAC unit is $P_{AC,1} = 2$ kW, $P_{AC,2} = 3.333$ kW, $P_{AC,3} = 1.795$ kW, $P_{AC,4} = 2.757$ kW, $P_{AC,5} =$

1.795kW respectively. Note that the power of HVAC 1 becomes saturated now after 5 iterations and the optimal frequency has a slight increase from 60.2061 Hz to 63.6146 Hz. The unsaturated HVAC units share more power with the growing frequency to compensate the effect of saturated HVAC device. However, the performance of local power mismatch and power balance for the entire system is not affected, as can be seen from Figure 4.4.2(c)(d)

4.4.3 Case study 3: Dynamic test

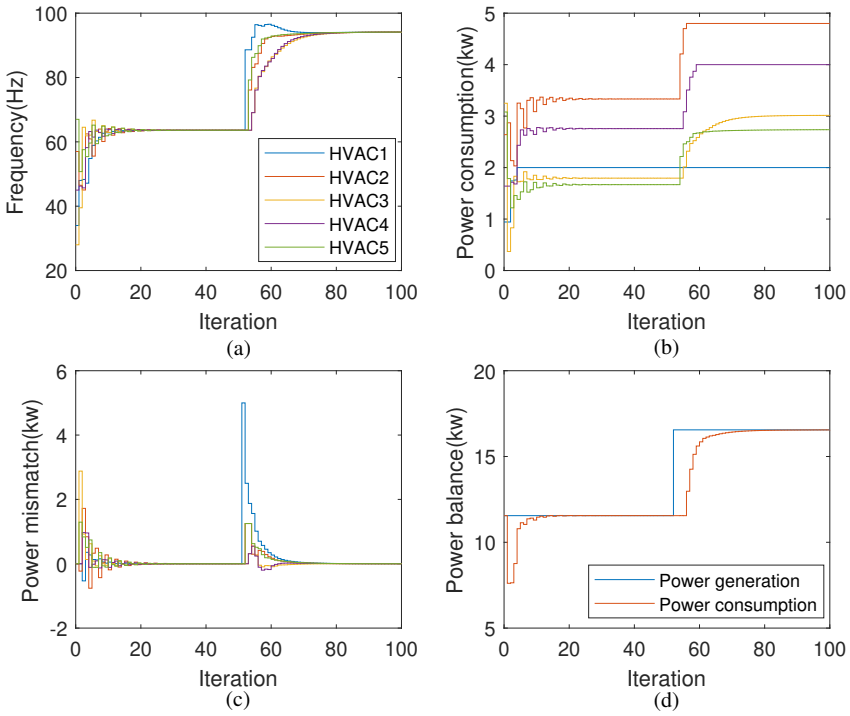

Figure 4.4.3: Results of HVAC-based consensus algorithm under time-varying power generation: (a) Frequency; (b) HVAC power consumption; (c) Estimated power mismatch and (d) Power balance.

This case investigates performance of the proposed algorithms under the time-

varying power generation, meaning there is a dynamic change for the supply-demand mismatch due to the presence of intermittent and uncontrollable renewable generators. We purposely increase 5 kW power generation (ΔG) at 1$^{\text{st}}$ local bus at the 50$^{\text{th}}$ iteration.

$$P_{G,i}(50) = \begin{cases} P_{G,i}(50) + \Delta G, & i = 1 \\ P_{G,i}(50), & i = 2,3,4,5 \end{cases} \tag{4.4.1}$$

As can be seen from Figure 4.4.3, before the 50$^{\text{th}}$ iteration, their transient response is the same as in Case 2. After the 50$^{\text{th}}$ iteration, consensus frequency increases from 63.61 Hz to 94.12 Hz to accommodate this power generation increase. The consensus power consumed for HVAC devices are now $P_{AC,1} = 2$ kW, $P_{AC,2} = 4.8$ kW, $P_{AC,3} = 3.014$ kW, $P_{AC,4} = 4$ kW, $P_{AC,5} = 2.736$ kW, respectively. These non-saturated HVAC units take more power to share the increased power generation due to power being saturated by those units (HVAC 1 and HVAC 4).

4.4.4 Case study 4: Anti-damage test

In this case, the HVAC fault is emulated to assess the robustness of the algorithm. It is assumed that at the 50$^{\text{th}}$ iteration, HVAC 1 fails, where a zero power is assigned to HVAC 1 before the next iteration. Thus, we define $\overline{P}_{AC,1}(50) = \underline{P}_{AC,1}(50) = 0$. The consensus frequency value increases up to 73.37 Hz due to the higher energy share for the remaining four HVACs (Figure 4.4.4(a)). Note that the simulated frequency is specified for faulty HVAC unit as a reference value. Practically, the faulty HVAC unit would not be able to operate at the specified frequency. The power consumed after the fault is $P_{AC,1} = 0$ kW, $P_{AC,2} = 4.016$ kW, $P_{AC,3} = 2.185$ kW, $P_{AC,4} = 3.342$ kW,

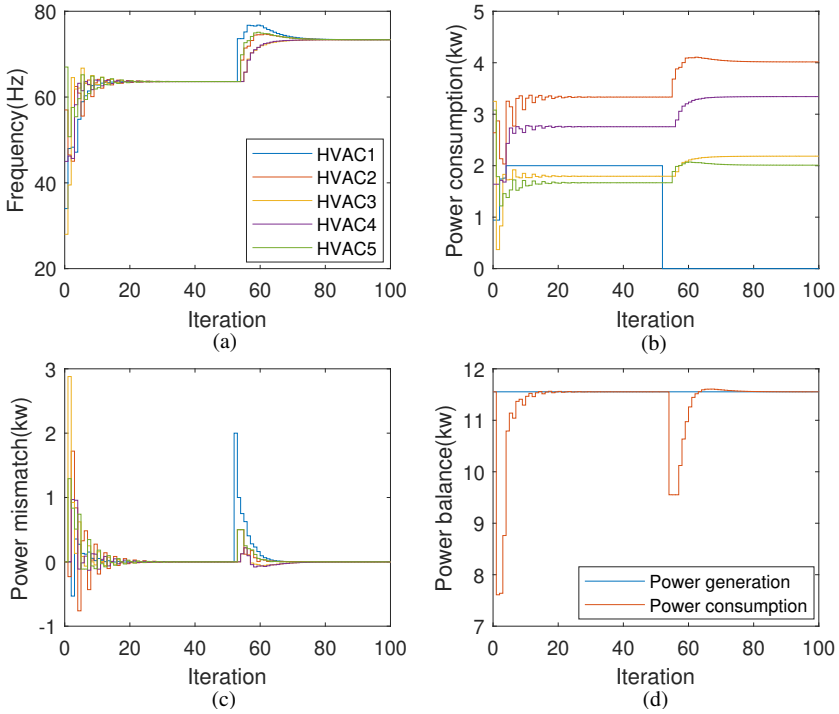

Figure 4.4.4: Results of HVAC-based consensus algorithm under anti-damage test: (a) Frequency; (b) HVAC power consumption; (c) Estimated power mismatch and (d) Power balance.

$P_{AC,5} = 2.01$ kW (Figure 4.4.4(b)). The performance shows that all power demands to HVACs are still within their power boundaries. The balance between the total power generation and load demand can still be achieved after the breakdown fault of a HVACs appears.

4.4.5 Case study 5: Scalability test

In order to explain the feasibility of the proposed approach for a large scale power system, the key point is to render the algorithm to converge in a timely manner. This case is conducted under IEEE 30-bus system (Figure 4.4.5) with 30 HVACs

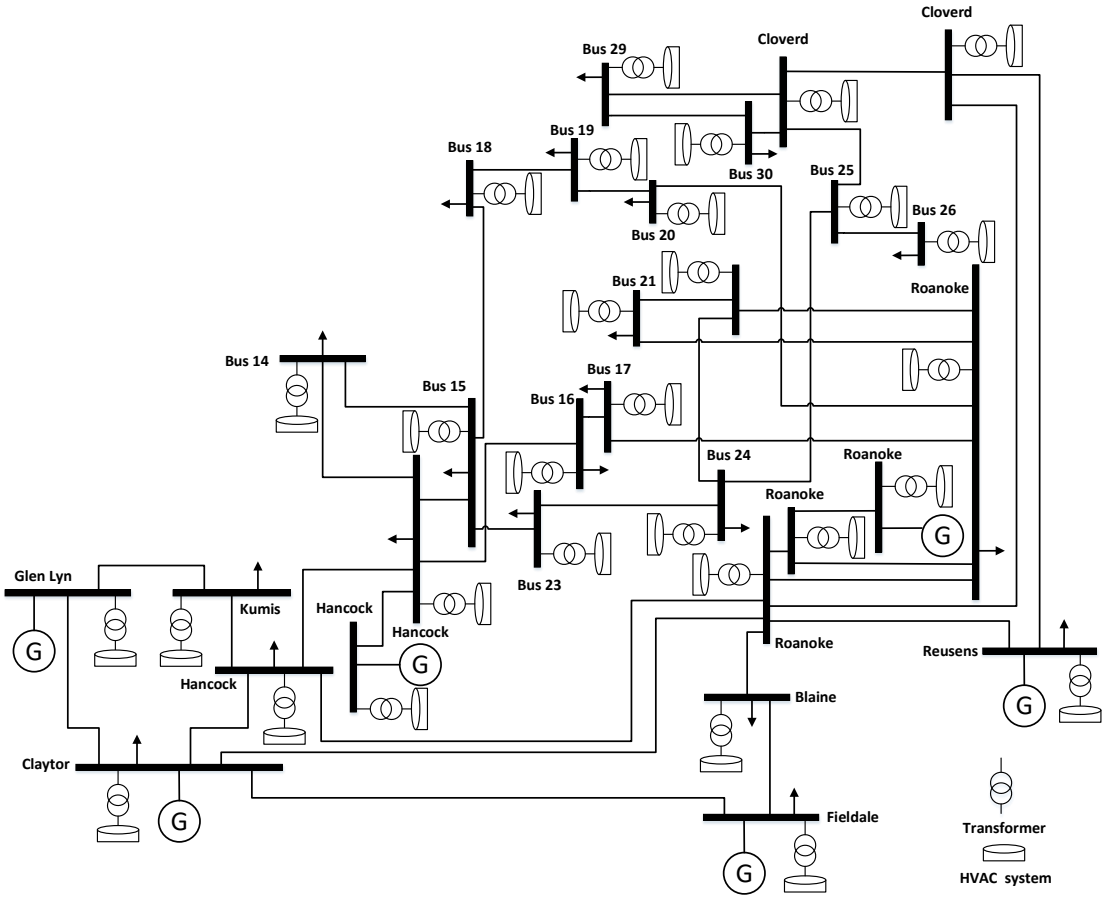

Figure 4.4.5: IEEE 30-bus system with multiple HVAC systems

connected to each bus line. The simulation parameters are adopted from [121] and the total power supply is set as 58 kW.

The designed communication network is strongly connected undirected graph with 30 bi-directional edges, which might be different with a physical power network. Thus, the associated stochastic matrix is determined by equation 4.1.6.

The simulation results are shown in Figure 4.4.6, the proposed algorithm converges within 600 iterations. The time consumed in a single cycle unit depends on the hardware and software implementation, such as computer and communication

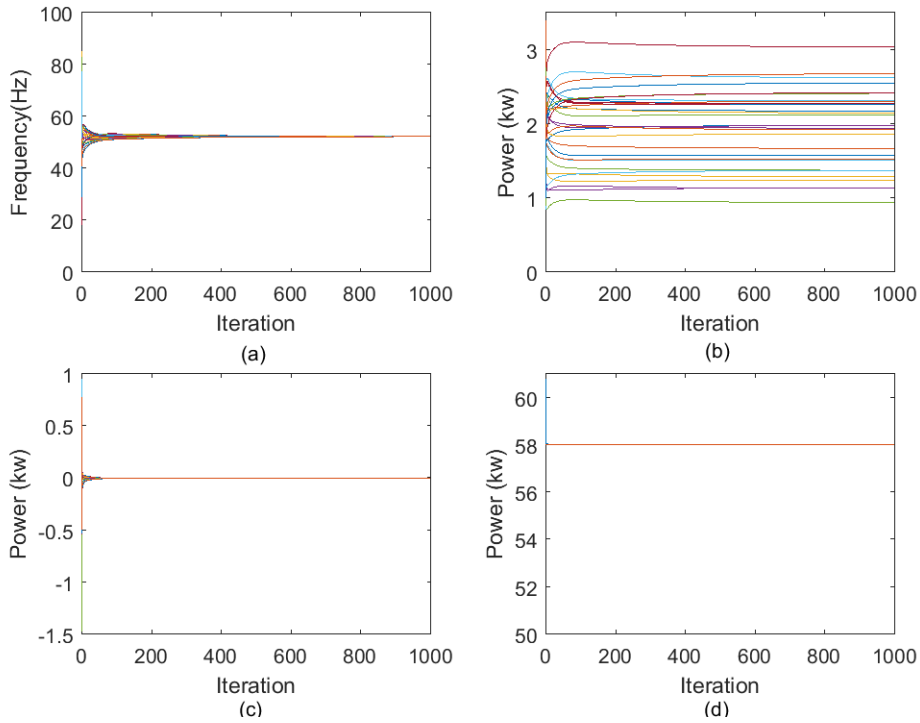

Figure 4.4.6: Results of HVAC-based consensus algorithm under scalability test: (a) Frequency; (b) HVAC power consumption; (c) Estimated power mismatch and (d) Power balance.

network, the efficiency of coding and compliers. Thus, the proposed approach shows a good prospect for large scale power system.

4.4.6 Case study 6: Switching topology test

In order to identify the effectiveness of the algorithm under the time-varying topology, we suppose the communication among HVAC units is a dynamic network in this case. Let define that the interaction topology is switching randomly within the set $\mathcal{G}(\mathcal{V}, \mathcal{E}) = \mathcal{G}_a, \mathcal{G}_b, \mathcal{G}_c$ at each iteration, as shown in Figure 4.4.7, where the associated matrices D_a, D_b, D_c are given. Apparently, the time-varying topology is a jointly

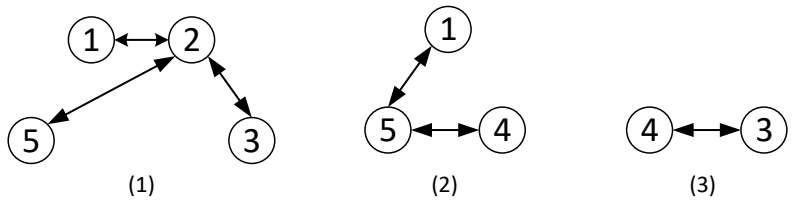

Figure 4.4.7: Switching topologies

strongly connected network, which satisfies the consensus condition. The results show that values at steady-state conditions are the same as those in Case Study 1 (Figure 4.4.8(a),(b)). However, the stability is not able to be achieved until the 50^{th} iteration, due to exchange of the intermittent information. Therefore, the algorithm presented in equations (4.3.23) and (4.3.24) under a dynamic topology will restrict the efficiency of information broadcast and thus increase the convergence time.

$$D_a = \begin{pmatrix} \frac{1}{2} & \frac{1}{2} & 0 & 0 & 0 \\ \frac{1}{4} & \frac{1}{4} & \frac{1}{4} & 0 & \frac{1}{4} \\ 0 & \frac{1}{2} & \frac{1}{2} & 0 & 0 \\ 0 & 0 & 0 & 1 & 0 \\ 0 & \frac{1}{2} & 0 & 0 & \frac{1}{2} \end{pmatrix} \quad D_b = \begin{pmatrix} \frac{1}{2} & 0 & 0 & 0 & \frac{1}{2} \\ 0 & 1 & 0 & 0 & 0 \\ 0 & 0 & 1 & 0 & 0 \\ 0 & 0 & 0 & \frac{1}{2} & \frac{1}{2} \\ \frac{1}{4} & 0 & 0 & \frac{1}{4} & \frac{1}{2} \end{pmatrix} \quad D_c = \begin{pmatrix} 1 & 0 & 0 & 0 & 0 \\ 0 & 1 & 0 & 0 & 0 \\ 0 & 0 & \frac{1}{2} & \frac{1}{2} & 0 \\ 0 & 0 & \frac{1}{2} & \frac{1}{2} & 0 \\ 0 & 0 & 0 & 0 & 1 \end{pmatrix}$$

4.5 Pre-scheduled energy dispatch scheme for HVAC systems

Considering the 24-hour solar radiance curve obtained in Figure 3.3.4, the pre-schedule energy dispatch scheme for each HVAC systems is developed, as shown in Figure 4.5.1.

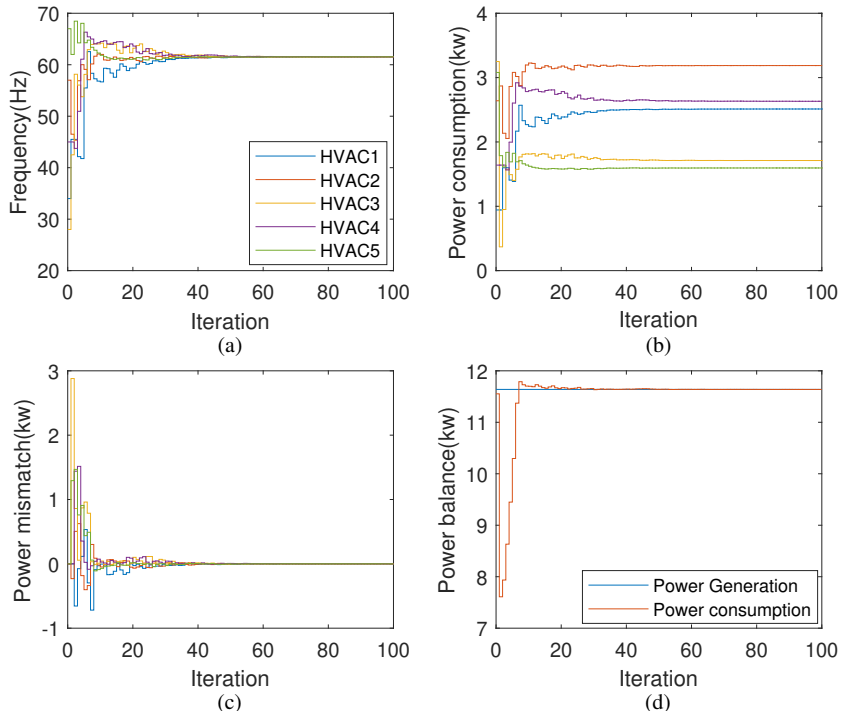

Figure 4.4.8: Results of revised cooperative algorithm under switching topology: (a) Frequency; (b) HVAC power consumption; (c) Estimated power mismatch and (d) Power balance.

Since the solar power is updated every 3 hours, all of state variables change every 3 hours correspondingly. Figure 4.5.1(a)(b) show the dynamic of the compressor frequency and power consumption of the HVAC devices in a day. Technically, the power reference signal will be sent to lower controller of each HVAC system through the interaction topology and the electrical circuit of HVAC unit is required to generate associated control signal for the compressor in order to achieve the desired power output. Figure 4.5.1(c) indicates that power mismatch for each local bus can be alleviated after each solar power generation update. The negative power appeared at 15^{th} hour results from the reduction in solar power generation. Figure 4.5.1(d)

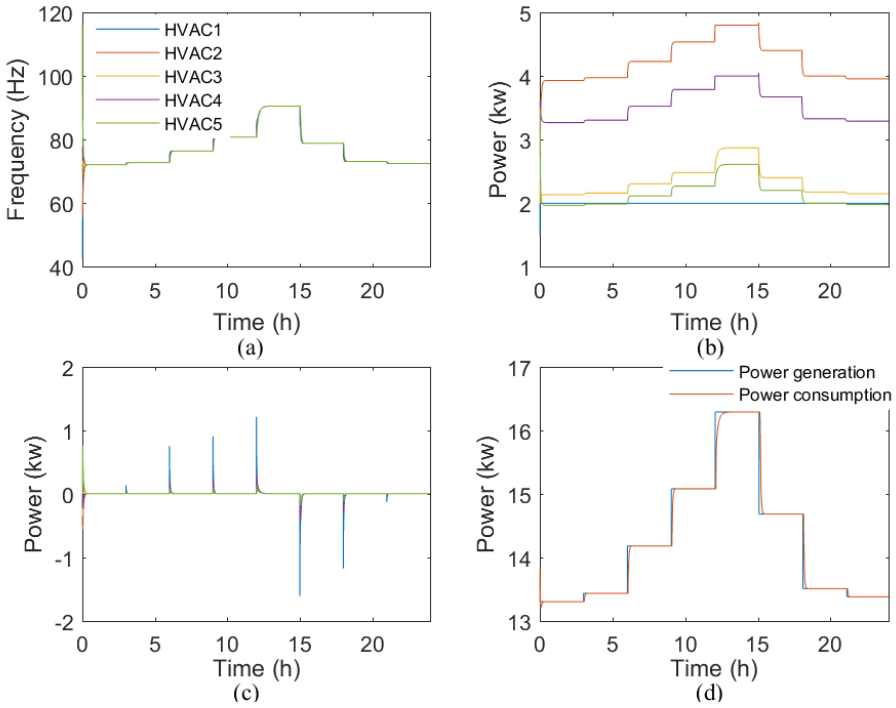

Figure 4.5.1: Results of HVAC-based consensus algorithm under 24-hour solar power forecasts: (a) Frequency; (b) HVAC power consumption; (c) Estimated power mismatch and (d) Power balance.

describes the renewable power generation can be dynamically balanced through the demand response of distributed HVAC systems. The simulation performance indicates that the proposed algorithm possesses good robustness and dynamics to overcome the weather uncertainty.

4.6 Summary and discussion

In this chapter, an energy dispatch scheme for HVAC systems is presented by designing an upper controller based on a MAS-based distributed algorithm, in order to eliminate

power imbalance due to the intermittent nature of the solar power and system fault. Algorithms are designed to manage HVAC units in a cooperative manner through the communication topology, based on the supply-demand mismatch of local bus lines. Furthermore, it is found that the state feedback gain has a significant influence on the convergence rate and stability of the control strategy. The stability proof and consensus condition of the algorithm under fixed topology and switching topology are presented, respectively.

A microgrid of 5-bus system is built to carry out the simulation studies. The tests are performed using MATLAB R2017a/Simulink, running on a laptop with a 2.59 GHz Intel Core i7 CPU and 8G RAM memory. The effectiveness of presented algorithms with or without power constraints are evaluated. The solutions converge to a common value in finite time duration. It is worthwhile to note that when arbitrary HVAC units are saturated, the unsaturated HVACs will increase the power consumed to maintain the power balance in the entire system. The renewable energy uncertainty and system fault are covered in cases studies to verify the dynamics and robustness of distributed algorithm. Moreover, a IEEE-30 bus system is introduced to evaluate the scalability of the proposed algorithm. For the revised algorithm under switching topology, it is found that the convergence time is longer than the fixed topology, due to the intermittent information exchange. Finally, an optimal energy dispatch scheme is developed for each HVAC system with the daily forecasting data of the solar power generation.

Chapter 5

Price-Comfort Optimization Algorithm

The utilization of distributed HVAC system to alleviate the power imbalance within the microgrid may sacrifice the comfortability and increase electricity costs for residential users. In this chapter, a price-comfort optimization model is established to minimize the discomfort level and electricity payment by introducing a virtual price variable to adjust the real time-of-use (ToU) price, whilst maintaining the global supply-demand match. An advanced proportional-integral-derivative (PID)-based distributed algorithm is developed to address the optimization problem, with the key parameters being determined. By comparing with ordinary distributed approach, the advantages of the proposed algorithm capable of reducing the steady-state error are illustrated. Case studies are carried out at 5-bus and IEEE 57-bus systems to test the algorithm under time-varying ToU price, variable renewable generation and the scalability. Section 5.1 introduces cost optimization approach of HVAC system

involving the discomfort model and electricity cost model. A PID-based distributed model is then presented in Section 5.2, where the solution of the optimization problem is given. Case studies and results are presented and discussed in Section 5.3, followed by a summary in Section 5.4.

5.1 Cost function model of HVAC system

As for customers, there is a trade-off between the electricity bill and discomfort level. A discomfort cost model and electricity payment model are introduced and a cost optimization model for HVAC system is formulated in this section.

5.1.1 Discomfort cost model

The consumers tend to schedule the power consumption of various loads in response to time-varying ToU price. Regarding shiftable appliances, such as washing machine, this type of appliance has flexible start time and operates continuously with constant power. It is an option to operate at time slots with lower electricity price in order to reduce the total payment. The appliances that also attract consumers are those schedulable appliances, such as HVACs in our study, which can make available with a flexible power demand within their scheduling horizons. Therefore, the use of these appliances will affect the level of comfort to end users. In this chapter, we only discuss about the schedulable appliance with controllable power output. Mathematically, the discomfort cost can be demonstrated according to the operation state of loads. Invoked by quality loss function in Taguchi's Quality Engineering Handbook [122],

the discomfort cost model $C_{a,i}$ for i^{th} HVAC unit can be denoted as a Taguchi loss function:

$$C_{a,i}(P_{AC,i}(t)) = \omega_{a,i}(P_{AC,i}(t) - \hat{P}_{AC,i})^2 \tag{5.1.1}$$

where $\omega_a(i)$ is a constant coefficient for i^{th} HVAC unit, $P_{AC,i}(t)$ is the power output of the i^{th} HVAC unit at time t and $\hat{P}_{AC,i}$ denotes the normal power consumption at the comfortable level. It can be observed that quadratic model of the loss function, as given in eq (5.1.1) can be minimized when $P_{AC,i}(t) = \hat{P}_{AC,i}$. The cost function will be increased as $P_{AC,i}(t)$ deviates from $\hat{P}_{AC,i}$. Taguchi loss function is used to define the relationship between the comfort loss and the deviation of power consumption from the normal power consumption. Suppose that the maximum power deviation is defined as Δ, which indicates the maximum operating power range of HVAC unit is $\hat{P}_{AC,i} \pm \Delta$. Once the system operates at the extreme power either $\hat{P}_{AC,i} + \Delta$ or $\hat{P}_{AC,i} - \Delta$, there are some actions needing to be taken by the consumers. Assume that the cost of action is A when $P_{AC,i}(t) = \hat{P}_{AC,i} + \Delta$ or $P_{AC,i}(t) = \hat{P}_{AC,i} - \Delta$, the parameter $\omega_a(i)$ can be defined as:

$$\omega_a(i) = \frac{A}{\Delta^2} \tag{5.1.2}$$

The above model clarify the discomfort cost model caused by HVAC units regarding the consumers [123].

5.1.2 Electricity price model

The electricity price in a certain scheduling horizon will be announced to the consumer one day ahead. The electricity cost $C_{p,i}$ regarding HVAC system i in unit time can

be estimated as:

$$C_{p,i}(P_{AC,i}(t)) = \rho(t)P_{AC,i}(t) \tag{5.1.3}$$

where $\rho(t)$ denotes the ToU price at time t. In reality, some consumers may tend to control the power consumption of schedulable loads to reduce the total electricity cost, even at the cost of comfortability.

5.1.3 Price-discomfort cost function model

With the aims of maximizing the customer's benefits in a comfortable and economical way whilst compensating the power mismatch, we formulate the power scheduling problem into the following optimization problem:

$$\begin{aligned} \min \quad & \nu_1 \sum_{i \in S_{AC}} C_{a,i}(P_{AC,i}) + \nu_2 \sum_{i \in S_{AC}} C_{p,i}(P_{AC,i}) \\ s.t. \quad & P_d = \sum_{i \in S_{AC}} P_{AC,i} \\ & \underline{P}_{AC,i} \leqslant P_{AC,i} \leqslant \overline{P}_{AC,i} \end{aligned} \tag{5.1.4}$$

The weighting coefficients ν_1 and ν_2 satisfy $\nu_1 + \nu_2 = 1$, which illustrate the trade-off between the economic loss and the discomfort level. There are three operation schemes with different parameter settings, as referred in [123]. Either one or both are considered in the model. Here, both electricity payment and discomfort are equally regarded as factors for consumers. Therefore, we define $\nu_1 = \nu_2 = \frac{1}{2}$ to realize an equal weighting for the payment and comfortability. As it was defined, $\underline{P}_{AC,i}$ and $\overline{P}_{AC,i}$ are the upper and lower bound of i^{th} HVAC system, respectively. The equality constraints indicate the power balance between power mismatch of the grid and the

power consumption of HVAC systems, whereas, the inequality describes the local power boundary for each HVAC unit to meet. Although the multiple HVAC units with various capacity have different flexibility and efficiency, we assume that all of the participants have equal weight in terms of their contribution.

The objective function in eq (5.1.4) can be rewritten as:

$$\min \quad \sum_{i \in S_{AC}} C_i(P_{AC,i}) \tag{5.1.5}$$

$$s.t. \quad P_d = \sum_{i \in S_{AC}} P_{AC,i} \tag{5.1.6}$$

$$H_i(P_{AC,i}) = (\overline{P}_{AC,i} - P_{AC,i})(\underline{P}_{AC,i} - P_{AC,i}) \leqslant 0 \tag{5.1.7}$$

where $C_i(P_{AC,i}) = \frac{1}{2}\rho(t)P_{AC,i} + \frac{1}{2}\omega_{a,i}(P_{AC,i} - \hat{P}_{AC,i})^2$.

5.2 PID-based consensus algorithm design

The formulated optimization problem in eq (5.1.5) is a convex function with equality and inequality constraints. The solution set of the constrained convex optimization problem is firstly characterized by Karush-Kuhn-Tucker (KKT) optimality condition. Then, a PID-based distributed cooperative algorithm is proposed for discovering the optimal solution of energy management problem.

5.2.1 Solution set for distributed energy management

As for problem (5.1.5)-(5.1.7), let define an Lagrangian function L

$$L = \sum_{i \in S_{AC}} \frac{1}{2}\omega_{a,i}P_{AC,i}^2 + \left(\frac{1}{2}\rho(t) - \omega_{a,i}\hat{P}_{AC,i}\right)P_{AC,i} + \frac{1}{2}\omega_{a,i}\hat{P}_{AC,i}^2 - \mu_i\left(\sum_{i \in S_{AC}} P_{AC,i} - P_d\right) \tag{5.2.1}$$

where μ_i is the so-called Lagrangian multiplier of problem (5.1.4) and let define $\mu = \{\mu_1, \mu_2, ..., \mu_n\}$

Note that the inequality constraint (5.1.7) is not considered in augmented function, due to that these local constraints can be treated as a boundary of the problem domain [124]. These inequality constraints can be taken into consideration by introducing additional projection operations. Meanwhile, the convergence analysis would not be affected by this condition, as demonstrated in [125]. We will not repeat it in this thesis. The function (5.2.1) can be rewritten as:

$$L = \sum_{i \in S_{AC}} \frac{1}{2}\omega_{a,i} P_{AC,i}^2 + \left(\frac{1}{2}\rho(t) - \omega_{a,i}\hat{P}_{AC,i} - \mu_i\right) P_{AC,i} + \frac{1}{2}\omega_{a,i}\hat{P}_{AC,i}^2 + \mu_i P_d \quad (5.2.2)$$

It can be noted that the Lagrange multiplier μ_i can be regarded as a virtual price signal to regulate the real ToU price $\rho(t)$, therefore the HVAC systems can be coordinated to achieve a maximum benefit point.

The aim of solving a constrained convex optimization problem is to obtain necessary and sufficient conditions satisfied by an optimum point. Its global optimality is ensured by using Karush-Kuhn-Tucker (KKT) optimality condition [126, 127], as shown below

Lemma 5.2.1: Consider an energy management problem (5.1.5)-(5.1.7) with only one affine equality constraints. Clearly, C_i is a differentiable and convex function on $\mathbb{R}$. The power point $P_{AC}^* = \{P_{AC,1}^*, P_{AC,2}^*, ..., P_{AC,n}^*\} \in \mathbb{R}^n$ is the solution of problem (5.1.5) if there there exist a $\mu^* \in \mathbb{R}$, such that

$$\bigtriangledown C_i(P_{AC}^*) - \mu^* = 0 \quad (5.2.3)$$

$$P_{AC,1}^* + ... + P_{AC,n}^* = P_d \quad (5.2.4)$$

Thus (μ^*, P_{AC}^*) is the KKT point of the Lagrange function (5.2.1) to find the optimal power operation point to address energy management problem [126]. The solution set $\mathcal{Y}^*$ is defined as below:

$$\mathcal{Y}^* = \{(\mu, P_{AC}) \in \mathbb{R}^{2n} | \bigtriangledown C(P_{AC}) - \mu = 0, \quad \sum_{i=1}^{n} P_{AC,i} - P_d = 0\} \tag{5.2.5}$$

where $\mu = [\mu_1, \mu_2, ..., \mu_n]^T$, $\bigtriangledown C(P_{AC}) = [\bigtriangledown C_1(P_{AC,1}), \bigtriangledown C_2(P_{AC,2}), ..., \bigtriangledown C_n(P_{AC,n})]^T$. Since $C_i(P_{AC,i})$ is a convex function, $\mathcal{Y}^*$ is singleton, i,e. the optimization problem has the unique solution.

We can show that following the [128], the saddle point dynamics below converge to the set $\mathcal{Y}^*$

$$\dot{\mu} = \sum_{i=1}^{n} P_{AC,i} - P_d \tag{5.2.6}$$

$$\dot{P}_{AC} = - \bigtriangledown C(P_{AC}) + \mu \tag{5.2.7}$$

That is, for initial state $(\mu(0), P_{AC}(0)) \in \mathbb{R}^{2n}$, every trajectory $(\mu(t), P_{AC}(t))$ converges to $\mathcal{Y}^*$, and eqs (5.2.6), (5.2.7) are a dynamical solver for the optimization problem (5.1.5).

5.2.2 PID-based distributed algorithm design

In this subsection, a distributed scheme is presented for energy management of HVAC system. The power dynamic of HVAC can be written as:

$$u_{AC,i} = \dot{P}_{AC,i}$$

where $u_{AC,i} \in \mathbb{R}$. Our aim is to design the control input of HVAC, such that $u_{AC,i}$ only depends on the local information of agent i and transmit data to neighbouring

HVAC. Then, $P_{AC,i}(t)$ converges asymptotically to the solution set by the optimization problem (5.1.4)

The solution for problem (5.1.4),is the following continuous-time PID-based distributed algorithm:

$$\dot{P}_{AC,i} = - \bigtriangledown C_i(P_{AC,i}) + \mu_i + u_{pid,i} \tag{5.2.8}$$

$$u_{pid,i} = K_P \left(P_d - \sum_{i \in S_{AC}} P_{AC,i} \right) + K_I \int \left(P_d - \sum_{i \in S_{AC}} P_{AC,i} \right) + K_D \frac{\mathrm{d}\left(P_d - \sum_{i \in S_{AC}} P_{AC,i} \right)}{\mathrm{d}t} \tag{5.2.9}$$

$$\dot{\mu}_i = -\Theta_1 \sum_{i \in N_i} a_{ij}(\mu_i - \mu_j) - \Theta_2 \sum_{i \in N_i} a_{ij}(z_i - z_j) \tag{5.2.10}$$

$$\dot{z}_i = \sum_{i \in N_i} a_{ij}(\mu_i - \mu_j) \tag{5.2.11}$$

where Θ_1 and Θ_2 are the positive constants, respectively. K_P, K_I,K_D denote tuning parameters for proportional, integral and derivative controller, respectively. a_{ij} is weighted information flow between agent i and j. z_i is an auxiliary variable for HVAC i. $u_{pid,i}$ is the control signal calculated by PID controller to alleviate the global power mismatch.

The proposed algorithm (5.2.8)-(5.2.11) can be rewritten in a matrix form, such as:

$$\dot{P}_{AC} = - \bigtriangledown C(P_{AC}) + \mu + U_{pid} \tag{5.2.12}$$

$$U_{pid} = \mathbf{1}_n \otimes K_P(P_d - \mathbf{1}_n P_{AC}) + \mathbf{1}_n \otimes K_I \int (P_d - \mathbf{1}_n P_{AC}) + \mathbf{1}_n \otimes K_D \frac{\mathrm{d}(P_d - \mathbf{1}_n P_{AC})}{\mathrm{d}t} \tag{5.2.13}$$

$$\dot{\mu} = -\Theta_1 \mathcal{L}\mu - \Theta_2 \mathcal{L} Z \tag{5.2.14}$$

$$\dot{Z} = \mathcal{L}\mu \tag{5.2.15}$$

where $U_{pid} = [u_{pid,1}, u_{pid,2}, ..., u_{pid,n}]^T$. $\mathbf{1}_n = [1, 1, ...]^T \in \mathbb{R}^n$ and $Z = [z_1, .., z_n]^T$, respectively. $\otimes$ denote the kronecker product. $\mathcal{L}$ is the Laplacian matrix defined by eq (4.1.3). The pseudo code of PID-based distributed algorithm is given in algorithm 2.

The design of the presented algorithm is inspired by the multiple time-scale analysis of the singularly perturbed dynamical system in control theory. Firstly, we assume that (5.2.14) and (5.2.15) run in a faster time scale than the rest of dynamics. We obtain $\dot{\mu} = 0$ and $\mu_i = \mu_j$, as $t \to \infty$. If the PID controller can eliminate the global power mismatch, from (5.2.12), we obtain $\dot{P}_{AC} = - \bigtriangledown C(P_{AC}) + \mu$. This along with $\dot{\mu} = 0$ becomes a copy of saddle-point dynamic (5.2.6) and (5.2.7) which will converge to the solution of problem (5.1.5). We introduce a mismatch estimator $(P_d - \mathbf{1}_n^T P_{AC})$ to observe the global information, where the PID control input u_{pid} is used to adjust the updated power mismatch. In comparison, the control strategy in [128] is not sufficiently robust to adapt to the change of different cases and power imbalance problem in the microgrid fails to be solved. The algorithm (5.2.8)-(5.2.11) solve the problem with the only required information being the state variable of i^{th} HVAC system, such as μ_i, $P_{AC,i}$ and z_i. Each HVAC system is required to send/receive μ_i and z_i to their neighbour HVACs. With addressing the privacy issue of HVACs, the proposed algorithm does not need HVACs to share the gradient of the cost function with neighbouring HVACs. Furthermore, the ToU signal $\rho(t)$ can be regulated by μ_i, so that multiple HVAC systems are coordinated to discover the optimal point.

Remark 5.2.1: Considering the problem in a practical case, various local constraints

can be added into the presented algorithm, such as CoP and maximum/minimum cooling capacity mentioned in Section 4.2. These constraints can be integrated by adding corresponding projection operation.

Algorithm 2 The Pseudo code of PID-based distributed algorithm

Input: $\mathcal{L} = \{\ell_{ij}\}$: Laplacian matrix; ρ: ToU price; Θ_1, Θ_2, K_P, K_I and K_D: Parameters;

Output: Optimal μ_i, z_i and $P_{AC,i}$

1: $P_{AC,i}(0)$, $\mu_i(0)$ and $z_i(0)$: state initialization;

2: **while** $T < T_{set}$ **do**

3: The derivative of state variable $\dot{\mu}_i$, $\dot{z}_i$ update with equation (5.2.10) (5.2.11);

4: Calculate the control signal $u_{pid,i}$ by PID controller with equation (5.2.9), based on the global power mismatch;

5: Update derivative of HVAC power consumption $\dot{P}_{AC,i}$ with (5.2.8)

6: Do integration of $\dot{\mu}_i$, $\dot{z}_i$ and $\dot{P}_{AC,i}$ to update μ_i, z_i and $P_{AC,i}$,respectively;

7: **end while**

The parameters of proportional controller, integral controller and derivative controller have direct impact on the dynamic response of the HVAC systems. In order to simplify the problem, these parameters are identical for each agent. The system performance and convergence time can be set by tuning the proportional parameter K_P. By fixing the value of K_I and K_D for demonstration purpose, different K_P are applied to the HVACs in the 5-bus system, as shown in Figure 5.2.1. It can be seen from the power response in HVAC 1 in Figure 5.2.1(a) that the convergence speed of the system will increase by selecting a higher proportional gain. When the gain is

relatively small, the system stability will be destroyed. Next, the steady state error of the system with different P_I are analysed, by choosing proper value of K_P and K_D for demonstration purpose. As shown in Figure 5.2.1(b), with a small K_I, the global error response of HVAC systems converge to zero in a longer time. Clearly, K_I is an indispensable parameter to control the steady state error. Moreover, the contribution of K_D to reducing overshoot is too limited to be considered.

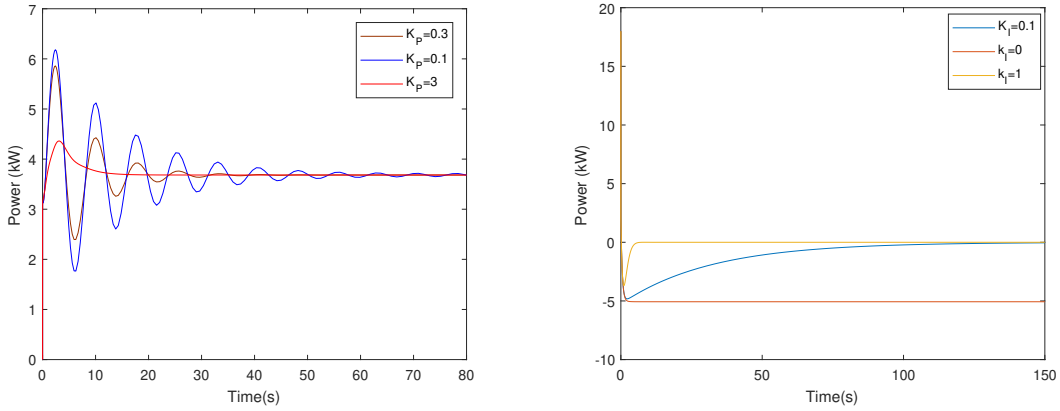

(a) Power consumption for different K_P (b) Power mismatch for different K_I

Figure 5.2.1: The simulation results of HVAC 1 for different K_I, K_P

5.3 Simulation studies and discussion

In this section, four case studies are given to demonstrate the effectiveness of presented algorithm. The microgrid system in Figure 2.5.1 is modified by adding a solar PV connected in Bus 4, as depicted in Figure 5.3.1, which is built in the MATLAB/Simulink. Initially, K_P, K_I and K_P are selected as 3.1, 4 and 1.3, respectively, for all agents, whereas they can be altered to accommodate different cases. In case 1, the algorithm

Table 5.3.1: Parameters of the HVAC in revised 5-bus system

	$\omega_{a,i}$	$\hat{P}_{AC,i}$	$\underline{P}_{AC,i}(kW)$	$\overline{P}_{AC,i}(kW)$
HVAC1	0.4	3.4	2.8	5.2
HVAC2	0.7	3.6	2.8	5.2
HVAC3	0.6	3.5	2.8	5.2
HVAC4	0.8	3.2	2.8	5.2
HVAC5	0.5	3.3	2.8	5.2

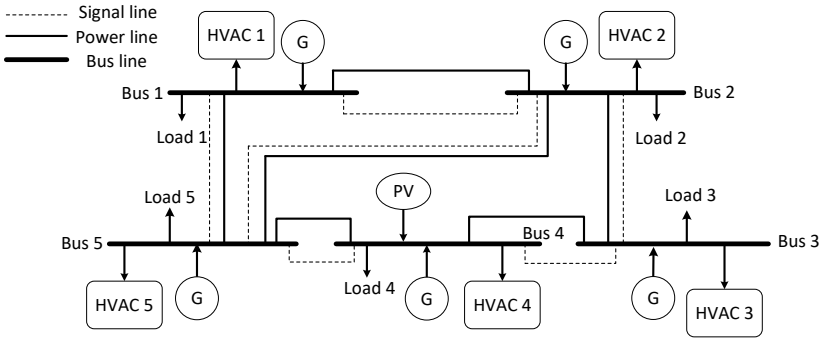

Figure 5.3.1: A modified 5-bus system

is compared with distributed algorithm in [6] to show the outperformance of proposed algorithm. Case 2 tests the convergence of the proposed algorithm to deal with time-varying ToU price. Case 3 is carried out under daily solar power forecasting obtained in Chapter 3. Case 4 investigates the scalability of the algorithm, where an IEEE 57-bus system is tested in MATLAB/Simulink. It is assumed that microgrid system operates in the islanded mode in all cases. The parameter setting of HVAC systems is shown in Table 5.3.1.

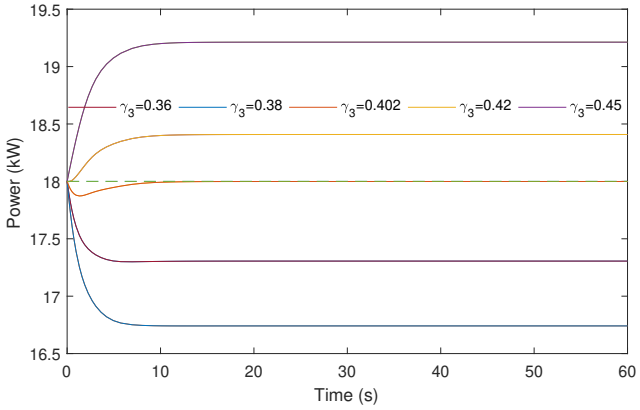

Figure 5.3.2: The power mismatch with parameter variation under algorithm in [6]

5.3.1 Case study 1: the feasibility study of the algorithm

In order to reveal the advance of the proposed algorithm, the algorithm is firstly compared with a continuous distributed algorithm in [6]. In reference [6] a mismatch estimator is introduced to observe the global information and the ToU price is adjusted by the state of BESS so that multiple BESSs are coordinated to discover the most efficient point. Without loss of generality, the ToU price and the supply-demand mismatch are assumed to be a constant value 14.44cent/kWh and 18 kW, respectively. The operation condition is supposed to be same for comparison study. From Figure 5.3.2, it is found that the steady-state error of the global power mismatch greatly depends on the value of γ_3 in [6]. Only if γ_3 is chosen by 0.402, the supply-demand power mismatch (18 kW) can be eliminated with the effects of distributed strategy. Moreover, γ_3 have to be adjusted to adapt to any changes in conditions, such as changes in ToU price or renewable power generations. The performance of proposed algorithm is facilitated by introducing a PID controller to ensure the global mismatch always converges to zero in Figure 5.3.3(c). Figure 5.3.3(a), 5.3.3(b), 5.3.3(d) depict

the incremental cost, output power reference and compressor frequency response of HVAC systems. Additionally, the proposed algorithm guarantees the efficiency and optimality without sacrificing the privacy of each participant.

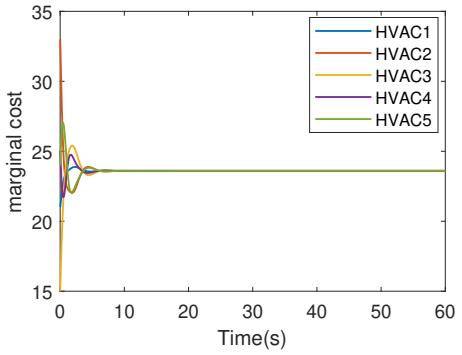

(a) Incremental cost.

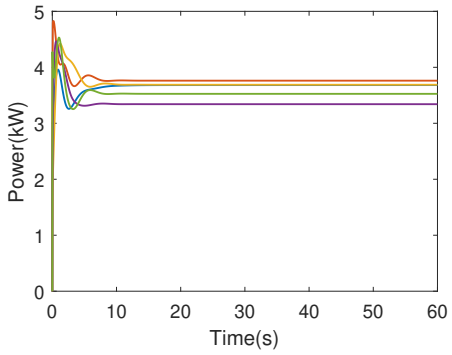

(b) Power consumption reference of HVACs

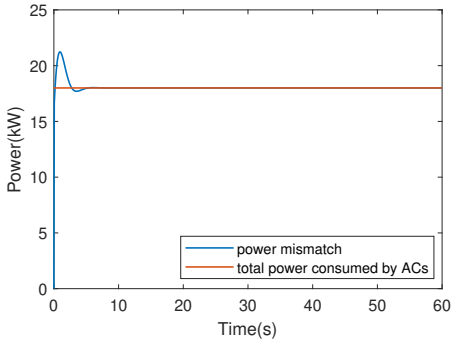

(c) Power mismatch

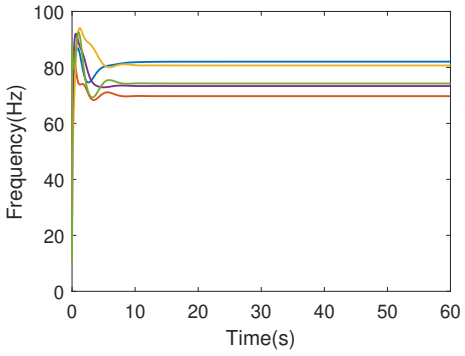

(d) Compressor frequency of HVAC system.

Figure 5.3.3: Results of PID-based distributed algorithm under constant condition

5.3.2 Case study 2: demand response to ToU price

In this case study, the global supply-demand mismatch in microgrid system is set to be a constant value as 18 kW. A ToU price curve fluctuating between 6 cent/kWh and 36 cent/kWh in a day is given in 5.3.4(a) [129, 130], the output power of HVAC

systems (Figure 5.3.4(b)) are updated corresponding to the price signal during the simulation. Figure 5.3.4(c) indicates the relationship of total output power of HVAC systems and supply-demand mismatch. The results show that the power consumption references converge to optimal value with the change of the ToU price. The supply-demand balance can be maintained without being affected by ToU price, which is a promising application in real-time control.

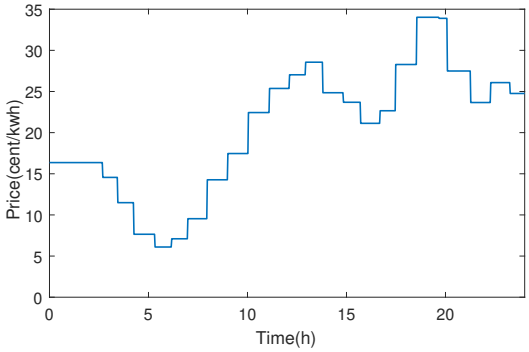

(a) ToU price

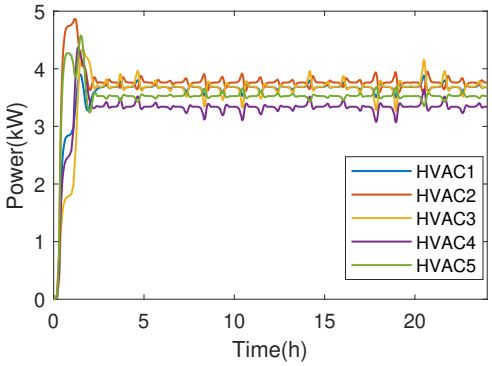

(b) Power consumption reference of HVAC

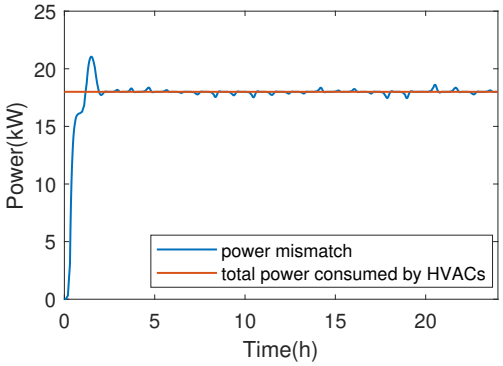

(c) Power mismatch

Figure 5.3.4: Results of PID-based distributed algorithm with time-varying ToU

5.3.3 Case study 3: demand response to renewable power generation

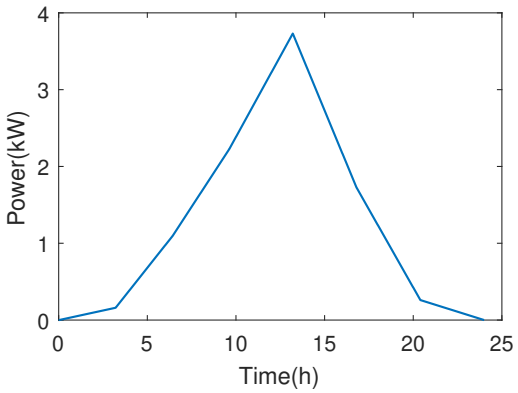

(a) Solar power generation

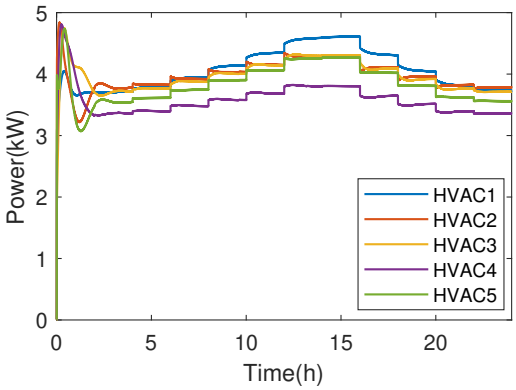

(b) Power consumption reference of HVAC

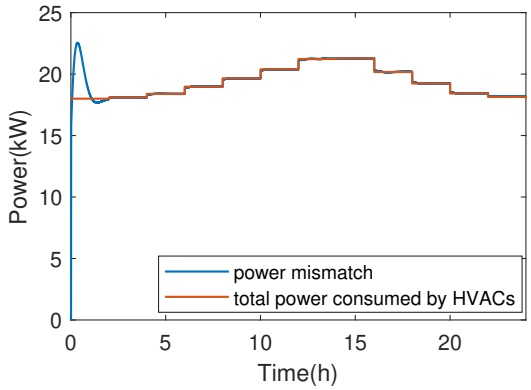

(c) Power mismatch

Figure 5.3.5: Results of PID-based distributed algorithm under solar power forecast

Case 3 focuses on the impact of renewable energy on the performance of distributed algorithm. Since the power generated by the PV array is a time-varying variable, the power consumption from HVAC system will be changeable correspondingly. Under this scenario, a simulation study is carried out based on the power output from the solar power generation, in order to test the dynamics of new-designed algorithm. As-

sume that the solar PV connected in Bus 4 is controlled in MPPT mode and the output power of PV panel is given in Figure 5.3.5(a). During the simulation time, each HVAC system follows the flow chart of a distributed algorithm implementation in Figure 4.3.3. By combining the existing power mismatch (18 kW) and solar power generation in Figure 5.3.5(a), Figure 5.3.5(b) and 5.3.5(c) give the results for the output power and power balance estimation, respectively. It can be seen that the power consumption of HVAC systems converges to an optimal value in finite time. Meanwhile, the power balance is maintained under the time-varying solar power generation. Based on the results in Case 2 and Case 3, the combined effects of solar power forecasts and ToU price can be considered. Therefore, Figure 5.3.6 gives the demand response of HVAC systems and power balance in the microgrid system.

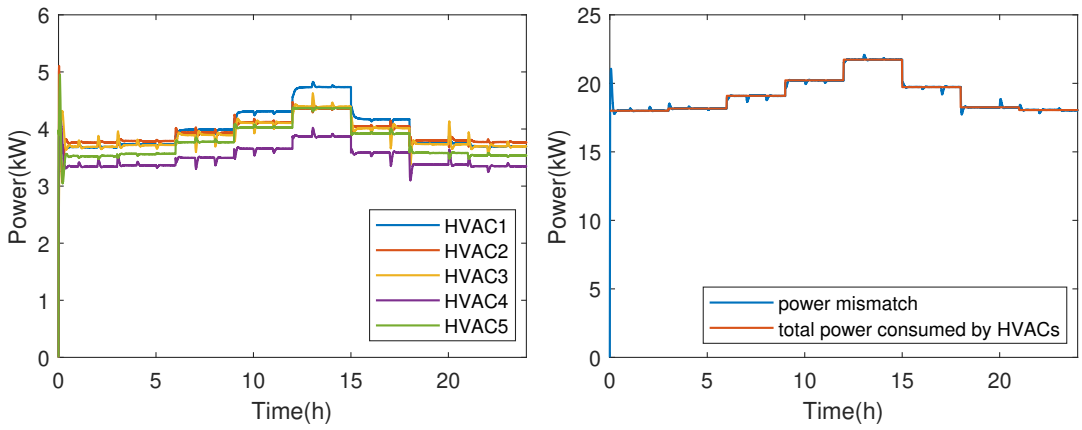

(a) Power consumption reference of HVAC (b) Power mismatch

Figure 5.3.6: Results of PID-based distributed algorithm under the combined effects

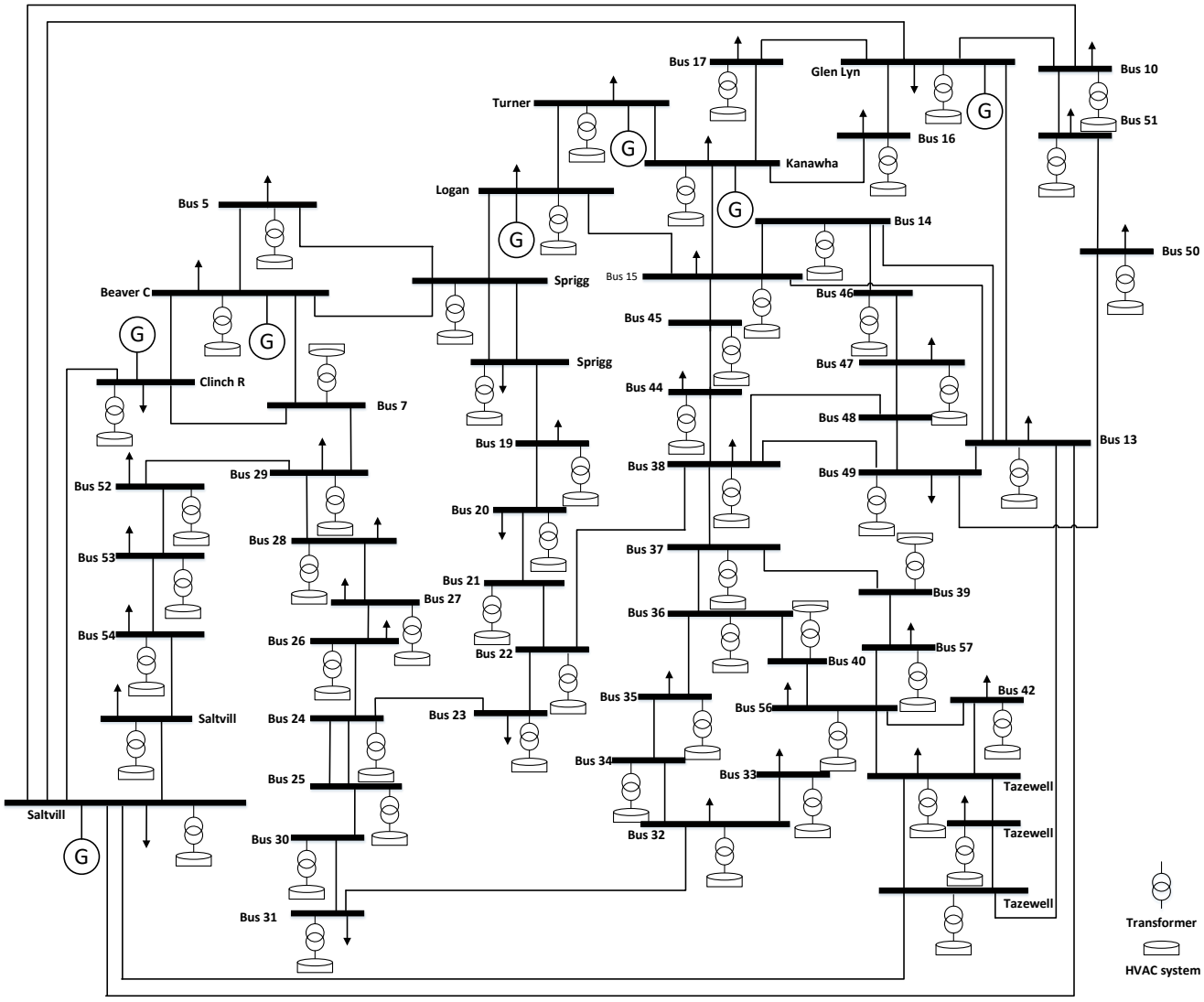

Figure 5.3.7: IEEE 57-bus system with multiple HVAC systems

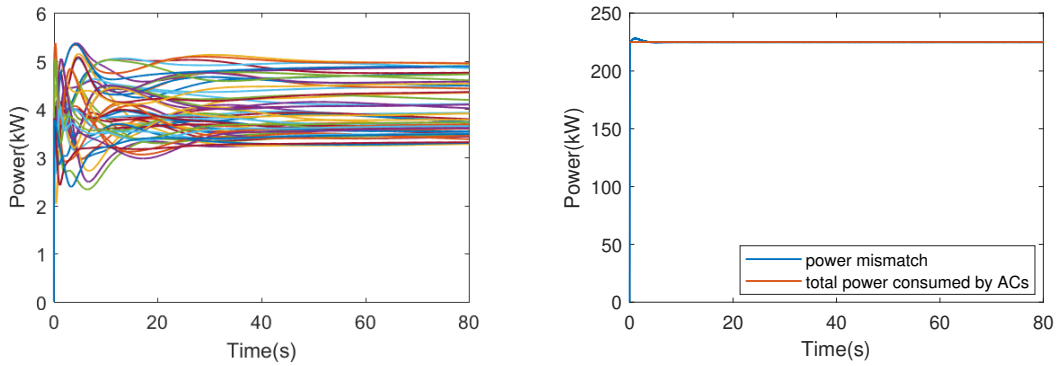

(a) Power consumption reference of HVACs (b) The power balance estimation

Figure 5.3.8: Results of PID-based distributed algorithm under scalability test

5.3.4 Case study 4: scalability of the algorithm

To extend the application of the presented algorithm to a large-scale system, the algorithm should be verified to converge to an optimal value in finite time. A IEEE 57-bus system with multiple HVAC systems is built in Matlab/Simulink with the diagram shown in Figure 5.3.7, where simulation parameters are adopted from [131]. The power constraints of all HVAC systems are between 2 kW and 5.5 kW. The communication network is designed to be strongly connected and the supply-demand mismatch is set as 225 kW. The scalability is demonstrated by observing Figure 5.3.8(a) and Figure 5.3.8(b). It shows that the output power of each HVAC system converges to an optimal value and power balance can be maintained with the utilization of HVAC systems.

5.4 Summary and discussion

In this chapter, both the user's comfortable level and ToU price are integrated into the HVAC system modelling framework. An optimization problem is formulated to reveal a trade-off between comfortability and electricity bill. A PID-based distributed algorithm is designed to solve the problem while maintaining the supply-demand balance and facilitating the total profits and energy efficiency. On the basis of MAS framework, the proposed approach is implemented in a distributed manner without a central controller. The results indicate that an optimal solution can be achieved without releasing the private information of each agent. Furthermore, by comparing with the algorithm proposed in [6], the approach ensures the steady-state error is within the threshold in any cases, instead of depending on the parameter selection. The effectiveness and scalability of the proposed strategy are verified on the 5-bus and IEEE 57-bus systems, respectively.

Chapter 6

Cooperative Control of HVAC-BESS System

In this chapter, the consensus-based distributed control protocol for HVAC system will be extended to accommodate hybrid loads. Battery energy storage system (BESS) has been regarded as the most widely-used energy storage system. A BESS-HVAC hybrid system would increase the storage capacity, thus providing an ancillary service for smart grid, including maintaining active power balance to stabilize system frequency and regulating reactive power to keep the voltage within an allowable range. Home microgrid or community microgrid with a certain scale of ESSs can improve its self-regulation ability and flexibility in response to intermittent renewable energy. By integrating the distributed algorithm into the microgrid system with hybrid loads, energy scheduling schemes of HVACs and BESS can be achieved. The remaining parts of this chapter is organized as follows. Section 6.1 introduces cost function models for BESS and HVAC system, respectively. The cooperative control of hybrid

system is described in Section 6.2, while results and discussions from case studies based on an IEEE 14-bus system are presented in Section 6.3. Conclusions are given in Section 6.4.

6.1 BESS model

In smart grid, energy storage devices can be utilized as buffer to absorb excessive power during peak generation periods and release the insufficient power during peak load periods. It helps adjust short-term variations in total net load. BESS has a fast response by the operator to deal with the requests for generation/demand changes. In an autonomous microgrid system, the employment of the BESSs aims to stabilize the system frequency and voltage by regulating the active power and reactive power. A number of literatures have conducted the research on control and optimization of BESSs [132, 133]. For example, a fast-acting storage technique is proposed in [132], with the aims of regulating grid frequency and mitigating the impacts of resource on dynamic performance. Generally, most of studies assume that the charging/discharging efficiency is a constant value under different charging/discharging rates. In order to control and manage the distributed BESS in a cost-efficient way, the charging-discharging efficiency need to be taken into account [104].

Due to the internal resistance in BESS, it will cause power losses when the BESS is operating in charging/discharging mode. The energy conversion efficiency model is shown as follows.

$$P_{B,i}^{cha} = P_{B,i}\eta_{C,i} \tag{6.1.1}$$

$$P_{B,i}^{dis} = \frac{P_{B,i}}{\eta_{D,i}} \tag{6.1.2}$$

where $P_{B,i}$ is the power input/output for i^{th} BESS, depending on the changing/discharging mode. $P_{B,i}^{cha}$, $P_{B,i}^{dis}$ are the power stored in and extracted from i^{th} BESS respectively. $\eta_{C,i}$ and $\eta_{D,i}$ are the charging and discharging efficiency. In order to be consistent with the demand response of controllable loads, this chapter only discusses the charging mode of BESSs. Let define S_B as the BESS group. The total actual power fed into BESS is calculated as

$$\sum_{i \in S_B} P_{B,i} \eta_{C,i} \tag{6.1.3}$$

In order to make the microgrid is operated in an economical way, the power loss occurring during BESS charging process should be minimized. It can be achieved by controlling the charging power references of BESSs to maximize equation 6.1.3.

The factors affecting charging efficiency are charging rate and SoC (State-of-Charging) of the BESS. The authors in [134, 135] showed in experiments that the charging efficiency is in a linear relationship with the input power, which is given by

$$\eta_{C,i} = b_{B,i} - a_{B,i} P_{B,i} \tag{6.1.4}$$

where $a_{B,i}$ and $b_{B,i}$ are constant coefficients for BESS i.

By substituting the equation (6.1.4) into (6.1.1). Then, the total power actually stored in BESSs is calculated as:

$$\sum_{i \in S_B} b_{B,i} P_{B,i} - a_{B,i} P_{B,i}^2 \tag{6.1.5}$$

In order to maximize the energy stored in BESSs whilst minimizing power loss during

charging process, the objective function for BESSs can be rewritten as:

$$\min \sum_{i \in S_B} C_i(P_{B,i}) \qquad (\underline{P}_{B,i} \leq P_{B,i} \leq \overline{P}_{B,i})$$
$$C_i(P_{B,i}) = a_{B,i} P_{B,i}^2 - b_{B,i} P_{B,i} \tag{6.1.6}$$

where the $P_{B,i}$ should satisfies the power constraint of BESS i. $\underline{P}_{B,i}$ and $\overline{P}_{B,i}$ are the lower and upper bounds of operating power of BESS i, respectively. C_i denotes the objective function of BESS i

6.2 Distributed hybrid controllable load management strategy

As demonstrated in Chapter 5, the cost function model of HVAC system is the combination of discomfort cost model (equation 5.1.1) and energy cost model (equation 5.1.3). It is worthwhile to note that this cost function can be generalized to describe other dispatchable and schedulable loads. As described in Chapter 5, the cost function of HVAC system j can be calculated as:

$$C_j(P_{AC,j}) = \frac{1}{2} a_{AC,j}(P_{AC,j}^2) + b_{AC,j} P_{AC,j} + c_{AC,j} \qquad (\underline{P}_{AC,j} \leq P_{AC,j} \leq \overline{P}_{AC,j}) \tag{6.2.1}$$

where $a_{AC,j} = w_{a,j}$, $b_{AC,j} = \frac{1}{2}\rho - w_{a,j}\hat{P}_{AC,j}$, $c_{AC,j} = \frac{1}{2} w_{a,j} \hat{P}_{AC,j}^2$. The objective of HVACs is to find a optimum point to achieve the minimization of financial cost and discomfort level for the residents. Therefore, we have:

$$\min \sum_{j \in S_{AC}} C_j(P_{AC,j}) \tag{6.2.2}$$

To ensure the total net power balance in an islanded microgrid, an appropriate dispatching strategy is required to share the global supply-demand power mismatch P_d among the distributed BESS and HVACs by adjusting their power reference, which can be indicated as:

$$\sum_{i \in S_B} P_{B,i} + \sum_{j \in S_{AC}} P_{AC,j} = P_d \tag{6.2.3}$$

Suppose that P_d is always positive.

A control scheme is introduced to coordinate all the participants to minimize operating cost, whilst maintaining active power balance and power constraints. The problem is formulated as:

$$\min \sum_{i \in S_B} C_i(P_{B,i}) + \sum_{j \in S_{AC}} C_j(P_{AC,j}) \tag{6.2.4}$$

$$\text{s.t.} \qquad \sum_{i \in S_B} P_{B,i} + \sum_{j \in S_{AC}} P_{AC,j} = P_d \tag{6.2.5}$$

$$\underline{P}_{AC,j} \leq P_{AC,j} \leq \overline{P}_{AC,j}, \quad \underline{P}_{B,i} \leq P_{B,i} \leq \overline{P}_{B,i} \tag{6.2.6}$$

For convenience, P_i is introduced to represent the power consumption of BESS and HVAC at Bus i ($P_i = \{P_{B,i}, P_{AC,j}\}$). We further define the incremental cost r_i of participant i as follow:

$$\frac{\partial C_i(P_i)}{\partial P_i} = r_i = a_i P_i + b_i \tag{6.2.7}$$

where $a_i = \{2a_{B,i}, a_{AC,j}\}$ and $b_i = \{-b_{B,i}, b_{AC,j}\}$. Similarly, let define $\overline{P}_i = \{\overline{P}_{B,i}, \overline{P}_{AC,j}\}$ and $\underline{P}_i = \{\underline{P}_{B,i}, \underline{P}_{AC,j}\}$. As it is demonstrated in equation (4.3.8), the optimal solution of objective function is the equal incremental cost criterion, which is represented

as:

$$\begin{cases} r^* = a_i P_i + b_i, & \underline{P}_i < P_i < \overline{P}_i \\ r^* > a_i P_i + b_i, & P_i = \overline{P}_i \\ r^* < a_i P_i + b_i, & P_i = \underline{P}_i \end{cases} \tag{6.2.8}$$

Conventionally, the optimal solution can be achieved with centralized strategy, which requires a central controller and bi-directional communication network between each agent and central controller. The central controller is responsible for collecting all local information e.g., power bounds of HVAC systems and BESSs, cost function and generation/demand information, and realizing centralized algorithm to compute the optimal operation point and broadcast the information to each agents. Due to the unexpected change in the power generation, high-frequent control update and high-speed processor is required. Thus, a high-efficiency distributed approach takes advantage of its flexibility and scalability, which has a promising prospect in the future.

Invoked by the algorithm in Chapter 4, a fully distributed energy storage management strategy based on consensus algorithm is presented, where each agent only utilizes the local information and exchanges with its neighbouring agents via the communication network. The update rules for agent's network are represented as:

$$r_i(k+1) = \sum_{j \in N_i} d_{ij} r_j(k) + \varepsilon_i P_{D,i}(k) \tag{6.2.9}$$

$$P_i(k+1) = \frac{r_i(k+1) - b_i}{a_i} \tag{6.2.10}$$

$$P'_{D,i}(k) = P_{D,i}(k) - (P_i(k+1) - P_i(k)) \tag{6.2.11}$$

$$P_{D,i}(k+1) = \sum_{j \in N_i} d_{ij} P'_{D,j}(k) \tag{6.2.12}$$

where $r_i(k)$ is the incremental cost of participant i at k^{th} iteration time. The coefficient ε_i is required to be adjusted to control convergence speed. $P_{D,i}(k)$ is the local power mismatch estimation in bus i. d_{ij} is the communication topology matrix as demonstrated in equation (4.1.6). The overall updating rules can be rewritten as a matrix form

$$R(k+1) = DR(k) + \varepsilon P_D(k) \tag{6.2.13}$$

$$P_D(k+1) = DP_D(k) - D(P(k+1) - P(k)) \tag{6.2.14}$$

$$P(k+1) = BR(k+1) + G \tag{6.2.15}$$

where R, P_D, P, G are column vectors of r_i, $P_{D,i}$, P_i, $-b_i/a_i$, respectively. $B = \text{diag}\{1/a_i\}$. Hence, a state equation with regard to $[R, P_D]^T$ can be formulated as:

$$\begin{pmatrix} R(k+1) \\ P_D(k+1) \end{pmatrix} = \begin{pmatrix} D & \varepsilon I_n \\ DB(D-I_n) & D + \varepsilon DB \end{pmatrix} \begin{pmatrix} R(k) \\ P_D(k) \end{pmatrix} \tag{6.2.16}$$

According to the convergence proof in Section 4.3.3, the system converges to span $[1_n, 0_n]^T$ as the time goes to infinity. Thus, the incremental cost of each agent converges to a common value r^* and $P_{D,i}$ alleviates to zero. The optimality is secured. Therefore,

$$\begin{pmatrix} R(\infty) \\ P_D(\infty) \end{pmatrix}_{2n\times 1} = r^* \begin{pmatrix} 1_n \\ 0_n \end{pmatrix} \tag{6.2.17}$$

Since the inequality power constraints is taken into consideration, the power update rule in equation (6.2.10) can be revised as:

$$P_i(k+1) = \begin{cases} \underline{P}_i, & \frac{r_i(t)-b_i}{a_i} < \underline{P}_i \\ \frac{r_i(t)-b_i}{a_i}, & \underline{P}_i \le \frac{r_i(t)-b_i}{a_i} \le \overline{P}_i \\ \overline{P}_i, & \frac{r_i(t)-b_i}{a_i} > \overline{P}_i \end{cases} \tag{6.2.18}$$

To investigate the impact of power constraints on the performance of presented algorithm, the revised algorithm is presented as:

$$\begin{pmatrix} R(k+1) \\ P_D(k+1) \end{pmatrix} = \begin{pmatrix} D & \varepsilon I_n \\ D\hat{B}(D-I_n) & D+\varepsilon D\hat{B} \end{pmatrix} \begin{pmatrix} R(k) \\ P_D(k) \end{pmatrix} \tag{6.2.19}$$

where $\hat{B} = \text{diag}\{b'_1, b'_2, ..., b'_n\}$ with

$$b'_i = \begin{cases} 0, & P_i \text{ is saturated} \\ \frac{1}{a_i}, & \text{Otherwise} \end{cases} \tag{6.2.20}$$

6.3 Simulation studies and discussion

6.3.1 System specifications

The proposed distributed control protocols is conducted in IEEE 14-bus system, which is a widely used test case in many studies. The standard system is revised to accommodate case studies, where it is composed of 14 buses, 1 solar PV, 1 wind turbine, 7 HVACs, 7 batteries and 10 loads, as shown in Figure 6.3.1. The introduction of wind turbine and solar PV is to evaluate the dynamics of the proposed algorithm. The parameters of HVACs and BESSs are summarized in Table 6.3.1. Note that the initial power mismatch for each local bus are set as zero.

The MAS is introduced to describe the information interaction in the system, where each local bus can be considered as an agent. It is worthwhile to note that the communication network among agents is independent from the physical connection.

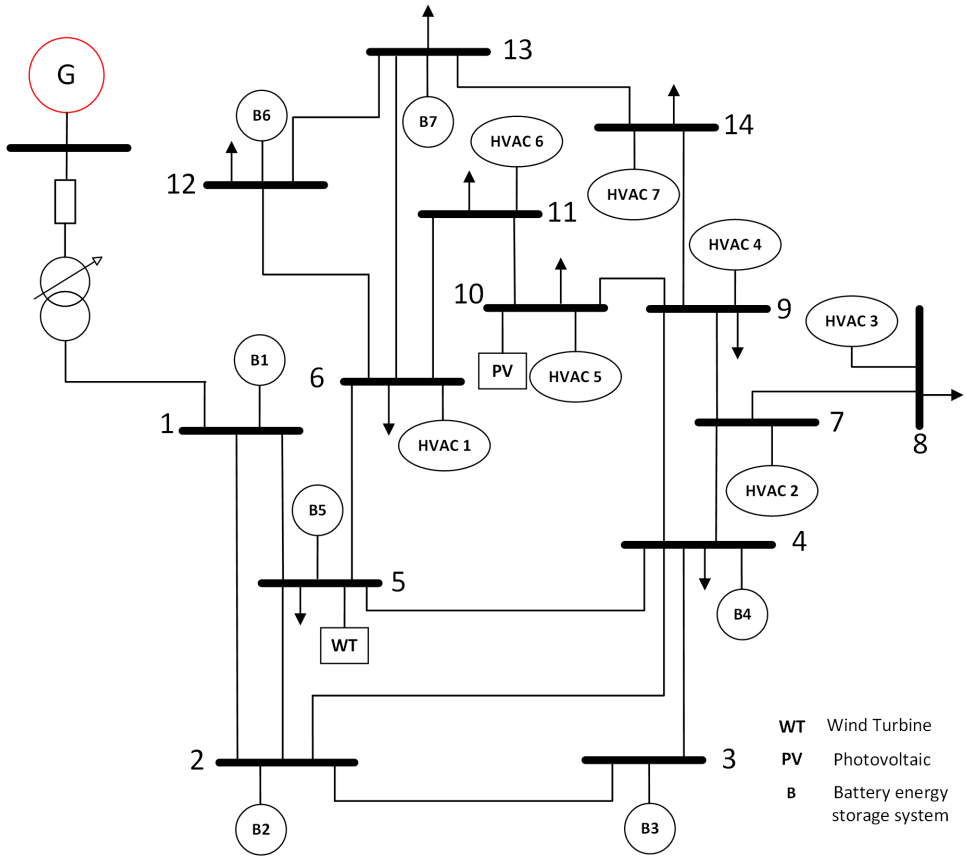

Figure 6.3.1: A IEEE 14-bus system with multiple HVACs and BESSs

It is assumed that each agent communicate with adjacent agents in a undirected way. Therefore, the information exchange between neighbouring agents is set as:

$$\mathcal{X} = \{(i-1,i),(i,i+1)|2<i<13\} \cup \{(14,1),(14,13),(2,1),(1,14)\}$$

where i represents the local bus. $\mathcal{X}$ specifies the communication topology in MAS. A 14×14 doubly stochastic matrix D can be determined according to equation 4.1.6. Suppose that microgrid is always operated in islanded mode. In first two cases, the total supply-demand mismatch is set to be a constant value at 290 kW. The demand response of HVAC systems and BESSs under different scenarios is investigated through case studies.

Table 6.3.1: Parameters of HVACs and BESSs in IEEE 14-bus System

Bus i	Agent	a_i	b_i	$\underline{P}_i(kW)$	$\overline{P}_i(kW)$	$r_i(0)$	$P_i(0)$
1	**B1**	0.094	1.22	30	60	7.8	35
2	**B2**	0.078	2.53	15	60	5.65	20
3	**B3**	0.105	4.41	15	35	7.56	15
4	**B4**	0.082	6.02	10	35	8.84	15
5	**B5**	0.074	3.17	15	60	6.13	20
6	**HVAC1**	0.11	4.5	15	35	7.8	15
7	**HVAC2**	0.095	4.8	18	35	8.6	20
8	**HVAC3**	0.07	4	21	55	8.2	30
9	**HVAC4**	0.098	4.5	12	36	7.44	15
10	**HVAC5**	0.065	5.4	12	46	8	20
11	**HVAC6**	0.094	5.6	5	20	8.232	14
12	**B6**	0.103	4.5	12	35	7.79	16
13	**B7**	0.075	3.3	20	55	7.05	25
14	**HVAC7**	0.08	2.5	15	60	5.7	30

6.3.2 Case study 1: without power constraints

In the first test, the power generation and load demand are considered as a constant value over the simulation time. Since is control cycle is set as 0.01s, the local information updates and data exchanges occur every 0.01 s. The updates of incremental cost, power consumption reference of hybrid loads, the supply-demand mismatch estimation of 14 local bus are shown in Figure 6.3.2. It can be seen in Figure 6.3.2(a), the incremental cost of all agents converge to a common value in 1 s. The power consumption reference curves in Figure 6.3.2(c) will be provided to BESSs and HVACs. The supply-demand mismatch can be alleviated to zero as shown in 6.3.2(b).

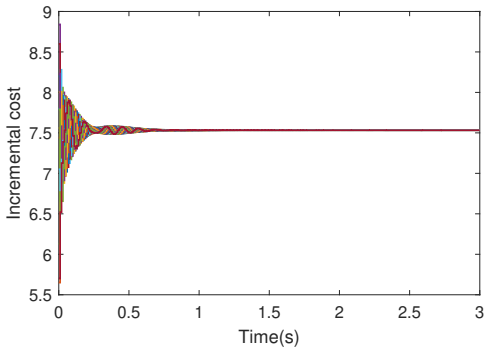

(a) Incremental cost

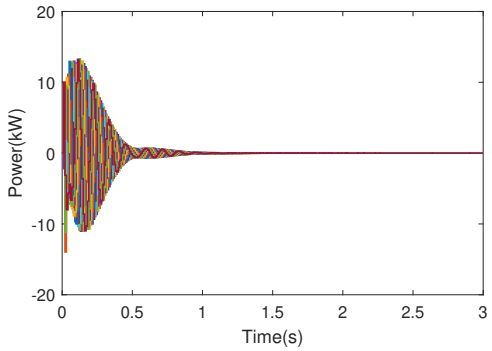

(b) Supply-demand mismatch

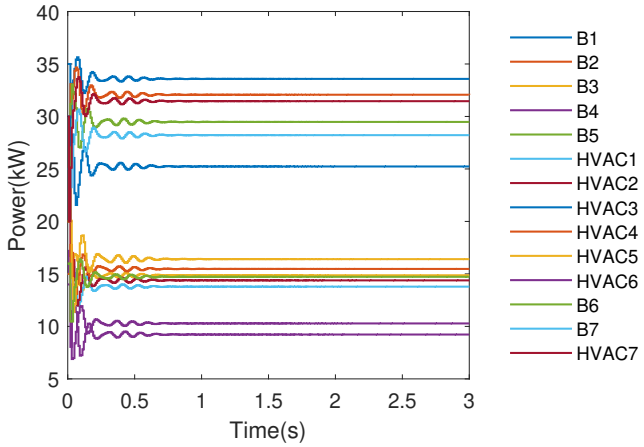

(c) Power reference of BESSs and HVACs

Figure 6.3.2: Results of HVAC-BESS without power constraints

6.3.3 Case study 2: with power constraints

As can be seen in Case 1, the charging power of BESS 3 and BESS 4 exceeds the lower limit, which is a infeasible solution. By considering revised algorithm equation 6.2.19, power constraints can be imposed to emulate a practical scenario in the case study. The simulation results are shown in Figure 6.3.3. Comparing Figure 6.3.2 with Figure 6.3.3, they both converge to an optimal solution, where $r^* = 7.527$. Furthermore, those unsaturated HVACs and BESSs are required to increase power consumption in order to alleviate the impact of saturated units, as shown in Figure 6.3.3(c). Mean-

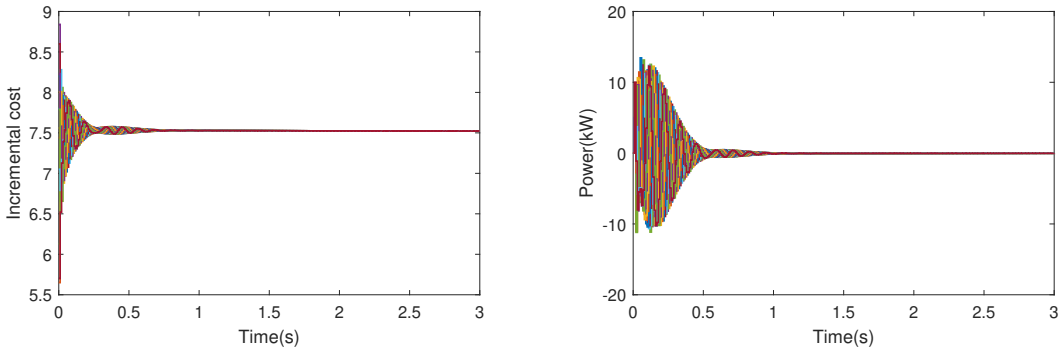

(a) Incremental cost

(b) Supply-demand mismatch

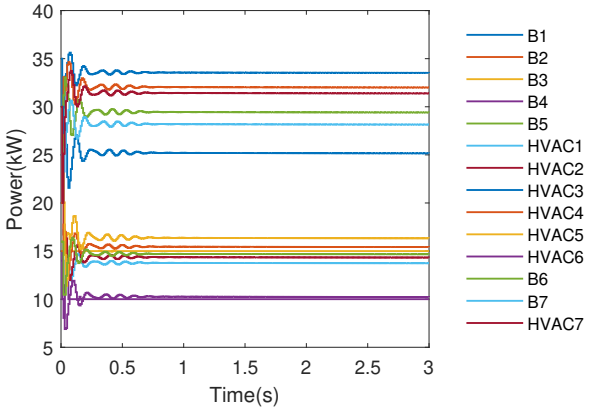

(c) Power reference of BESSs and HVACs

Figure 6.3.3: Results of HVAC-BESS with power constraints

while, the local power mismatch can be adjusted to zero (Figure 6.3.3(b)).

6.3.4 Case study 3: demand response of dynamic power mismatch

The proposed control solution is further tested under time-varying supply-demand mismatch. The generations from renewable energy and load demand are variable and intermittent. Therefore, the global supply-demand mismatch is also time-varying. In Figure 6.3.1, there is a wind turbine and a solar PV connected in Bus 5 and Bus 10.

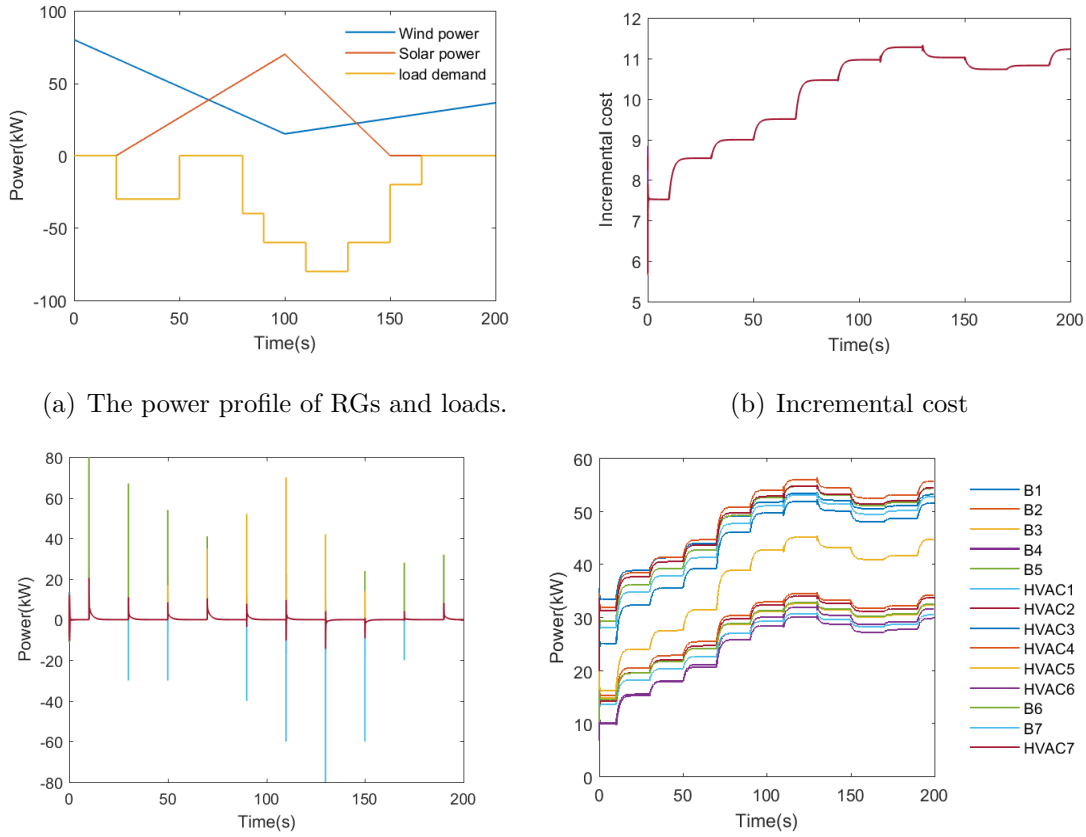

(a) The power profile of RGs and loads.

(b) Incremental cost

(c) Supply-demand mismatch

(d) Power reference of BESSs and HVACs

Figure 6.3.4: Results of HVAC-BESS under time-varying power mismatch

The profiles of wind turbine, solar PV and load demand are given in Figure 6.3.4(a), respectively. As an example, these disturbances are added to the system at 10s and the information of generation and load is updated every 20s ($T_d = 20s$).

Each agent in the system measures the local supply and demand then calculates the local power mismatch every 0.01s. During each control cycle ($T_c = 0.01$), agents implement the proposed distributed control strategy as explained in equation 6.2.18 and float chart 4.3.3. As shown in Figure 6.3.4(b), the local incremental costs converge to a common value within each T_d, which indicates the objective is achieved for each information update cycle. Figure 6.3.4(d) and 6.3.4(c) present power reference

update and local power mismatch estimation for each participant, respectively. The local estimated mismatch converges to zero within each information update cycle; consequently the total BESSs and HVACs power consumption equals the measured global power mismatch.

6.3.5 Case study 4: anti-damage test

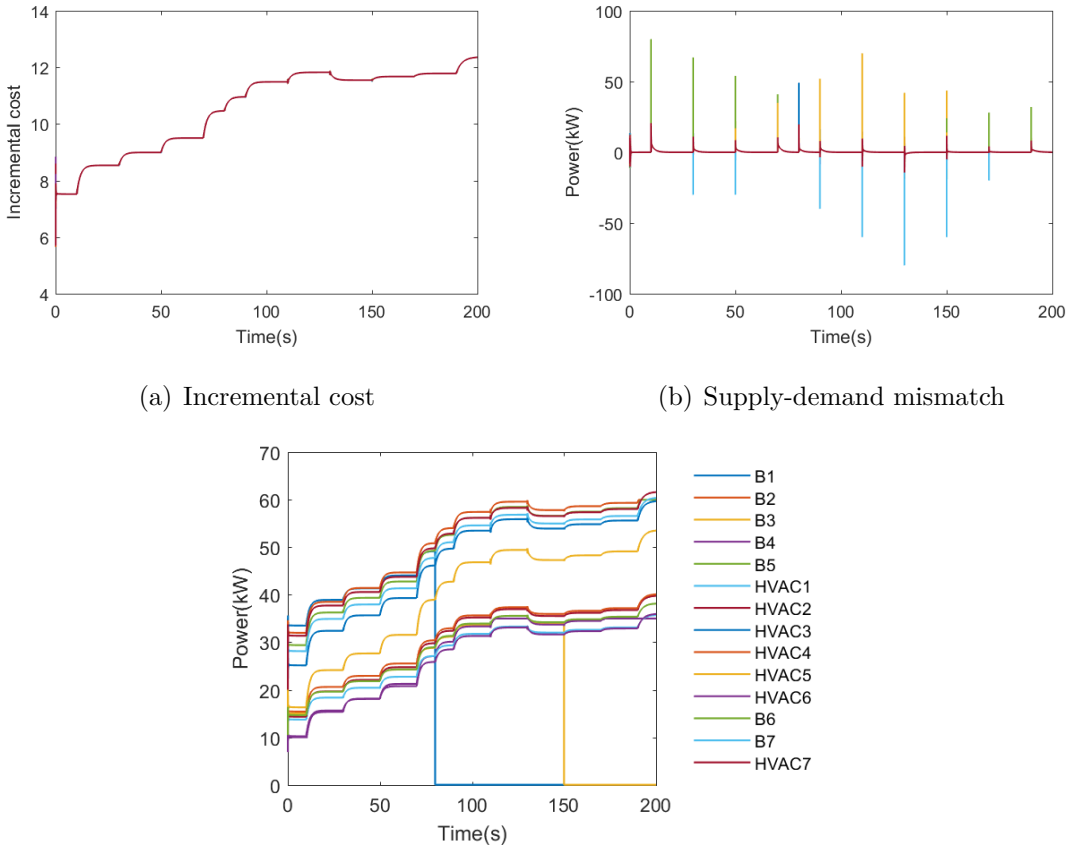

(a) Incremental cost

(b) Supply-demand mismatch

(c) Power reference of BESSs and HVACs

Figure 6.3.5: Results of HVAC-BESS for anti-damage test

This case evaluates the effectiveness of control strategy when a BESS or HVAC fault occurs. Before 80s, all participants work properly. It is assumed that BESSs

at bus 1 and bus 3 are broken down at 80s and 150s respectively and others work properly. In reality, this change is received by the sensor in bus 1 and 5 and sensors reset the corresponding limited BESSs and cost parameters before executing next updating iteration. That is $\overline{P}_1 = \underline{P}_1 = 0$, $\overline{P}_3 = \underline{P}_3 = 0$ and other parameters remain unchanged. Before 80s, all participants work properly, so the optimal power consumptions are the same as in Case 2. After the fault occurring in Bus 1 and Bus 3 at 80s and 150s, the incremental cost increases correspondingly, in order to maintain supply-demand balance, as described in Figure 6.3.5(a). The new power output references are shown in Figure 6.3.5(c). The mismatch converges to zero, as indicated in Figure 6.3.5(b).

6.3.6 Case study 5: Energy dispatch scheme for HVAC-BESS under short-term solar power forecasts

This case focuses on developing a pre-schedule energy dispatch scheme for HVAC-BESS systems, shown in Figure 6.3.6. Based on solar radiance forecasts in Figure 3.4.2, Figure 6.3.6(a) gives the 24-hour solar power curve in a solar PV array. The dynamic of the incremental cost and power consumption of HVACs and BESSs are shown in Figure 6.3.6(b)(c). Technically, the power reference signal will be broadcast to local controller of HVACs and BESSs via the communication network and the control system of these agents is responsible for generating associated control signal to adjust power consumption to track designed signal.

In order to evaluate the feasibility of control strategy in a short-term solar power

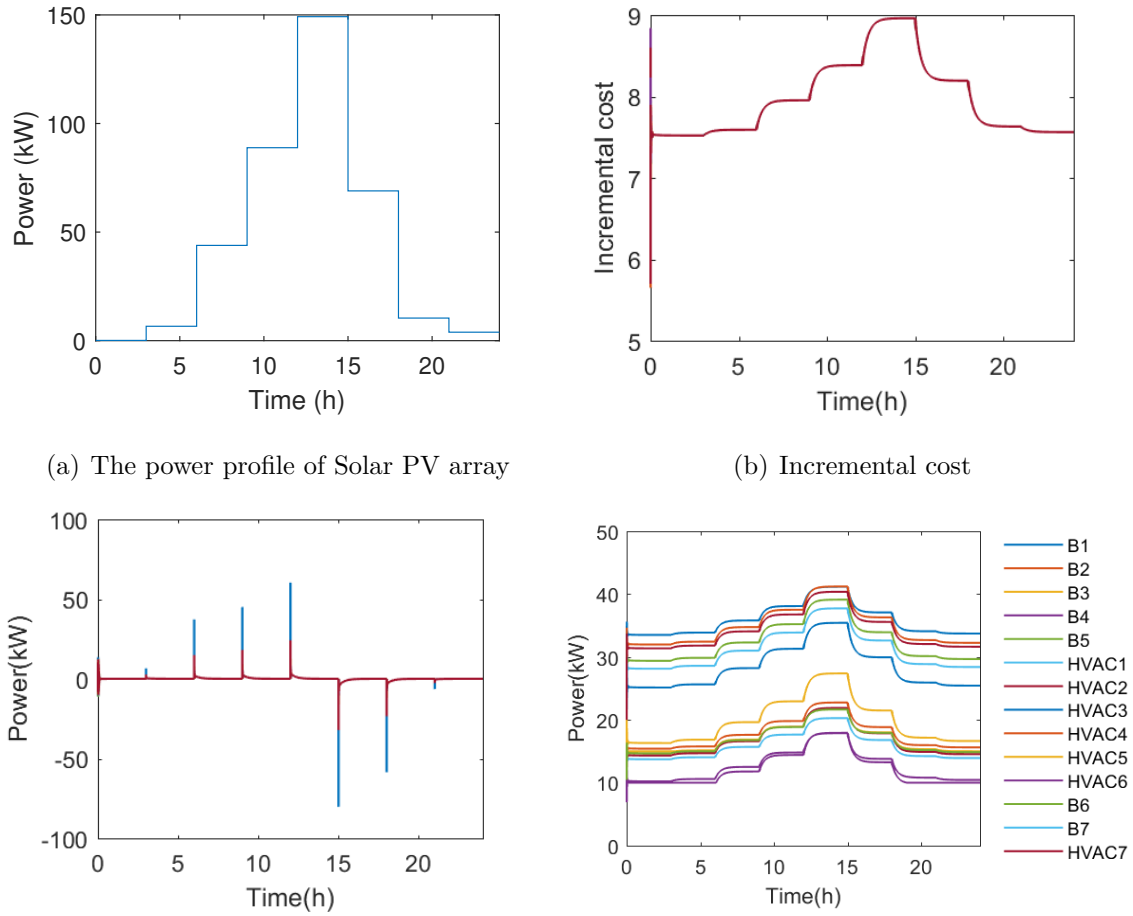

(a) The power profile of Solar PV array

(b) Incremental cost

(c) Supply-demand mismatch

(d) Power reference of BESSs and HVACs

Figure 6.3.6: Results of HVAC-BESS under 24-hour solar power forecasts

forecast, the results obtained by MAPAx-PCA model in Figure 3.2.2 is employed to carry out the test. Figure 6.3.7 shows the power consumption reference for HVAC-BESS system in a month. Clearly, the power signal varies with the change of daily solar radiance.

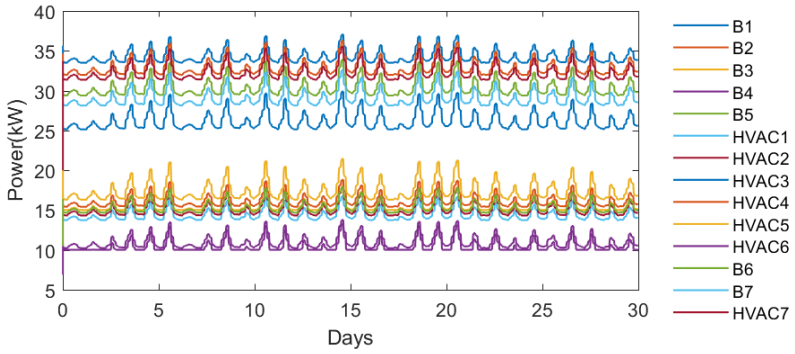

Figure 6.3.7: Results of HVAC-BESS under 1 month solar power forecasts

6.4 Summary and discussion

In this chapter, the MAS-based consensus algorithm is extended to achieve the coordination of hybrid HVAC-BESS systems. The cost function models of BESS and HVAC units can be generalised as quadratic functions to accommodate the distributed algorithm model. Case studies are carried out in IEEE 14-bus microgrid model built in MATLAB/Simulink. The simulation results demonstrate the effectiveness of proposed solution under the representative scenarios. The results demonstrate that a distributed coordination of heterogeneous controllable loads would be feasible to alleviate supply-demand imbalance under with/without power constraints, time-varying power mismatch, anti-damage test, 24-hour and one-month solar power forecasts, which can be a promising DSM scheme.

Chapter 7

Conclusions

7.1 Conclusions

This work is motivated by the Entrust Microgrid LLP, who is dedicated to promoting smart microgrid technology. With high penetration of DC-type loads and DC-based DERs, the company currently engages in design a home-based hybrid DC&AC networks, comprising embedded renewable power generators (solar PV panels), energy storage, controllable AC&DC loads. HVAC system, as a commonly-used electric appliance in the home, can be easily embedded into network to involve in DSM program. This research has aimed to investigate an coordination scheme for multiple HVAC systems to contribute to the upgrading and improvement of microgrid technology.

The growing capacity of renewable generators with uncertain generation patterns results in the need for increased system flexibility [136]. A novel concept "microgrid" is evolving that can help manage the variability of renewable resources and intelligently regulate power balance between local demand and power supply in a small-scale

electricity network. In addition to traditional energy storage device, i.e., BESSs, it is worthwhile to note that the introduction of TCL devices (HVAC) can be an alternative choice to provide a short-term ancillary service, such as balancing and frequency regulation in the microgrid. Furthermore, the HVAC system has a "slack" characteristic in nature in terms of temperature, running time and power output, which represents a promising end-user category to engage in the grid service.

A hierarchical energy management system (Figure 2.5.1) is proposed to provide a forecasting-management-optimization comprehensive solution. The integration of a cooperative algorithm into a cluster of HVAC units is an optimal solution to address issues in DSM, where the local load consumption pattern can be influenced to follow the change of on-site renewable energy generation. With an accurate estimation of distributed generation, a pre-scheduled energy dispatch scheme is designed for each HVAC. The proposed method aims to maximize the on-site power generation, reduce peak load demand, curtail the storage capacity and decrease the construction cost of transmission system. This would provide a comprehensive solution to development of next generation power system, for meeting the global challenge in energy security, affordability and sustainability, and battling climate change and environment pollution. More importantly, it is a great opportunity for local residents to obtain financial incentive, such as feed-in tariff, from the grid operator by providing an ancillary service. In the future, more and more customers will change inherent behaviour of electricity usage and be encouraged to participate in DSM activities and energy trade. On the other hand, with the utilization of HVAC systems in the grid service, the comfortable level of end users would be affected to some extent. Thus, a price-comfort optimiza-

tion problem is formulated to reveal the trade-off between electricity payment and comfortable level for residential users.

Firstly, an accurate forecasting of solar power/irradiance is critical to secure economic operation of the microgrid system. A MAPA-PCA hybrid forecasting model is designed to forecast one-month solar radiance in Lancaster area based on historical weather data at Hazelrigg meteorological enclosure and nearby weather forecast at walney island. The results indicate that the hybrid model outperforms the MLR and ARIMAX, with MAPE being 65.0355 and R-square being 0.803. Correspondingly, the daily power generation curve of a PV array can be estimated by a set of solar power calculation models.

Secondly, HVACs need to be properly coordinated through a cooperative control strategy to compensate the power imbalance and an energy dispatch scheme for a group of HVACs in a time horizon of 24 hours is developed, based on local solar power forecast results. Note that the numerical analysis for the convergence speed against feedback gain is given and fastest performance can be achieved when the gain is equal to 3.6. Meanwhile, the convergence proof of the algorithm under switching communication topology is given by using Lyapunov stability theorem. It is verified that a jointly strongly connected topology is a sufficient condition in order to achieve average consensus for a time-varying topology. The power constraints, dynamics, robustness, scalability, topology of the proposed algorithm have been investigated through case studies.

The financial and discomfort cost affected by DSM activities are also considered to formulate a optimization problem, where the objective function is designed to

maximize the total welfare of HVAC systems and maintain the total power balance. A PID-based distributed algorithm is proposed to maintain comfortability of end users and active power balance by adjusting a virtual price. The advantages of the algorithm capable of eliminating the steady-state error are proved by comparing with the related literature. Case studies are carried out under different conditions on the changes of ToU price, renewable power generation and different scales of IEEE bus systems.

Furthermore, the distributed algorithm is expanded to include other controllable components, i.e., BESSs. It is utilized to coordinate power sharing among heterogeneous energy storage devices distributed in IEEE 14-bus system. The sufficient condition to achieve average consensus is the communication network by ensuring to provide a spanning tree to access all BESSs and HVACs. The effectiveness of proposed algorithm and its robustness against unexpected power imbalance, equipment failure and short-term solar power forecasts are verified through case studies on a microgrid test-bed built in MATLAB/Simulink.

7.2 Future perspectives

The work presented in this thesis proposes a hierarchical DSM model framework for controllable household appliances, considering HVACs, BESSs, renewable energy forecasting technologies, distributed energy management and DSM optimization algorithms. As an industrial-lead PhD project, the final target of the research is to transfer the key knowledge to the company for business use. Along this direction, the

following research avenues may be of interest to academia and industry:

- Presently, a few assumptions are made in this research. Firstly, the energy loss in the microgrid systems is not considered during the problem formulation. Secondly, the price-comfort model is optimized by minimizing comfort loss and electricity bills in response to the ToU price. It is valuable to study the indoor temperature and CO2 level, since the fluctuations in the outdoor temperature may also cause dissatisfaction. Furthermore, the dynamics of the BESSs including charging/discharging cycles, SoC state, degradation and ageing problem are not considered in the models. Nevertheless, the proposed HVAC-based energy management system has demonstrated its operational feasibility as well as the interests from the company. Further work will continue to investigate the requirement for practical use in consultation with the company.

- The work will be to develop a real-time online distributed control system to accommodate multiple end users with controllable loads that can be jointly managed through communication network. The distributed controller can be implemented and integrated into the microgrid operator. This distributed controller can be composed of three modules. The data acquisition block is a data centre to extract real-time weather forecast information from the Met-office website. The power forecasting module is utilized to implement time-series forecast algorithm and produce a daily solar power curve. DSM block is responsible for the hardware implementation of the distributed algorithm and providing a power consumption signal to each HVAC based on the overall power available.

After receiving the signal, the local controller in each HVAC unit will generate associated control signal to control and regulate its power output.

- The HVAC applied in this study is a popular household appliance with small capacity and large quantity. Similarly, the immersion heater can be another back-up energy storage system. It can preheat the cold water and reduce the workload of water boiler. The immersion heaters at different houses can be cooperated to consume the excessive power during peak generation of the electrical grid. The thermal resistance voltage in the heater can be adjusted to track the desired power consumption assigned by a distributed controller. It helps mitigate the negative impact of renewable power generation on the main grid, such as voltage fluctuation and maximize the on-site power generation.

- The heterogeneity of BESS should be taken into account. The employment of the consensus-based method would achieves energy level balancing, active/reactive power sharing and voltage/frequency synchronization of energy storage devices by using inter-BESS communications.

- With the population of electrical vehicles (EV), the battery pack as the core part of EV can be considered to participant in DSM activities. The proposed coordination strategy can be used to deal with large-scale EV charging coordination, such as minimizing the charging power loss and maximizing the available EV power for vehicle-to-grid (V2G) services. The corresponding incremental cost functions can be formulated for these objectives. The consensus algorithm can be applied to realize the local information updating and external informa-

tion exchanging among neighbouring EVs, whilst satisfying the EV charging requirements specified by the vehicle drivers [137].

Appendix A

Appendix

```
<?xml version="1.0" encoding="ISO-8859-1"?>
<SiteRep>
  <Wx>
    <Param units="C" name="F">Feels Like Temperature</Param>
    <Param units="mph" name="G">Wind Gust</Param>
    <Param units="%" name="H">Screen Relative Humidity</Param>
    <Param units="C" name="T">Temperature</Param>
    <Param units="" name="V">Visibility</Param>
    <Param units="compass" name="D">Wind Direction</Param>
    <Param units="mph" name="S">Wind Speed</Param>
    <Param units="" name="U">Max UV Index</Param>
    <Param units="" name="W">Weather Type</Param>
    <Param units="%" name="Pp">Precipitation Probability</Param>
  </Wx>
  <DV type="Forecast" dataDate="2017-04-01T05:00:00Z">
    <Location name="WALNEY ISLAND" elevation="15.0" continent="EUROPE" country="ENGLAND" lon="-3.257"
    lat="54.125" i="3214">
      <Period type="Day" value="2017-04-01Z">
        <Rep U="0" W="12" V="GO" T="10" S="4" Pp="78" H="91" G="22" F="7" D="SE">0</Rep>
        <Rep U="0" W="12" V="EX" T="9" S="4" Pp="57" H="97" G="16" F="9" D="SSW">180</Rep>
        <Rep U="1" W="12" V="MO" T="9" S="2" Pp="85" H="97" G="4" F="9" D="E">360</Rep>
        <Rep U="1" W="15" V="MO" T="9" S="7" Pp="81" H="92" G="9" F="8" D="ENE">540</Rep>
        <Rep U="3" W="12" V="VG" T="10" S="9" Pp="53" H="92" G="13" F="8" D="WNW">720</Rep>
        <Rep U="2" W="7" V="GO" T="10" S="11" Pp="8" H="86" G="20" F="8" D="WNW">900</Rep>
        <Rep U="1" W="3" V="VG" T="9" S="11" Pp="6" H="87" G="20" F="6" D="WNW">1080</Rep>
        <Rep U="0" W="0" V="VG" T="8" S="13" Pp="0" H="89" G="22" F="5" D="NW">1260</Rep>
      </Period>
      <Period type="Day" value="2017-04-02Z">
        <Rep U="0" W="0" V="VG" T="8" S="13" Pp="0" H="88" G="22" F="4" D="NW">0</Rep>
        <Rep U="0" W="0" V="VG" T="7" S="11" Pp="0" H="92" G="18" F="3" D="NW">180</Rep>
        <Rep U="1" W="1" V="VG" T="6" S="9" Pp="0" H="93" G="16" F="3" D="NW">360</Rep>
        <Rep U="2" W="1" V="VG" T="9" S="7" Pp="0" H="79" G="11" F="7" D="NW">540</Rep>
        <Rep U="3" W="3" V="VG" T="10" S="9" Pp="1" H="74" G="13" F="9" D="W">720</Rep>
        <Rep U="2" W="1" V="VG" T="10" S="7" Pp="0" H="71" G="13" F="9" D="WSW">900</Rep>
        <Rep U="1" W="1" V="VG" T="9" S="4" Pp="0" H="78" G="7" F="8" D="SW">1080</Rep>
        <Rep U="0" W="0" V="GO" T="7" S="4" Pp="0" H="92" G="7" F="6" D="SSE">1260</Rep>
      </Period>
      <Period type="Day" value="2017-04-03Z">
        <Rep U="0" W="0" V="GO" T="7" S="7" Pp="1" H="91" G="11" F="5" D="SE">0</Rep>
        <Rep U="0" W="0" V="GO" T="7" S="7" Pp="1" H="89" G="11" F="4" D="SSE">180</Rep>
        <Rep U="1" W="7" V="GO" T="6" S="9" Pp="4" H="89" G="16" F="4" D="SSE">360</Rep>
        <Rep U="2" W="7" V="VG" T="9" S="11" Pp="4" H="72" G="22" F="6" D="S">540</Rep>
        <Rep U="3" W="7" V="VG" T="11" S="13" Pp="4" H="61" G="25" F="9" D="S">720</Rep>
        <Rep U="1" W="7" V="GO" T="11" S="11" Pp="10" H="67" G="22" F="8" D="SSW">900</Rep>
        <Rep U="1" W="12" V="MO" T="10" S="13" Pp="49" H="79" G="25" F="7" D="SSW">1080</Rep>
        <Rep U="0" W="15" V="GO" T="9" S="13" Pp="78" H="89" G="25" F="6" D="SSW">1260</Rep>
      </Period>
      <Period type="Day" value="2017-04-04Z">
        <Rep U="0" W="12" V="GO" T="9" S="13" Pp="55" H="92" G="22" F="6" D="SW">0</Rep>
        <Rep U="0" W="9" V="GO" T="8" S="11" Pp="40" H="89" G="22" F="5" D="W">180</Rep>
        <Rep U="1" W="12" V="GO" T="8" S="13" Pp="48" H="86" G="20" F="4" D="NW">360</Rep>
        <Rep U="2" W="3" V="VG" T="9" S="13" Pp="8" H="72" G="25" F="5" D="NW">540</Rep>
        <Rep U="3" W="7" V="VG" T="10" S="16" Pp="6" H="62" G="27" F="7" D="WNW">720</Rep>
        <Rep U="2" W="7" V="VG" T="10" S="13" Pp="4" H="63" G="27" F="7" D="WNW">900</Rep>
        <Rep U="1" W="7" V="VG" T="9" S="11" Pp="5" H="70" G="20" F="6" D="WNW">1080</Rep>
        <Rep U="0" W="7" V="VG" T="8" S="11" Pp="5" H="72" G="20" F="5" D="WNW">1260</Rep>
      </Period>
      <Period type="Day" value="2017-04-05Z">
        <Rep U="0" W="8" V="VG" T="8" S="13" Pp="8" H="76" G="22" F="5" D="WNW">0</Rep>
        <Rep U="0" W="7" V="VG" T="8" S="13" Pp="6" H="79" G="25" F="4" D="WNW">180</Rep>
        <Rep U="1" W="7" V="VG" T="7" S="13" Pp="7" H="81" G="27" F="4" D="WNW">360</Rep>
        <Rep U="2" W="7" V="VG" T="9" S="16" Pp="6" H="76" G="29" F="5" D="WNW">540</Rep>
        <Rep U="3" W="7" V="VG" T="10" S="16" Pp="5" H="73" G="29" F="6" D="WNW">720</Rep>
        <Rep U="1" W="7" V="VG" T="10" S="13" Pp="5" H="73" G="27" F="6" D="WNW">900</Rep>
        <Rep U="1" W="7" V="VG" T="9" S="11" Pp="4" H="77" G="20" F="6" D="WNW">1080</Rep>
        <Rep U="0" W="7" V="VG" T="8" S="9" Pp="5" H="83" G="16" F="5" D="WNW">1260</Rep>
      </Period>
    </Location>
  </DV>
</SiteRep>
```


Figure A.0.1: Forecast information from Met Office Data Point.

Bibliography

[1] E. Microgrid. Entrust smart hot water. [Online]. Available: https://www.entrustmicrogrid.com/

[2] T. Kaur, S. Kumar, and R. Segal, "Application of artificial neural network for short term wind speed forecasting," in *Biennial International Conference on Power & Energy Systems: Towards Sustainable Energy. IEEE*, 2016.

[3] A. Barbato and A. Capone, "Optimization models and methods for demand-side management of residential users: A survey," *Energies*, vol. 7, pp. 5787–5824, 2014.

[4] N. Kourentzes, F. Petropoulos, and J. R. Trapero, "Improving forecasting by estimating time series structural components across multiple frequencies," *International Journal of Forecasting*, vol. 30, no. 2, pp. 291 – 302, 2014.

[5] Nikolaos, Kourentzes, Fotios, and Petropoulos, "Forecasting with multivariate temporal aggregation: The case of promotional modelling," *International Journal of Production Economics*, vol. 181, pp. 145–153, 2016.

[6] T. Zhao and Z. Ding, "Cooperative optimal control of battery energy storage

system under wind uncertainties in a microgrid," *IEEE Transactions on Power Systems*, vol. 33, no. 2, pp. 2292–2300, 2018.

[7] M. Mokhtar, M. Stables, X. Liu, and J. Howe, "Intelligent multi-agent system for building heat distribution control with combined gas boilers and ground source heat pump," *Energy and Buildings*, vol. 62, pp. 615 – 626, 2013.

[8] N. Kourentzes, F. Petropoulos, and J. R. Trapero, "Improving forecasting by estimating time series structural components across multiple frequencies," *International Journal of Forecasting*, vol. 30, no. 2, pp. 291 – 302, 2014.

[9] J. Ma and X. Ma, "A review of forecasting algorithms and energy management strategies for microgrids," *Systems Science & Control Engineering*, vol. 6, no. 1, pp. 237–248, 2018.

[10] X. Liu, I. Chilvers, M. Mokhtar, A. Bedford, K. Stitt, and J. Yazdani, "Microgrid development for properties," in *2011 2nd IEEE PES International Conference and Exhibition on Innovative Smart Grid Technologies*, 2011, pp. 1–7.

[11] F. Martin-Martinez, A. Sanchez-Miralles, and M. Rivier, "A literature review of microgrids: A functional layer based classification," *Renewable & Sustainable Energy Reviews*, vol. 62, no. sep., pp. 1133–1153, 2016.

[12] X. Ma, Y. Wang, and J. Qin, "Generic model of a community-based microgrid integrating wind turbines, photovoltaics and chp generations," *Applied Energy*, vol. 112, pp. 1475 – 1482, 2013.

[13] A. Kaur, J. Kaushal, and P. Basak, "A review on microgrid central controller," *Renewable & Sustainable Energy Reviews*, vol. 55, pp. 338–345, 2016.

[14] L. Mariam, M. Basu, and M. F. Conlon, "Microgrid: Architecture, policy and future trends," *Renewable & Sustainable Energy Reviews*, vol. 64, pp. 477–489, 2016.

[15] J. J. Justo, F. Mwasilu, J. Lee, and J.-W. Jung, "Ac-microgrids versus dc-microgrids with distributed energy resources: A review," *Renewable & Sustainable Energy Reviews*, vol. 24, pp. 387 – 405, 2013.

[16] V. Nasirian, Q. Shafiee, J. M. Guerrero, F. L. Lewis, and A. Davoudi, "Droop-free distributed control for ac microgrids," *IEEE Transactions on Power Electronics*, vol. 31, no. 2, pp. 1600–1617, 2016.

[17] R. H. Lasseter, J. H. Eto, B. Schenkman, J. Stevens, H. Vollkommer, D. Klapp, E. Linton, H. Hurtado, and J. Roy, "Certs microgrid laboratory test bed," *IEEE Transactions on Power Delivery*, vol. 26, no. 1, pp. 325–332, 2011.

[18] J. Eto, R. Lasseter, B. Schenkman, J. Stevens, and J. Roy, "Overview of the certs microgrid laboratory test bed," in *Integration of Wide-scale Renewable Resources Into the Power Delivery System, Cigre/ieee Pes Joint Symposium*, 2009.

[19] L. Che, M. Shahidehpour, A. Alabdulwahab, and Y. Al-Turki, "Hierarchical coordination of a community microgrid with ac and dc microgrids," *IEEE Transactions on Smart Grid*, vol. 6, no. 6, pp. 3042–3051, 2015.

[20] S. Lu, L. Wang, T. Lo, and A. V. Prokhorov, "Integration of wind power and wave power generation systems using a dc microgrid," *IEEE Transactions on Industry Applications*, vol. 51, no. 4, pp. 2753–2761, 2015.

[21] T. Dragičević, X. Lu, J. C. Vasquez, and J. M. Guerrero, "Dc microgrids—part ii: A review of power architectures, applications, and standardization issues," *IEEE Transactions on Power Electronics*, vol. 31, no. 5, pp. 3528–3549, 2016.

[22] P. Flores, A. Tapia, and G. Tapia, "Application of a control algorithm for wind speed prediction and active power generation," *Renewable Energy*, vol. 30, no. 4, pp. 523–536, 2005.

[23] T. Kaur, S. Kumar, and R. Segal, "Application of artificial neural network for short term wind speed forecasting," in *2016 Biennial International Conference on Power and Energy Systems: Towards Sustainable Energy (PESTSE)*, 2016, pp. 1–5.

[24] Shuhui Li, D. C. Wunsch, E. A. O'Hair, and M. G. Giesselmann, "Using neural networks to estimate wind turbine power generation," *IEEE Transactions on Energy Conversion*, vol. 16, no. 3, pp. 276–282, 2001.

[25] M. C. Alexiadis, P. S. Dokopoulos, H. S. Sahsamanoglou, and I. M. Manousaridis, "Short-term forecasting of wind speed and related electrical power," *Solar Energy*, vol. 63, no. 1, pp. 61–68, 1998.

[26] M. C. Mabel and E. Fernandez, "Analysis of wind power generation and predic-

tion using ann: A case study," *Renewable Energy*, vol. 33, no. 5, pp. p.986–992, 2008.

[27] P. Qian, X. Ma, D. Zhang, and J. Wang, "Data-driven condition monitoring approaches to improving power output of wind turbines," *IEEE Transactions on Industrial Electronics*, vol. 66, no. 8, pp. 6012–6020, 2019.

[28] M. Diagne, M. David, P. Lauret, J. Boland, and N. Schmutz, "Review of solar irradiance forecasting methods and a proposition for small-scale insular grids," *Renewable & Sustainable Energy Reviews*, vol. 27, no. Complete, pp. 65–76, 2013.

[29] A. Sharma and A. Kakkar, "Forecasting daily global solar irradiance generation using machine learning," *Renewable & Sustainable Energy Reviews*, vol. 82, pp. 2254–2269, 2018.

[30] S. Sobrina, K.-K. Sam, and A. R. Nasrudin, "Solar photovoltaic generation forecasting methods: A review," *Energy Conversion and Management*, vol. 156, pp. 459–497, 2018.

[31] T. Khatib, A. Mohamed, and K. Sopian, "A review of solar energy modeling techniques," *Renewable and Sustainable Energy Reviews*, vol. 16, no. 5, pp. 2864 – 2869, 2012.

[32] M. Chaabene and M. B. Ammar], "Neuro-fuzzy dynamic model with kalman filter to forecast irradiance and temperature for solar energy systems," *Renewable Energy*, vol. 33, no. 7, pp. 1435 – 1443, 2008.

[33] A. Mellit and A. M. Pavan, "A 24-h forecast of solar irradiance using artificial neural network: Application for performance prediction of a grid-connected pv plant at trieste, italy," *Solar Energy*, vol. 84, no. 5, pp. 807 – 821, 2010.

[34] Z. Dong, D. Yang, T. Reindl, and W. M. Walsh, "A novel hybrid approach based on self-organizing maps, support vector regression and particle swarm optimization to forecast solar irradiance," *Energy*, vol. 82, pp. 570 – 577, 2015.

[35] S. Chen, H. Gooi, and M. Wang, "Solar radiation forecast based on fuzzy logic and neural networks," *Renewable Energy*, vol. 60, pp. 195 – 201, 2013.

[36] L. Wang, O. Kisi, M. Zounemat-Kermani, G. A. Salazar, Z. Zhu, and W. Gong, "Solar radiation prediction using different techniques: model evaluation and comparison," *Renewable and Sustainable Energy Reviews*, vol. 61, pp. 384 – 397, 2016.

[37] H. Nazaripouya, B. Wang, Y. Wang, P. Chu, H. R. Pota, and R. Gadh, "Univariate time series prediction of solar power using a hybrid wavelet-arma-narx prediction method," in *2016 IEEE/PES Transmission and Distribution Conference and Exposition (T D)*, 2016, pp. 1–5.

[38] X. Huang, J. Shi, B. Gao, Y. Tai, Z. Chen, and J. Zhang, "Forecasting hourly solar irradiance using hybrid wavelet transformation and elman model in smart grid," *IEEE Access*, vol. 7, pp. 139 909–139 923, 2019.

[39] K. Mohammadi, S. Shamshirband, A. Kamsin, P. Lai, and Z. Mansor, "Identifying the most significant input parameters for predicting global solar radiation

using an anfis selection procedure," *Renewable and Sustainable Energy Reviews*, vol. 63, pp. 423 – 434, 2016.

[40] R. Ahmed, V. Sreeram, Y. Mishra, and M. Arif, "A review and evaluation of the state-of-the-art in pv solar power forecasting: Techniques and optimization," *Renewable and Sustainable Energy Reviews*, vol. 124, p. 109792, 2020.

[41] S. Ghimire, R. C. Deo, N. Raj, and J. Mi, "Deep solar radiation forecasting with convolutional neural network and long short-term memory network algorithms," *Applied Energy*, vol. 253, p. 113541, 2019.

[42] N. Dong, J.-F. Chang, A.-G. Wu, and Z.-K. Gao, "A novel convolutional neural network framework based solar irradiance prediction method," *International Journal of Electrical Power & Energy Systems*, vol. 114, p. 105411, 2020.

[43] Z. Pang, F. Niu, and Z. O'Neill, "Solar radiation prediction using recurrent neural network and artificial neural network: A case study with comparisons," *Renewable Energy*, vol. 156, pp. 279 – 289, 2020.

[44] D. Yang, P. Jirutitijaroen, and W. M. Walsh, "Hourly solar irradiance time series forecasting using cloud cover index," *Solar Energy*, vol. 86, no. 12, pp. 3531 – 3543, 2012.

[45] C. Yang, A. A. Thatte, and L. Xie, "Multitime-scale data-driven spatio-temporal forecast of photovoltaic generation," *IEEE Transactions on Sustainable Energy*, vol. 6, no. 1, pp. 104–112, 2015.

[46] G. Wang, Y. Su, and L. Shu, "One-day-ahead daily power forecasting of photovoltaic systems based on partial functional linear regression models," *Renewable Energy*, vol. 96, pp. 469 – 478, 2016.

[47] Y. Li, Y. He, Y. Su, and L. Shu, "Forecasting the daily power output of a grid-connected photovoltaic system based on multivariate adaptive regression splines," *Applied Energy*, vol. 180, pp. 392–401, 2016.

[48] L. Massidda and M. Marrocu, "Use of multilinear adaptive regression splines and numerical weather prediction to forecast the power output of a pv plant in borkum, germany," *Solar Energy*, vol. 146, pp. 141 – 149, 2017.

[49] A. Mellit, M. Menghanem, and M. Bendekhis, "Artificial neural network model for prediction solar radiation data: application for sizing stand-alone photovoltaic power system," in *IEEE Power Engineering Society General Meeting, 2005*, 2005, pp. 40–44.

[50] M. A, M. P. A, and L. V, "Short-term forecasting of power production in a large-scale photovoltaic plant," *Solar Energy*, vol. 105, pp. 401–413, 2014.

[51] E. G. Kardakos, M. C. Alexiadis, S. I. Vagropoulos, C. K. Simoglou, P. N. Biskas, and A. G. Bakirtzis, "Application of time series and artificial neural network models in short-term forecasting of pv power generation," in *2013 48th International Universities' Power Engineering Conference*, 2013, pp. 40–44.

[52] K. Wang, X. Qi, and H. Liu, "A comparison of day-ahead photovoltaic power

forecasting models based on deep learning neural network," *Applied Energy*, vol. 251, p. 113315, 2019.

[53] M. David, F. Ramahatana, P. Trombe, and P. Lauret, "Probabilistic forecasting of the solar irradiance with recursive arma and garch models," *Solar Energy*, vol. 133, pp. 55 – 72, 2016.

[54] M. Guermoui, F. Melgani, K. Gairaa, and M. L. Mekhalfi, "A comprehensive review of hybrid models for solar radiation forecasting," *Journal of Cleaner Production*, vol. 258, p. 120357, 2020.

[55] H. Sun, D. Yan, N. Zhao, and J. Zhou, "Empirical investigation on modeling solar radiation series with arma–garch models," *Energy Conversion and Management*, vol. 92, pp. 385 – 395, 2015.

[56] M. A. F. Lima, P. C. Carvalho, L. M. Fernández-Ramírez, and A. P. Braga, "Improving solar forecasting using deep learning and portfolio theory integration," *Energy*, vol. 195, p. 117016, 2020.

[57] Z. Yang, M. Mourshed, K. Liu, X. Xu, and S. Feng, "A novel competitive swarm optimized rbf neural network model for short-term solar power generation forecasting," *Neurocomputing*, vol. 397, pp. 415 – 421, 2020.

[58] A. R. Pazikadin, D. Rifai, K. Ali, M. Z. Malik, A. N. Abdalla, and M. A. Faraj, "Solar irradiance measurement instrumentation and power solar generation forecasting based on artificial neural networks (ann): A review of five years research trend," *Science of The Total Environment*, vol. 715, p. 136848, 2020.

[59] H. Lan, C. Zhang, Y.-Y. Hong, Y. He, and S. Wen, "Day-ahead spatiotemporal solar irradiation forecasting using frequency-based hybrid principal component analysis and neural network," *Applied Energy*, vol. 247, pp. 389 – 402, 2019.

[60] F. Wang, Z. Mi, S. Su, and H. Zhao, "Short-term solar irradiance forecasting model based on artificial neural network using statistical feature parameters," *Energies*, vol. 5, no. 5, pp. 1355–1370, 2012.

[61] J. Liu, W. Fang, X. Zhang, and C. Yang, "An improved photovoltaic power forecasting model with the assistance of aerosol index data," *IEEE Transactions on Sustainable Energy*, vol. 6, no. 2, pp. 434–442, 2015.

[62] M. Bouzerdoum, A. Mellit, and A. M. Pavan, "A hybrid model (sarima-svm) for short-term power forecasting of a small-scale grid-connected photovoltaic plant," *Solar Energy*, vol. 98, no. pt.C, pp. 226–235, 2013.

[63] S. X. Chen, H. B. Gooi, and M. Q. Wang, "Solar radiation forecast based on fuzzy logic and neural networks," *Renewable Energy*, vol. 60, pp. 195–201, 2013.

[64] D. E. Olivares, C. A. Canizares, and M. Kazerani, "A centralized energy management system for isolated microgrids," *IEEE Transactions on Smart Grid*, vol. 5, no. 4, pp. 1864–1875, 2014.

[65] R. Palma-Behnke, C. Benavides, F. Lanas, B. Severino, L. Reyes, J. Llanos, and D. Sáez, "A microgrid energy management system based on the rolling horizon strategy," *IEEE Transactions on Smart Grid*, vol. 4, no. 2, pp. 996–1006, 2013.

[66] A. Chaouachi, R. M. Kamel, R. Andoulsi, and K. Nagasaka, "Multi-objective intelligent energy management for a microgrid," *IEEE Transactions on Industrial Electronics*, vol. 60, no. 4, pp. p.1688–1699, 2013.

[67] W. Fan, N. Liu, and J. Zhang, "Multi-objective optimization model for energy management of household micro-grids participating in demand response," in *IEEE Innovative Smart Grid Technologies-asia*, 2015.

[68] M. B. Wafaa and L. Dessaint, "Multi-objective stochastic optimal power flow considering voltage stability and demand response with significant wind penetration," *IET Generation, Transmission & Distribution*, vol. 11, no. 14, pp. 3499–3509, 2017.

[69] Y. Han, K. Zhang, H. Li, E. A. A. Coelho, and J. M. Guerrero, "Mas-based distributed coordinated control and optimization in microgrid and microgrid clusters: A comprehensive overview," *IEEE Transactions on Power Electronics*, vol. 33, no. 8, pp. 6488–6508, 2018.

[70] X. Lu, X. Yu, J. Lai, Y. Wang, and J. M. Guerrero, "A novel distributed secondary coordination control approach for islanded microgrids," *IEEE Transactions on Smart Grid*, vol. 9, no. 4, pp. 2726–2740, 2018.

[71] Y. Han, H. Li, P. Shen, E. A. A. Coelho, and J. M. Guerrero, "Review of active and reactive power sharing strategies in hierarchical controlled microgrids," *IEEE Transactions on Power Electronics*, vol. 32, no. 3, pp. 2427–2451, 2017.

[72] Y. Zhang and H. Ma, "Theoretical and experimental investigation of networked

control for parallel operation of inverters," *IEEE Transactions on Industrial Electronics*, vol. 59, no. 4, pp. 1961–1970, 2012.

[73] J. Qin, Q. Ma, Y. Shi, and L. Wang, "Recent advances in consensus of multi-agent systems: A brief survey," *IEEE Transactions on Industrial Electronics*, vol. 64, no. 6, pp. 4972–4983, 2017.

[74] W. Li, T. Logenthiran, W. L. Woo, V. Phan, and D. Srinivasan, "Implementation of demand side management of a smart home using multi-agent system," in *2016 IEEE Congress on Evolutionary Computation (CEC)*, 2016, pp. 2028–2035.

[75] F. Brazier, H. L. Poutre, A. R. Abhyankar, K. Saxena, S. N. Singh, and K. K. Tomar, "A review of multi agent based decentralised energy management issues," in *2015 International Conference on Energy Economics and Environment (ICEEE)*, 2015, pp. 1–5.

[76] S. Yang, S. Tan, and J. Xu, "Consensus based approach for economic dispatch problem in a smart grid," *IEEE Transactions on Power Systems*, vol. 28, no. 4, pp. 4416–4426, 2013.

[77] W. Liu, W. Gu, W. Sheng, X. Meng, Z. Wu, and W. Chen, "Decentralized multi-agent system-based cooperative frequency control for autonomous microgrids with communication constraints," *IEEE Transactions on Sustainable Energy*, vol. 5, no. 2, pp. 446–456, 2014.

[78] Y. Xu and Z. Li, "Distributed optimal resource management based on the con-

sensus algorithm in a microgrid," *IEEE Transactions on Industrial Electronics*, vol. 62, no. 4, pp. 2584–2592, 2015.

[79] J. Hu and A. Lanzon, "Distributed finite-time consensus control for heterogeneous battery energy storage systems in droop-controlled microgrids," *IEEE Transactions on Smart Grid*, vol. 10, no. 5, pp. 4751–4761, 2019.

[80] H. S. V. S. K. Nunna and D. Srinivasan, "A multi-agent system for energy management in smart microgrids with distributed energy storage and demand response," in *2016 IEEE International Conference on Power Electronics, Drives and Energy Systems (PEDES)*, 2016, pp. 1–5.

[81] X. Lu, K. Sun, J. M. Guerrero, J. C. Vasquez, and L. Huang, "State-of-charge balance using adaptive droop control for distributed energy storage systems in dc microgrid applications," *IEEE Transactions on Industrial Electronics*, vol. 61, no. 6, pp. 2804–2815, 2014.

[82] T. Morstyn, B. Hredzak, and V. G. Agelidis, "Cooperative multi-agent control of heterogeneous storage devices distributed in a dc microgrid," *IEEE Transactions on Power Systems*, vol. 31, no. 4, pp. 2974–2986, 2016.

[83] L. Gelazanskas and K. A. Gamage, "Demand side management in smart grid: A review and proposals for future direction," *Sustainable Cities and Society*, vol. 11, pp. 22 – 30, 2014.

[84] B. P. Esther and K. S. Kumar, "A survey on residential demand side manage-

ment architecture, approaches, optimization models and methods," *Renewable and Sustainable Energy Reviews*, vol. 59, pp. 342 – 351, 2016.

[85] J. C. Vasquez, J. M. Guerrero, J. Miret, M. Castilla, and L. G. de Vicuña, "Hierarchical control of intelligent microgrids," *IEEE Industrial Electronics Magazine*, vol. 4, no. 4, pp. 23–29, 2010.

[86] P. Palensky and D. Dietrich, "Demand side management: Demand response, intelligent energy systems, and smart loads," *IEEE Transactions on Industrial Informatics*, vol. 7, no. 3, pp. 381–388, 2011.

[87] S. Ramchurn, P. Vytelingum, A. Rogers, and N. Jennings, "Agent-based control for decentralised demand side management in the smart grid," in *Proceedings of the 10th international conference on autonomous agents and multi agent systems (AAMAS2011)*, 2011.

[88] W. Zhang, J. Liang, C. Y. Chang, and K. Kalsi, "Aggregated modeling and control of air conditioning loads for demand response," *IEEE Transactions on Power Systems*, vol. 28, no. 4, pp. 4655–4664, 2013.

[89] J. Hlava and N. Zemtsov, "Aggregated control of electrical heaters for ancillary services provision," in *19th International Conference on System Theory, Control and Computing (ICSTCC)*, 2015, pp. 1–5.

[90] S. H. Tindermans, V. Trovato, and G. Strbac, "Decentralized control of thermostatic loads for flexible demand response," *IEEE Transactions on Control Systems Technology*, vol. 23, no. 5, pp. 1685–1700, 2015.

[91] M. Liu, Y. Shi, and X. Liu, "Distributed mpc of aggregated heterogeneous thermostatically controlled loads in smart grid," *IEEE Transactions on Industrial Electronics*, vol. 63, no. 2, pp. 1120–1129, 2016.

[92] X. Wu, J. He, Y. Xu, J. Lu, N. Lu, and X. Wang, "Hierarchical control of residential hvac units for primary frequency regulation," *IEEE Transactions on Smart Grid*, vol. 9, no. 4, pp. 3844–3856, 2018.

[93] D. H. Blum, T. Zakula, and L. K. Norford, "Opportunity cost quantification for ancillary services provided by heating, ventilating, and air-conditioning systems," *IEEE Transactions on Smart Grid*, vol. 8, no. 3, pp. 1264–1273, 2017.

[94] S. Bashash and H. K. Fathy, "Modeling and control insights into demand-side energy management through setpoint control of thermostatic loads," in *Proceedings of the 2011 American Control Conference*, 2011, pp. 4546–4553.

[95] A. Aswani, N. Master, J. Taneja, D. Culler, and C. Tomlin, "Reducing transient and steady state electricity consumption in hvac using learning-based model-predictive control," *Proceedings of the IEEE*, vol. 100, no. 1, pp. 240–253, 2012.

[96] W. Zhang, J. Lian, C. Chang, and K. Kalsi, "Aggregated modeling and control of air conditioning loads for demand response," in *2014 IEEE PES General Meeting | Conference Exposition*, 2014.

[97] M. Hu, F. Xiao, J. B. Jørgensen, and S. Wang, "Frequency control of air conditioners in response to real-time dynamic electricity prices in smart grids," *Applied Energy*, vol. 242, pp. 92 – 106, 2019.

[98] Z. Liang, D. Bian, X. Zhang, D. Shi, R. Diao, and Z. Wang, "Optimal energy management for commercial buildings considering comprehensive comfort levels in a retail electricity market," *Applied Energy*, vol. 236, pp. 916 – 926, 2019.

[99] M. Hu and F. Xiao, "Price-responsive model-based optimal demand response control of inverter air conditioners using genetic algorithm," *Applied Energy*, vol. 219, pp. 151–164, 2018.

[100] B. Wang, T. Zhang, X. Hu, Y. Bao, and H. Su, "Consensus control strategy of an inverter air conditioning group for renewable energy integration based on the demand response," *IET Renewable Power Generation*, vol. 12, no. 14, pp. 1633–1639, 2018.

[101] R. Wang, Q. Li, B. Zhang, and L. Wang, "Distributed consensus based algorithm for economic dispatch in a microgrid," *IEEE Transactions on Smart Grid*, vol. 10, no. 4, pp. 3630–3640, 2019.

[102] L.-Y. Chiu, D. J. Arcega Rustia, C.-Y. Lu, and T.-T. Lin, "Modelling and forecasting of greenhouse whitefly incidence using time-series and arimax analysis," *IFAC-PapersOnLine*, vol. 52, no. 30, pp. 196 – 201, 2019, 6th IFAC Conference on Sensing, Control and Automation Technologies for Agriculture AGRICONTROL 2019.

[103] J. Ma and X. Ma, "Consensus-based hierachical demand side management in microgrid," in *2019 25th International Conference on Automation and Computing (ICAC)*, 2019, pp. 1–6.

[104] J. Ma and X. Ma, "Distributed control of battery energy storage system in a microgrid," in *2019 8th International Conference on Renewable Energy Research and Applications*, 2019, pp. 320–325.

[105] B. Moore, "Principal component analysis in linear systems: Controllability, observability, and model reduction," *IEEE Transactions on Automatic Control*, vol. 26, no. 1, pp. 17–32, 1981.

[106] A. M. Martinez and A. C. Kak, "Pca versus lda," *IEEE Transactions on Pattern Analysis and Machine Intelligence*, vol. 23, no. 2, pp. 228–233, 2001.

[107] Y. Wang, X. Ma, and P. Qian, "Wind turbine fault detection and identification through pca-based optimal variable selection," *IEEE Transactions on Sustainable Energy*, vol. 9, no. 4, pp. 1627–1635, 2018.

[108] Y. Wang, X. Ma, and M. J. Joyce, "Reducing sensor complexity for monitoring wind turbine performance using principal component analysis," *Renewable Energy*, vol. 97, pp. 444 – 456, 2016.

[109] M. Mao, L. Cui, Q. Zhang, K. Guo, L. Zhou, and H. Huang, "Classification and summarization of solar photovoltaic mppt techniques: A review based on traditional and intelligent control strategies," *Energy Reports*, vol. 6, pp. 1312 – 1327, 2020.

[110] S. Sumathi, L. A. Kumar, and P. Surekha, *Solar PV and Wind Energy Conversion Systems*. Switzerland: Springer, 2015.

[111] X. Zhang and R. Cao, *Grid-connected solar photovoltaic power generation and its inverter control (Chinese)*. China Machine Press, 2011.

[112] R. Wei and R. W. Beard, *Distributed consensus in multi-vechicle cooperative control*. Berlin, Germany: Springer-Verlag, 2008.

[113] R. Horn and C. Johnson, *Matrix Analysis*. Cambrige UK: Cambridge University Press, 1985.

[114] Y. C. Park, Y. C. Kim, and M.-K. Min, "Performance analysis on a multi-type inverter air conditioner," *Energy Conversion and Management*, vol. 42, no. 13, pp. 1607 – 1621, 2001.

[115] M. Song, C. Gao, H. Yan, and J. Yang, "Thermal battery modeling of inverter air conditioning for demand response," *IEEE Transactions on Smart Grid*, vol. 9, no. 6, pp. 5522–5534, 2018.

[116] S. Shao, W. Shi, X. Li, and H. Chen, "Performance representation of variable-speed compressor for inverter air conditioners based on experimental data," *International Journal of Refrigeration*, vol. 27, no. 8, pp. 805 – 815, 2004.

[117] K. Cai and H. Ishii, "Average consensus on general strongly connected digraphs," *Automatica*, vol. 48, no. 11, pp. 2750 – 2761, 2012.

[118] K. Cai and H. Ishii, "Average consensus on arbitrary strongly connected digraphs with time-varying topologies," *IEEE Transactions on Automatic Control*, vol. 59, no. 4, pp. 1066–1071, 2014.

[119] L. Moreau, "Stability of multiagent systems with time-dependent communication links," *IEEE Transactions on Automatic Control*, vol. 50, no. 2, pp. 169–182, 2005.

[120] R. Olfati-Saber, J. A. Fax, and R. M. Murray, "Consensus and cooperation in networked multi-agent systems," *Proceedings of the IEEE*, vol. 95, no. 1, pp. 215–233, 2007.

[121] (1993, 08) Power systems test case archive. "30 bus power flow test case". [Online]. Available: http://labs.ece.uw.edu/pstca/pf30/ieee30cdf.txt

[122] G. Taguchi, S. Chowdhury, and Y. Wu, *Taguchi's Quality Engineering Handbook*. USA: Wiley, 2007.

[123] K. Ma, T. Yao, J. Yang, and X. Guan, "Residential power scheduling for demand response in smart grid," *International Journal of Electrical Power & Energy Systems*, vol. 78, no. jun., pp. 320–325, 2016.

[124] N. Rahbari-Asr, U. Ojha, Z. Zhang, and M. Chow, "Incremental welfare consensus algorithm for cooperative distributed generation/demand response in smart grid," *IEEE Transactions on Smart Grid*, vol. 5, no. 6, pp. 2836–2845, 2014.

[125] F. Chen, M. Chen, Q. Li, K. Meng, Y. Zheng, J. M. Guerrero, and D. Abbott, "Cost-based droop schemes for economic dispatch in islanded microgrids," *IEEE Transactions on Smart Grid*, vol. 8, no. 1, pp. 63–74, 2017.

[126] A. Mordecai, *Nonlinear Programming: Analysis and Methods*. Dover Publications, 01 1976.

[127] D. G. Luenberger and Y. Ye, *Linear and Nonlinear Programming (Third Edition)*. Berlin, Germany: Springer, 2008.

[128] S. S. Kia, "A distributed dynamical solver for an optimal resource allocation problem over networked systems," in *2015 54th IEEE Conference on Decision and Control (CDC)*, 2015, pp. 7482–7487.

[129] C. Eid, E. Koliou, M. Valles, J. Reneses, and R. Hakvoort, "Time-based pricing and electricity demand response: Existing barriers and next steps," *Utilities Policy*, vol. 40, pp. 15 – 25, 2016.

[130] J. Kohlmann, M. C. H. van der Vossen, J. D. Knigge, C. B. A. Kobus, and J. G. Slootweg, "Integrated design of a demand-side management system," in *2011 2nd IEEE PES International Conference and Exhibition on Innovative Smart Grid Technologies*, 2011, pp. 1–8.

[131] (1993, 08) Power systems test case archive. "ieee 57-bus system". [Online]. Available: http://labs.ece.uw.edu/pstca/pf57/ieee57cdf.txt

[132] G. Delille, B. Francois, and G. Malarange, "Dynamic frequency control support by energy storage to reduce the impact of wind and solar generation on isolated power system's inertia," *IEEE Transactions on Sustainable Energy*, vol. 3, no. 4, pp. 931–939, 2012.

[133] T. Dragičević, X. Lu, J. C. Vasquez, and J. M. Guerrero, "Dc microgrids—part i: A review of control strategies and stabilization techniques," *IEEE Transactions on Power Electronics*, vol. 31, no. 7, pp. 4876–4891, 2016.

[134] J. Choi, I. Choi, G. An, and D. J. Won, "Advanced power sharing method for energy efficiency improvement of multiple battery energy storages system," *IEEE Transactions on Smart Grid*, pp. 1–1, 2016.

[135] F. A. Amoroso and G. Cappuccino, "Advantages of efficiency-aware smart charging strategies for pevs," *Energy Conversion and Management*, vol. 54, no. 1, pp. 1 – 6, 2012.

[136] Y. V. Makarov, C. Loutan, J. Ma, and P. de Mello, "Operational impacts of wind generation on california power systems," *IEEE Transactions on Power Systems*, vol. 24, no. 2, pp. 1039–1050, 2009.

[137] L. Wang and B. Chen, "Distributed control for large-scale plug-in electric vehicle charging with a consensus algorithm," *International Journal of Electrical Power & Energy Systems*, vol. 109, pp. 369 – 383, 2019.